
Analysis of Dscam1 diversity in regulating dendritic morphology of Lobula Plate Tangential Cells

Dissertation

zur Erlangung des Doktorgrades
der Naturwissenschaften (Dr. rer. nat.)
an der Fakultät für Biologie
der Ludwig-Maximilians-Universität München

Angefertigt am Max-Planck-Institut für Neurobiologie
Abteilung Neuronale Informationsverarbeitung

vorgelegt von
Jing Claussen (geb. Shi)
aus Shanghai

München 08.05.2014

Erstgutachter: Prof. Dr. Alexander Borst

Zweitgutachter: Prof. Dr. Hans Straka

Tag der mündlichen Prüfung: 11.11.2014

I. Table of Contents

I.	Table of Contents	1
II.	Abbreviations.....	5
III.	Table of Figures	10
1	Abstract	12
2	Introduction.....	14
2.1	The motion detection pathway in flies	14
2.1.1	The compound eye	14
2.1.2	Signaling pathways	15
2.1.3	The Reichardt detector model.....	17
2.1.4	LPTCs in <i>Calliphora</i>	19
2.1.5	LPTCs in <i>Drosophila</i>	22
2.2	The function of Dscams in neuronal wiring.....	26
2.2.1	Self-avoidance and <i>Dscam1</i>	26
2.2.1.1	Isoform diversity	26
2.2.1.2	Homophilic interactions	28
2.2.1.3	Repulsion mechanism	29
2.2.1.4	Structural basis.....	29
2.2.1.5	Functions in dendritic morphogenesis	29
2.2.1.6	Functions in axonal morphogenesis	31
2.2.1.7	Reduced <i>Dscam1</i> variability	33
2.2.1.8	Further functions.....	33
2.2.2	Tiling and <i>Dscam2</i>	35
2.2.3	The function of <i>DSCAM</i> in mammals	35
2.3	Genetic tools in <i>Drosophila</i>	36
2.3.1	The Gal4/ UAS system.....	37
2.3.1.1	Gal80/ Gal80 ^{ts}	38
2.3.1.2	Split-Gal4.....	39
2.3.1.3	The FRT/ FLP recombination system	39
2.3.1.4	MARCM	39
2.3.2	Gene knockdown with RNAi.....	41
2.3.3	Cell ablation using genetic encoded RicinA	41

Table of contents

2.3.4	Genetically encoded calcium indicator TN-XXL	42
2.4	Tracing neuronal circuits using viruses	43
2.5	Aims and project outline	46
3	Materials and methods	48
3.1	Materials.....	48
3.1.1	Buffers, solutions and media	48
3.1.2	Flystocks	49
3.1.3	Consumables	50
3.1.4	Antibodies	52
3.1.5	Electronic equipment.....	53
3.1.6	Primers.....	53
3.2	Methods	57
3.2.1	Molecular biology	57
3.2.1.1	Plasmid DNA Extraction	57
3.2.1.2	Polymerase Chain Reaction	58
3.2.1.3	Restriction of DNA vector backbone and insert	58
3.2.1.4	Preparation of DNA for ligation	59
3.2.1.5	Vector backbone purification	59
3.2.1.6	Insert purification	60
3.2.1.7	Ligation.....	60
3.2.1.8	Gateway cloning system.....	61
3.2.1.9	Transformation of chemical competent cells.....	62
3.2.1.10	Rapid small-scale isolation of DNA.....	62
3.2.1.11	Degenerative PCR.....	63
3.2.2	Transgenic flies	66
3.2.2.1	Production of flyfood.....	66
3.2.2.2	Breeding of flies.....	66
3.2.2.3	Production of egg-laying medium	66
3.2.2.4	Generation of transgenic flies.....	66
3.2.3	Anatomical analysis	68
3.2.3.1	Fly crossings.....	68
3.2.3.1.1	Dscam1 project.....	68
3.2.3.1.2	RicinA project.....	70
3.2.3.1.3	UAS>Stop>TN-XXL project.....	70

Table of contents

3.2.3.1.4	Virus project.....	71
3.2.3.2	Immunohistochemistry.....	71
3.2.3.3	Confocal microscopy.....	71
3.2.3.4	Image post-processing.....	72
3.2.3.5	Cell reconstructions.....	72
3.2.4	RicinA project.....	73
3.2.4.1	Development of LPTCs.....	73
3.2.4.2	Heatshock protocol.....	73
3.2.4.3	Cell vitality test.....	74
3.2.5	TN-XXL project.....	75
3.2.6	Virus project.....	76
3.2.6.1	Brain culture.....	76
3.2.6.2	The UAS-TVA-2Alike-dsRed construct.....	77
3.2.6.3	The UAS-G-protein constructs.....	79
4	Results.....	80
4.1	Manipulations of the <i>Dscam1</i> expression in LPTCs.....	80
4.1.1	Immunolabeling against <i>Dscam1</i>	80
4.1.2	Reduced <i>Dscam1</i> expression level.....	82
4.1.2.1	Silencing <i>Dscam1</i> with RNAi.....	82
4.1.2.2	MARCM.....	85
4.1.2.3	MARCM with residual flippase activity.....	86
4.1.3	Reduced <i>Dscam1</i> diversity.....	90
4.1.4	Misexpression of single <i>Dscam1</i> isoforms.....	93
4.1.4.1	<i>Dscam1</i> ^{+7.6.19.2}	93
4.1.4.2	<i>Dscam1</i> ^{+11.31.25.1}	96
4.1.4.2.1	Horizontal connectivity.....	100
4.1.4.2.2	MARCM analysis.....	101
4.1.4.2.3	Time-point analysis.....	102
4.1.4.2.4	Misexpression in T4/ T5 cells.....	105
4.2	RicinA induced ablation of LPTCs.....	108
4.3	Refined expression pattern of TN-XXL.....	112
4.4	Viral labeling of LPTCs.....	113
5	Discussion.....	116
5.1	<i>Dscam1</i> manipulation in LPTCs.....	116

Table of contents

5.1.1	Anatomical changes and underlying mechanisms	116
5.1.1.1	Reduced <i>Dscam1</i> expression level	116
5.1.1.2	Reduced <i>Dscam1</i> expression diversity.....	117
5.1.1.3	Misexpression of single <i>Dscam1</i> isoforms.....	119
5.1.2	Correlations between anatomy and function	122
5.1.3	Correlations between anatomy and behavior	124
5.2	Efficacy of RicinA cell ablation	125
5.2.1	Insights into developmental mechanisms.....	127
5.2.2	Correlation between anatomy and behavior.....	128
5.3	Recording cellular response properties with TN-XXL	128
5.4	Virus based neural tracer in <i>Drososphila</i>	128
6	Conclusion.....	130
7	References	131
IV.	Acknowledgement.....	151
V.	Ehrenwörtliche Versicherung.....	152
VI.	Curriculum vitae	153

Abbreviations

II. Abbreviations

ASLV-A	Avian Sarcoma Leucosis Virus -A
BH	Rabies virus strain
BI	Bristle
bNOS	Brain Nitric Oxide Synthase
bp	Base pair
C	Cytoplasmic
cDNA	Complementary DNA
CFP	Cyan Fluorescent Protein
CH	Centrifugal Horizontal
CNS	Central Nervous System
CVS	Rabies Virus strain
CyO	Curly of Oyster
CyO _{GB}	CyO with a green balancer
Cyto	Cytosolic
da	Dendritic arborization
Dcr	Dicer
DEPC	Diethylpyrocarbonate
dG	Deletion of G-protein
Dlg	Discs large
DNA	Deoxyribonucleic Acid
DPBS	Dulbecco's PBS
DSCAM	Down syndrome cell adhesion molecule in vertebrates
Dscam1	Down syndrome cell adhesion molecule 1
Dscam1 ^{Δ21/Δ23}	Dscam1 loss-of-function alleles
Dscam1 ^{+11.31.25.1}	Misexpression with single Dscam1 isoform 11.31.25.1
Dscam1 ^{+7.6.19.2}	Misexpression with single Dscam1 isoform 7.6.19.2
Dscam1 ^{FLP}	Dscam1 MARCM experiment using UAS-flippase
Dscam1-IC	Antibody targeting against Dscam1 intracellular domain

Abbreviations

Dscam1 ^{LOF}	Dscam1 loss-of-function allele
Dscam1 ^{single}	Knock-in mutant
Dscam2	Down syndrome cell adhesion molecule 2
dsRed	Red fluorescent protein
dsRNA	Double-stranded RNA
EDTA	Ethylen-Diamino-Tetra-Acetation
EGFP	Enhanced GFP
EM	Electronmicroscope
EMD	Elementary Motion Detector
EnvA	Envelope A
FLP	Flippase
FMRP	Fragile X mental retardation protein
FN	Fibronectin type III
FRET	Fluorescence Resonance Energy Transfer
FRT	Flippase Recognition Target
GABA	Gamma-Aminobutyric Acid
Gal4	Yeast transcription factor, positive regulator of Galactose-induced genes
Gal80	Gal4 inhibitor, binds and inhibits the transcription activation domain of Gal4
Gal80 ^{ts}	Temperature sensitive Gal80
GECI	Genetically Encoded Calcium Indicators
GFP	Green Fluorescent Protein
G-protein	Glycoprotein
HA	Hemagglutinin
HP	High-Pass
HS	Horizontal System
HSE	Horizontal System Equatorial
hs-FLP	Heatshock induced FLP activity
HSN	Horizontal System Northern

Abbreviations

HSS	Horizontal Sensitive Southern
Ig	Immunoglobulin
KDS	Potassium Dodecyl Sulfate
L1-L5	Lamina Monopolarcell 1-5
L2	2nd instar
L3	3rd instar
LB	Lysogeny Broth
LED	Light Emitting Diode
LP	Low-Pass
Lpt	Lobula plate tangential
LPTC	Lobula Plate Tangential Cell
M	Multiplication
MARCM	Mosaic Analysis with a Repressible Cell Marker
MB	Mushroom Body
Mi	Medulla intrinsic
MKRS	Balancer for third chromosome: stubble
Mokkola	Rabies virus strain
mRNA	Messenger RNA
MS	Mechanosensory
nAChR	Nicotinic Acetylcholine Receptor
ND	Null Direction
Nipagin	Methyl hydroxybenzoate
N-terminal	Amino-terminal
ORN	Olfactory Receptor Neuron
PBS	Phosphate Buffered Saline
PBT	PBS, pH 7.2, including 1% Triton X-100
PCR	Polymerase Chain Reaction
PD	Preferred Direction
P-element	A transposon that is present specifically in <i>Drosophila melanogaster</i>

Abbreviations

PFA	Paraformaldehyde
PI	Propidium Iodide
PN	Projection Neuron
PNS	Peripheral Nervous System
Px	Pupa stage x
R1-R8	Photoreceptor 1-8
RicinA	A-chain of Ricin
RISC	RNA-Induced Silencing Complex
RNA	Ribonucleic Acid
RNAi	RNA interference
RT	Room temperature
RT-PCR	Reverse Transcription-PCR
S2 cells	Drosophila Schneider 2 cells
SAD	Rabies virus strain: St. Augustine Decline
SADdG-EGFPs(EnvA)	SAD in which the coding sequence for G-protein synthesis is replaced by that of EGFP and pseudotyped with the encoding sequence for EnvA
Sb	Stubble
SDS	Sodium Dodecyl Sulfate
siRNA	Small interfering RNA
SOC	Super Optimal Broth with Glucose
ssRNA	single-stranded RNA
T	Translobulaplate
TAE	Tris-Acetate-EDTA
TE	Tris-EDTA
TM	Transmembrane
Tm	Transmedulla
TM 6	Third Multiple 6
TN-XXL	Genetically encoded calcium biosensor that consists of YFP and CFP interlinked by the troponin C based calcium binding domain

Abbreviations

Tris	Trisaminomethane
Tub-Gal80	Tubulin driven Gal80 expression
Tub-Gal80 ^{ts}	Temperature sensitive tub-Gal80
TVA	Avian receptor protein
UAS	Upstream Activating Sequence
UV	Ultraviolette
VS	Vertical System
VSV	Vesicular Stomatitis Virus
VSVdG-EGFP	VSV in which the coding sequence for G-protein synthesis is replaced by that of EGFP
WT	Wild-type
YFP	Yellow Fluorescent Protein
α -Btx	Alpha-Bungarotoxin

III. Table of Figures

Fig. 1: The neural superposition eye.	14
Fig. 2: The motion pathways.....	16
Fig. 3: The Reichardt detector model.	18
Fig. 4: The horizontal system in <i>Calliphora</i>	20
Fig. 5: The vertical system in <i>Calliphora</i>	21
Fig. 6: The horizontal system in <i>Drosophila</i>	23
Fig. 7: The vertical system in <i>Drosophila</i>	24
Fig. 8: Isoform diversity and binding specificity of Dscam1.	28
Fig. 9: Dendritic self-avoidance and tiling.	30
Fig. 10: Axonal morphogenesis of MB neurons.....	32
Fig. 11: Axonal morphogenesis of MS neurons.....	34
Fig. 12: <i>Dscam2</i> mediates tiling in the fly visual system.....	35
Fig. 13: The Gal4/ UAS-System	38
Fig. 14: Restrictions of the Gal4/ UAS system.....	40
Fig. 15: The EnvA/ TVA system.....	45
Fig. 16: Neurite outgrowth of LPTCs.	73
Fig. 17: The UAS>Stop>TNXXL plasmid.....	75
Fig. 18: Ex vivo fly brain culture.....	77
Fig. 19: The UAS-TVA-2Alike-dsRed plasmid.	78
Fig. 20: The UAS-G-protein plasmids.....	79
Fig. 21: <i>Dscam1</i> expression in the optical lobe.	81
Fig. 22: <i>Dscam1</i> knockdown with RNAi.....	84
Fig. 23: The effects of <i>Dscam1</i> ^{FLP} on lobula plate cells.....	88
Fig. 24: Computer based reconstructions.....	89
Fig. 25: Schematic description of Exon6 deletion.....	91
Fig. 26: Reduction of Exon6 variability.	92
Fig. 27: Misexpression of <i>Dscam1</i> ^{+7.6.19.2}	95
Fig. 28: Misexpression of <i>Dscam1</i> ^{+11.31.25.1}	98
Fig. 29: Computer based analysis of the <i>Dscam1</i> ^{+11.31.25.1} phenotype.....	99
Fig. 30: Electric coupling between <i>Dscam1</i> ^{+11.31.25.1} HS cells.....	100
Fig. 31: Misexpression of <i>Dscam1</i> ^{+11.31.25.1} in a single HSN cell.....	102

Table of figures

Fig. 32: Time-point analysis of the Dscam1 ^{+11.31.25.1} phenotype.	104
Fig. 33: Misexpression of Dscam1 ^{+11.31.25.1} in T4/ T5 cells.	106
Fig. 34: Statistical analysis of the ablation rate.	109
Fig. 35: Expression patterns after RicninA induced ablation.	110
Fig. 36: Restricted expression patterns of TN-XXL expressing LPTCs.	112
Fig. 37: TVA expression in flies	114
Fig. 38: Viral labeling of LPTCs.	115

1 Abstract

In arthropods like *Drosophila*, Down syndrome cell adhesion molecules (*Dscam1*) exhibit enormous molecular diversity. A single *Dscam1* gene encodes a large superfamily of neuronal cell recognition proteins that control neuronal outgrowth and anatomy. A comparable function is exhibited by the vertebrates DSCAMs of which only few isoforms exist. However, it is largely unknown, if and how this function of *Dscams* affects neuronal function and the control of behavior by the nervous system. In this thesis, I employed an arsenal of genetic techniques to perturb the expression level of *Dscam1* isoforms in directionally selective Lobula Plate Tangential Cells (LPTCs). LPTCs of the Vertical (VS) and the Horizontal System (HS) were chosen as a model system because of their well-documented anatomy, role in information processing and behavior. Though, only little is known about the developmental mechanisms and molecular factors controlling the morphogenesis and wiring of these cells. The central aim of my study thus is to reveal a possible role of *Dscam1* in the growth and development of the complex dendrites of in particular HS cells. Furthermore, my work aims at establishing a novel model system for integrated studies on the development and function of LPTCs by genetic manipulations of *Dscam1* expression.

My results demonstrate that *Dscam1* is expressed broadly in the fly visual system including HS-cells (immunolabeling of the conserved intracellular domain). Loss of *Dscam1* function and reduced isoform diversity consistently elicited misrouting and self-crossings of neurites in LPTC dendrites. In contrast, misexpression of selected single *Dscam1* isoforms caused a severe reduction in the size and branching complexity of LPTC dendrites. The dendritic gain-of-function phenotype (ectopic expression of the *Dscam1* isoform 11.31.25.1) was strongly dependent on the time of onset of misexpression during development. These results demonstrate that *Dscam1* contributes to the development of LPTC dendrites. This system can now be used to (A) address a possible role of *Dscam1* in the function of neurons and circuitries and (B) to address the interplay of anatomy and function of LPTC dendrites.

In further side projects I aimed at the development of additional genetic tools for the investigation of the role of LPTCs in behavior and for studies on the wiring of LPTCs to the presynaptic circuitry. I established a heat-shock protocol for the ablation of

specified LPTCs by RicinA expression and I generated a fly line for the expression of TN-XXL (a genetically encoded calcium biosensor) in small cell clusters or individual cells. Finally, I participated in efforts to establish a virus based retrograde labeling method in *Drosophila*.

2 Introduction

2.1 The motion detection pathway in flies

For almost all animals, the sense of sight is pivotal for survival and reproduction (Land and Fernald, 1992). Motion vision is a major function of all visual systems. Especially for flies, this ability is crucial for survival behaviors like obstacle avoidance and escape from predators.

2.1.1 The compound eye

Eyes are adapted to the environment and life requirements of the animal, which bears them. Just looking at the outer appearance of the fly's eyes, the differences to those of humans are striking; not only their shape and structure but also their relative proportion to the rest of the body is outstanding. Each compound eye of the fly consists of around 750 ommatidia (Hardie, 1985).

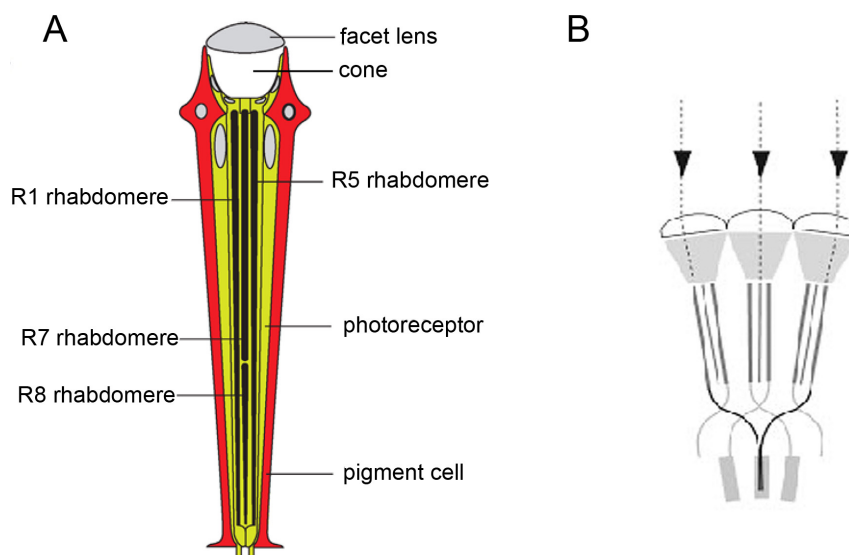


Fig. 1: The neural superposition eye.

(A) Each ommatidium possesses a transparent cornea and cone. Both bundle the light towards the 8 photoreceptor cells located in the center of each ommatidium. Pigment cells are surrounding each ommatidium, separating them from each other. (B) Flies have an open rhabdom in which the rhabdomeres of one ommatidium have different optical axes whereas the optical axes of seven rhabdomeres in seven adjacent ommatidia are parallel. The axons of such retinula cells project onto a common cartridge in the first optical ganglion, the lamina. Thus, each lamina cartridge looks at one

point in the visual space. This kind of neural superposition eye allows vision under lower light levels without sacrificing optical resolution. Modified from Moses, 2006.

Each ommatidium is a dioptic apparatus with a lens system, pigment and receptor cells (Fig. 1A). The light conducting rod structures in arthropods are called rhabdomeres. They accommodate millions of light receptor molecules required for efficient photon collection. Flies like *Drosophila melanogaster* possess an open rhabdom system, in which the seven rhabdomeres of one ommatidium are optically separated from each other (Kirschfeld and Franceschini, 1968). Therefore, these rhabdomeres function as independent light guides. The central rhabdomere contains two photoreceptors, R7 and R8. It is surrounded by six peripheral non-fused rhabdomeres with the photoreceptors R1-R6 (Franceschini, 1975).

2.1.2 Signaling pathways

Photoreceptors are signaling components that capture and transform photons into an electrical signal that is conveyed to higher visual brain regions. All outer photoreceptors in one ommatidium have divergent optical axes. Whereas seven rhabdomeres located in neighboring ommatidia have the same orientation and thus, direct towards the same environmental point (Fig. 1B) (Kirschfeld, 1967). The axons of such retinula cells (except the central R7 and R8, which pass through to the second optic ganglion, the medulla (Boschek, 1971) converge onto the same cartridge of secondary neurons in the first optic ganglion, the lamina. With that, each lamina cartridge 'looks at' one point in space (Braitenberg, 1967). Visual information is thereby processed from the photoreceptors down to all neuropil layers in a strictly retinotopic way (i.e. information from two neighboring spots in the visual field is processed via axons to two neighboring columns throughout all neuropils). The neuronal superposition eye is built by two parts (Kirschfeld, 1973): The first part, R1-R6 is used at low light intensities and for motion detection (Hardie, 1985; Heisenberg and Wolf, 1984). Previous studies revealed that in their absence the optomotor responses of the fly were missing, i.e. the fly was not reacting to visual stimulations anymore (Heisenberg and Buchner, 1977; Yamaguchi et al., 2008). The conclusion was therefore drawn, that R1-R6 are necessary and sufficient for motion vision. The

second part is built by R7 and R8 and is used at high light intensities and for color vision (Cook and Desplan, 2001; Hardie and Raghu, 2001).

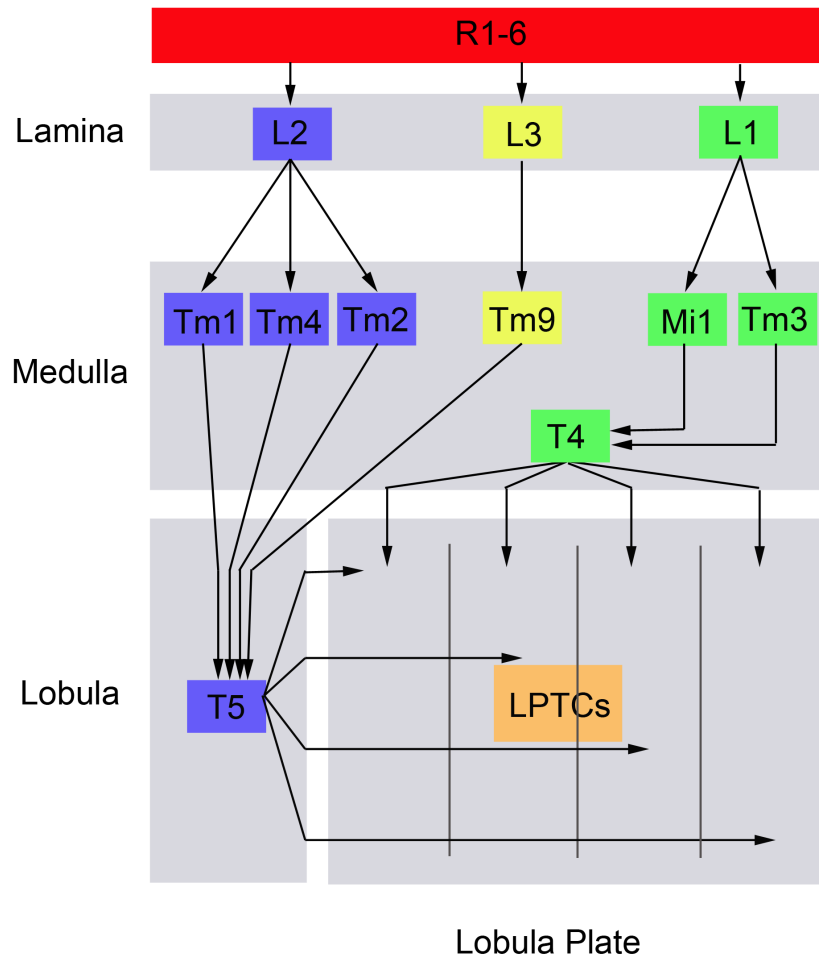


Fig. 2: The motion pathways.

In the fly's visual system three motion pathways have been revealed so far. In first pathway, L1 (Lamina Monopolar cells) provide input to Mi1 (Medulla intrinsic) and TM3 (Transmedulla 3) cells which then give input to motion-sensitive T4 (Tanslobulaplate) cells. In the second pathway, L2 cells feed to Tm1, Tm2 and Tm4 cells which connect to motion-sensitive T5 cells. Additional input to T5 cells is provided from Tm9 cells which are the target from L3 cells. T4 and T5 cells feed into motion-sensitive LPTCs. Modified from Shinomiya et al., 2014.

In the lamina, photoreceptors R1-R6 provide input to five different lamina monopolar cells: L1-L5 via chemical synapses. Three of them, L1, L2 cells and L3 have been proposed to be the major input elements to the motion detection circuitry (Fig. 2) (Bausenwein et al., 1992; Shinomiya et al., 2014). Based on the co-stratification of columnar neurons (Fischbach and Dittrich, 1989; Bausenwein et al., 1992) and

experiments employing the deoxyglucose technique (physiologically active neurons take up and accumulate radioactive material that can be localized in anatomical sections by autoradiography) (Sokoloff et al., 1977; Buchner and Buchner, 1980), some neurons have been predicted long ago. Recent studies revealed not only the presence of a third motion detection pathway but also identified further cells constituting to the motion detection circuitry (Shinomiya et al., 2014; Takemura et al., 2013). The L1 pathway is built up by L1 neurons which connect to Mi1 and Tm3. They provide input to motion-sensitive T4 cells. The L2 pathway goes from L2 neurons via Tm1, Tm2 and Tm4 neurons which synapse onto the dendrites of T5 cells. Additional input to T5 cells comes from Tm9 cells that are targeted from L3 neurons. T4 and T5 cells are the first known neurons in the motion pathways that are direction-selective to small-field motion (Schnell et al., 2012; Maisak et al., 2013; Mauss et al., 2014). They provide input to wide-field motion-sensitive LPTCs (Schnell et al., 2010; Joesch et al., 2008).

2.1.3 The Reichardt detector model

Despite the anatomy-based predictions of the motion detection pathways, columnar neurons in the medulla have so far escaped electrophysiological analysis due to their small sizes. Here, the so-called Reichardt detector model (Fig. 3) (Hassenstein and Reichardt, 1956; Reichardt, 1961) describes how the direction sensitivity of motion could be computed by the brain (Borst and Egelhaaf, 1989; Borst and Haag, 2002). This correlation-type or EMD (Elementary Motion Detector) model relies on at least two neighboring input channels, as motion is a vector in the spatiotemporal domain that needs two points for its representation.

The interaction between both input channels must be non-linear in order to preserve the information about temporal order of the incoming signals, which is mathematically easiest done by multiplication. This step leads to a maximal response to motion in one direction and no or weaker response to motion in the other direction. Output signals from both half-detectors are then subtracted from each other in order to achieve full direction selectivity (Borst and Haag, 2002).

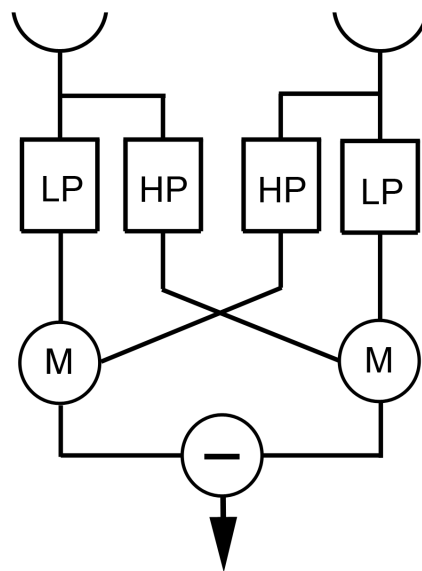


Fig. 3: The Reichardt detector model.

The Reichardt detector model represents a simple principle mechanism of how motion can be extracted from incoming signals of neighboring photoreceptors. This model includes two essential steps: First, the asymmetric temporal filtering through a HP (High-Pass) and a LP (Low-Pass) filter. Second, the nonlinear integration of the signals in which the filtered information is multiplied (M). This composition makes the detector sensitive to the direction of the motion, the stimulus pattern, and its velocity. At each image location, at least two detectors responsive to opposite directions are needed. Modified from Borst et al., 2003.

Many studies of the mechanisms underlying direction selectivity have been performed first on the visual system in big flies, where motion-sensitive LPTCs spatially pool the output signals on their dendrites from many thousands of directionally selective neurons. Two fields of Reichardt detectors are supposed to provide input from columnar neurons, one inhibitory, and the other excitatory. Spatially integrated arrays of motion detectors exhibit a velocity optimum, i.e. moving patterns with a speed beyond that optimum elicit only declined responses. In addition, the responses also depend on the structure of the moving pattern, i.e. high contrast elicits greater responses than lower contrast despite the same moving velocity. Moreover, the optimum velocity depends on the spatial pattern wavelength leading to an invariant temporal frequency optimum (Reichardt, 1986; Borst and Haag, 2002). The axonal signals of these neurons represent the global detector signal in the fly visual system. Using optical recordings of free cytosolic calcium have demonstrated that stimulation by uniformly moving gratings elicit local modulations in the dendritic

tips of integrating motion-sensitive neurons like LPTCs (Single and Borst, 1998). These modulations are synchronous with the temporal frequency of the moving pattern and phase-shifted with respect to each other in different parts of the dendrite, thus providing clear evidence in favor of Reichardt-type motion processing in the fly visual system (Haag et al., 2004).

In *Drosophila*, functional studies have revealed that motion sensitivity of *Drosophila* LPTCs also relies on the Reichardt detector model (Jösch et al., 2008; Schnell et al., 2010; Silies et al., 2013; Takemura et al., 2013, Borst, 2014).

Studies in the past have revealed that signals received from photoreceptors segregate into an ON-channel constituted by the L1 pathway and an OFF-channel that is propagated by the L2 pathway (Joesch et al., 2010). However, in L2 cells the input signals are first half-wave rectified before they enter the next relay station in the medulla. With that L2 cells predominantly transmit brightness decrements to downstream circuits (Reiff et al., 2010) and L1 cells code preferably bright edges. Both of them lack sensitivity to motion. The L3 cells act combinatorially with the L1 and L2 pathways and is specialized to detect moving light and dark edges (Silies et al., 2013). Interneurons within each pathway were found to have corresponding selectivity for light-ON or light-OFF and thereby provide the evidence that motion is computed in parallel light-on and light-off pathways (Strother et al., 2014; Meier et al., 2014). The interneurons Tm2 and Tm9 synapse spatially segregated on the dendrites of T5 cells.

These anatomical findings suggest that Tm1 cells and TM2 cells might build one arm of a T5 EMD circuit and TM9 cells provide the opposing arm (Shinomiya et al., 2014). In the T4 EMD circuit Mi1 cells might build one arm whose counterpart is provided by Tm3 cells (Takemura et al., 2013, Maisak et al., 2013).

2.1.4 LPTCs in *Calliphora*

LPTCs are giant tangential neurons, which can be grouped into horizontal sensitive and vertical sensitive systems (Pierantoni, 1976). The HS system consists of three neurons whose dendritic ramifications extend over the entire innermost layer of the lobula plate. The dendrites are distributed along the dorsal-ventral axis where HSN is

the northern, HSE the equatorial, and HSS the southern horizontal neuron. HSN and HSE cells give rise to many branches over the lateral border of the lobula plate and overlap widely at the para-equatorial level. The HSS cell, on the other hand, occupies space at the lowermost region in the lobula plate and overlaps with HSE at its dorsal territory (Fig. 4).

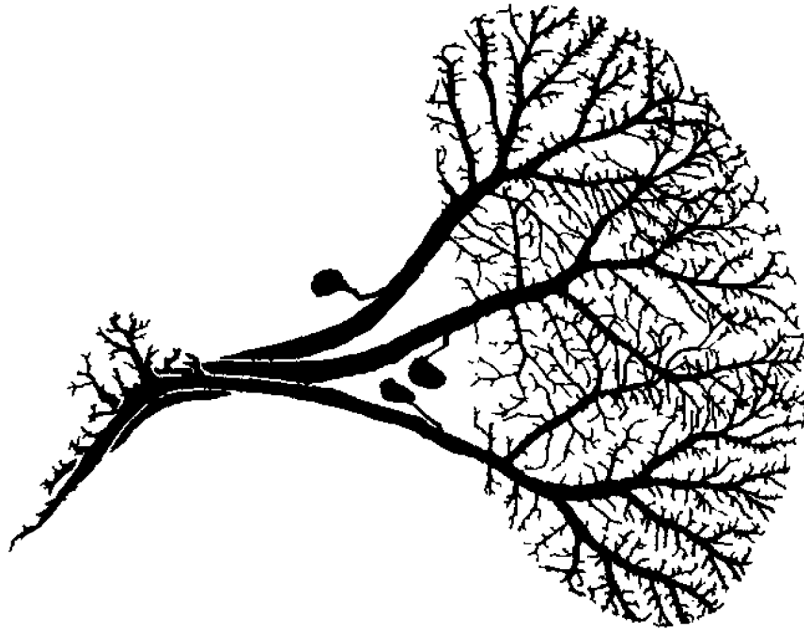


Fig. 4: The horizontal system in *Calliphora*.

Frontal view of the 3 horizontal cells of the right lobula plate. The cobalt diffusion technique allows simultaneous impregnation of all three horizontal cells, thus resolving not only their complete arborization patterns, but also the relative positions of their dendritic fields and the degree of overlap between them. Modified from Hausen et al., 1980.

Electron microscopy has revealed that all fibers in the lobula plate are postsynaptic. The dendritic trees are built in such a way that the number of branches increases with distance from the main stem and reaches its maximum at the lateral border of the lobula plate. Despite the high density of ramifications, the fibers of one HS cell never synapse with each other (Pierantoni, 1976; Hausen et al., 1980). It has been shown that not only the arborization density, but also the number of branches and hence the density of input synapses in each horizontal cell increases from the proximal to the lateral margin of the lobula plate, the later represents the frontal part of the visual field (Hausen et al., 1980). Electrical connections were found between

HS and CH (Centrifugal Horizontal) cells (Haag and Borst, 2005). The two CH cells in each optical lobe, one ventrally and the other one dorsally located, are both, pre- and postsynaptic in the lobula plate. Much is known about the anatomical aspects of HS cell dendrites however, the presynaptic elements have yet to be identified.

Within the lobula plate, the fibers of the 3 HS cells run independently from each other. Around 200 μm from the lobula plate, they converge to a large and very long branch descending towards the ipsilateral posterior slope of the central brain. Their endings terminate close to the external face of the connective and below the esophagus. During their way, the axon fibers connect to three other large units that descend along the esophageal connective. HS cell fibers stay at the ipsilateral hemisphere of the brain and do not enter the contralateral side. At the level of the midbrain, the HS cell fibers are simultaneously pre- and postsynaptic; at their endings, in the periesophageal region, the fibers of HS cells show a presynaptic nature. Cell bodies of HS neurons can be found between the ventral medial edge of the lobula plate and the bundle of the VS cell fibers (Dvorak et al., 1975).

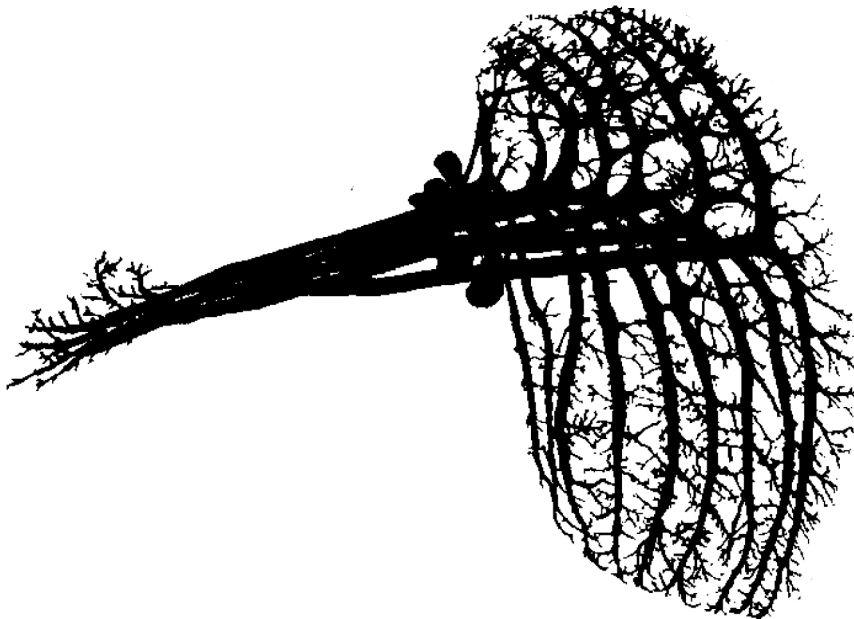


Fig. 5: The vertical system in *Calliphora*.

The dendritic fibers of VS neurons ramify along the proximal-distal axis of the lobula plate. Their axonal terminals innervate the periesophageal region. Modified from Hausen et al., 1980.

The vertical system in *Calliphora* consists of eleven neurons, which have vertically oriented dendrites in the most posterior layer of the lobula plate (Fig. 5) (Hengstenberg et al., 1982). The dendritic fibers in the lobula plate are T-shaped. They enter the lobula plate dorsally and their main dendrite turns ventrally. Therefore, VS cells cover the proximal-distal parts of the retinotopic area. The branching points of all fibers follow the equator of the lobula plate. Like in HS cells, the main branches give rise to a large number of secondary ones and those in turn give origin to tertiary endings. In the lobula plate, VS cells have been found to be postsynaptic. The distribution of secondary branches is highly asymmetric: almost all of them are oriented towards the lateral edge of the lobula plate and largely overlap with the following main fiber. Electrical connections exist between neighboring VS cells (Haag and Borst, 2004; Farrow et al., 2005). Postsynaptic sites comparable to those in the horizontal cell collaterals are also present at the axon terminals (Hausen et al., 1980). The fibers of VS cells gather in a bundle at the equatorial level along the medial edge of lobula plate. Approximately 200 μm after the emergence from the lobula plate, the fibers give rise to long and tiny branches. Their terminals innervate the region slightly above the esophagus and remain ipsilateral to the neuropil from which they originate (Pierantoni, 1976). The somata of VS cells can be found in close proximity to the cell bodies of HS cells. The dendritic fibers of HS and VS neurons run along the curved shape of the lobula plate.

2.1.5 LPTCs in *Drosophila*

The general architecture of the lobula plate resembles that in big flies: There are four neuropils, of which two are covered by the dendrites of HS and VS cells. All main fibers of LPTCs join into horizontal bundles within the lobula plate and run towards the periesophageal region of the central brain (Heisenberg et al., 1978).

There are 3 HS cells contributing to the horizontal motion detection (Fig. 6). Their dendritic fibers, which lie on the frontal surface along the dorsal-ventral axis of the lobula plate, can be distinguished from each other by their arborization domains: north, equatorial and south. In *Drosophila*, the dendrites of all 3 HS cells overlap considerably with each other (Heisenberg et al., 1978). At the lateral border of the lobula plate, their ramifications are tilted in respect to the surface of the plate. There,

the HS cells have a very rich dendritic ramification pattern like in big flies. Golgi stainings have revealed a large number of terminal spines along the secondary and tertiary branches (Hausen, 1976; Heisenberg et al., 1978). The northern and equatorial fibers join the horizontal bundle where they leave the lobula plate; the southern fibers join them laterally to the retractor muscle of the proboscis. Immediately medially to the retractor, the 3 HS cells leave the bundle, bend downward and split each into two branches, one going further down along the posterior slope, the other turning forward into the depth of the brain. Notably, CH cells are missing in *Drosophila* (Schnell et al., 2010) and thus, HS cells are directly connected with each other or indirectly coupled via a yet unidentified cell type.

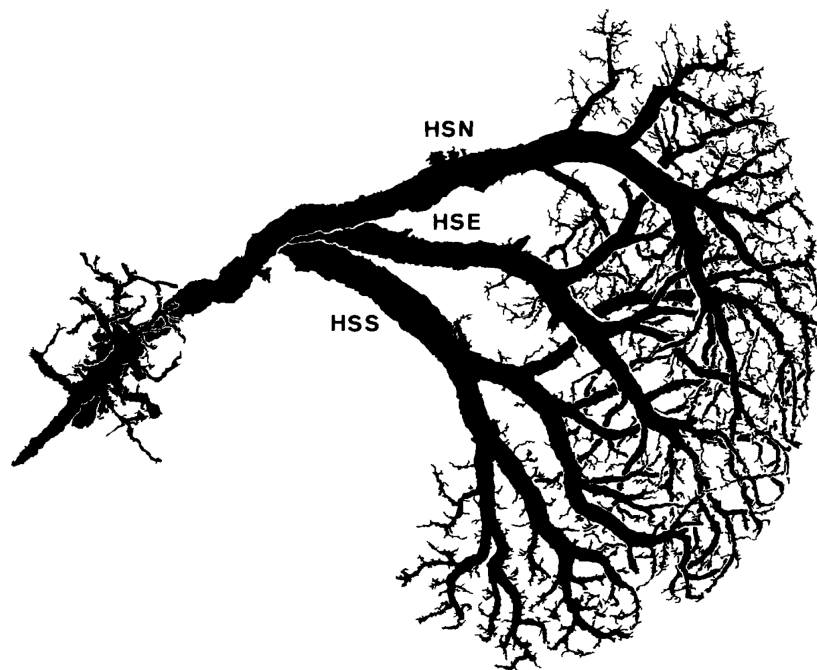


Fig. 6: The horizontal system in *Drosophila*.

The dendritic fibers of HSN cells cover the dorsal part of the lobula plate whereas the dendrites of HSE cells ramify at the equatorial part and those of HSS cells in the ventral region. The axons terminate in the periesophageal region of the central brain. Modified from Fischbach and Dittrich, 1989.

In *Drosophila* the total number of VS cells (Fig. 7) is still illusive. So far, six of them have been identified based on the expression patterns of available Gal4 fly strains.

The general shape of VS cells is comparable to those in big flies (Heisenberg et al., 1978).

The *Drosophila* vertical system closely resembles the system in big flies, with each neuron in *Drosophila* having an approximate counterpart in big flies (Scott et al., 2002). The giant fiber bundle of VS cells enters the lobula plate dorsally. Around 3/4 of the height of the plate is covered by the prominent branches of VS1 and VS2 cells. All branches run parallel to each other. Those of VS1, VS4 and VS5 cells are closer together than the others. The branches of the neurons VS1, VS2, and VS3 are accompanied by satellite fibers. The upward extending branches are much smaller and less well oriented.

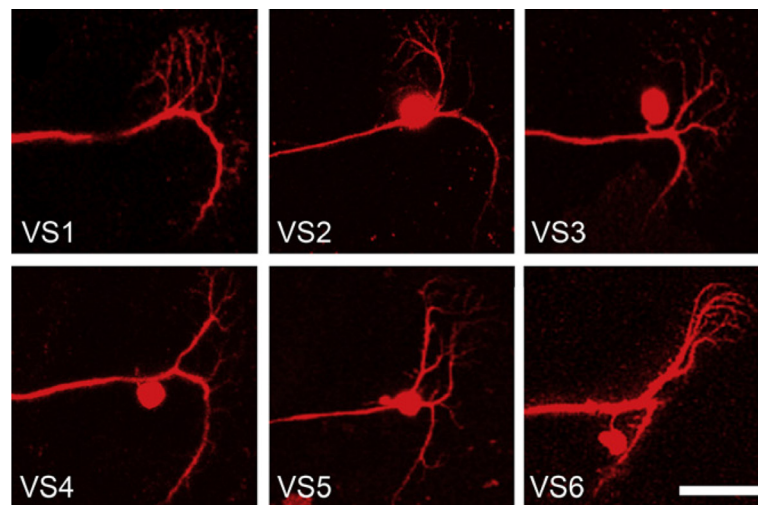


Fig. 7: The vertical system in *Drosophila*.

VS cells were loaded via the patch pipette with Alexa-568. VS cells have vertically oriented dendrites in the most posterior layer of the plate. The VS neurons enter the lobula plate dorsally and their main dendrite turns ventrally. A smaller dendrite branches to the most anterior layer of the lobula plate (Fischbach and Dittrich, 1989). Scale bar 25 μ m. Modified from Joesch et al., 2008.

What distinguishes the VS cells of *Drosophila* from those of big flies is that several of these collaterals run towards the frontal surface of the lobula plate where they have arborizations within the plane of HS cells (Heisenberg et al., 1978), thereby leaving speculations about potential interactions between VS and HS cells. These VS cell branches end in a part of the lobula plate, which presumably corresponds to the upper frontal part of the visual field. A large branch of the VS2 cell enters the middle

plane of the lobula plate and fills the upper frontal part of the projection of the visual field. The VS cells have long horizontal axonal projections to the upper posterior slope. Close to the esophagus, they split into an ascending and a descending branch and end in a region where they meet some of the ocellar giant fibers and a branch of a huge fiber of the cervical connective (Heisenberg et al., 1978).

A detailed analysis of presynaptic release and postsynaptic inhibitory and excitatory sites in LPTCs was carried out by Raghu and coworkers (2007, 2009). HS and VS cells express in their dendritic region within the lobula plate both GABA (Gamma-Aminobutyric Acid) receptors and $\alpha 7$ -type nAChR (nicotinic Acetylcholine Receptor) subunits. Specifically on higher-order dendritic branches, the density of receptors increases. These findings underline the postsynaptic nature of HS and VS cell neurites in the lobula plate and shed light on their presynaptic columnar partners, which provide inhibitory and excitatory inputs to these cells. Moreover, the presence of these receptors supports a model in which directional selectivity of LPTCs is achieved by dendritic integration of excitatory, cholinergic, and inhibitory GABAergic input from local motion detectors with opposite preferred direction (Brotz and Borst, 1996; Raghu et al., 2009; Borst, 2014; Mauss et al., 2014).

The terminals of LPTC neurites in the protocerebrum express synaptobrevin, an integral membrane protein of secretory vesicles. This suggests the presence of presynaptic specializations of the neurites in the central brain. HS cell and VS cell terminals additionally show evidence of postsynaptic GABAergic input (Raghu et al., 2007).

2.2 The function of Dscams in neuronal wiring

In LPTCs dendritic branches which originate from the same neuron (sister branches) do not cross or fasciculate. This self-avoidance mechanism ensures that dendritic arbors will spread evenly across their territory during morphogenesis. By contrast, branches from different LPTCs can co-exist (Fischbach and Dittrich, 1989). The question how LPTC dendrites recognize and avoid self-crossings of sister branches on the one hand but allow overlappings with branches from neighbouring cells on the other hand, still needs to be elucidated. In theory, each LPTC could possess a unique surface identity, but this would demand a high degree of molecular diversity. Several studies in *Drosophila* demonstrated that *Dscams* provide a requisite diversity and play a crucial role in maintaining the self-avoidance mechanism in many neuronal cell types (Corty et al., 2009, Zipursky and Grueber, 2013). In total, there are four *Dscam* paralogs in *Drosophila* (*Dscam1-4*). However, the generated diversity through alternative splicing is unique to *Dscam1*. This gene locus encodes several thousands of cell surface proteins through alternative splicing.

2.2.1 Self-avoidance and *Dscam1*

2.2.1.1 Isoform diversity

Dscam1 isoforms share a common domain structure with 10 Ig (Immunoglobulin) domains and 6 FN (Fibronectin type III) domains, a single TM (Transmembrane) segment, and a C (Cytoplasmic) terminal (Schmucker et al., 2000; Yamakawa et al., 1998; Millard et al., 2007). Three of the Ig domains are built by blocks of alternative exons encoding for variable amino acids. They contribute to the interaction specificity of each isoform. 12 alternative exons encode for the first half of Ig2, 48 alternative exons encode the first half of Ig3, 33 alternative exons encode for Ig7 and finally, 2 exons encode for the transmembrane domain. Together, *Dscam1* gives rise to 38,016 different Isoforms and 19,008 different ectodomains, respectively (Fig. 8A) (Hattori et al., 2008, 2009).

Quantitative analysis based on RT-PCRs (Reverse Transcription-PCR) of photoreceptor cells and mushroom body neurons provided evidences of a stochastic yet biased expression of different *Dscam1* isoforms in neighboring cells (Neves et al.,

2004; Zhan et al., 2004). It has been shown that even neurons of the same type differ in the sets of expressed *Dscam1* isoforms. For example, directly neighboring photoreceptors express between 10-50 distinct mRNAs (messenger RNA) and with that each of them engages a unique *Dscam1* cell surface code (Neves et al., 2004). Furthermore, it has been demonstrated that a probabilistic splicing occurs on single cell level and can even change over time (Miura et al., 2013).

Recent studies have demonstrated that two pathways, involving dual leucine zipper kinase and FMRP (fragile X mental retardation protein), control *Dscam1* expression through protein translation (Kim et al., 2013). Disruption of the members of either pathway resulted in uncontrolled growth of dendritic arbors in larval da neurons. This result revealed the role of both pathways in restricting dendritic outgrowth through the posttranscriptional regulation of *Dscam1* expression. Same function of FMRP has also been found in MS (mechanosensory) neurons (Cvetkovska et al., 2013).

2.2.1.2 Homophilic interactions

Homophilic binding of Dscam1 isoforms is mediated by matching of all three hypervariable domains. This interaction initiates a repulsion mechanism between opposing cell surfaces (Fig. 8B).

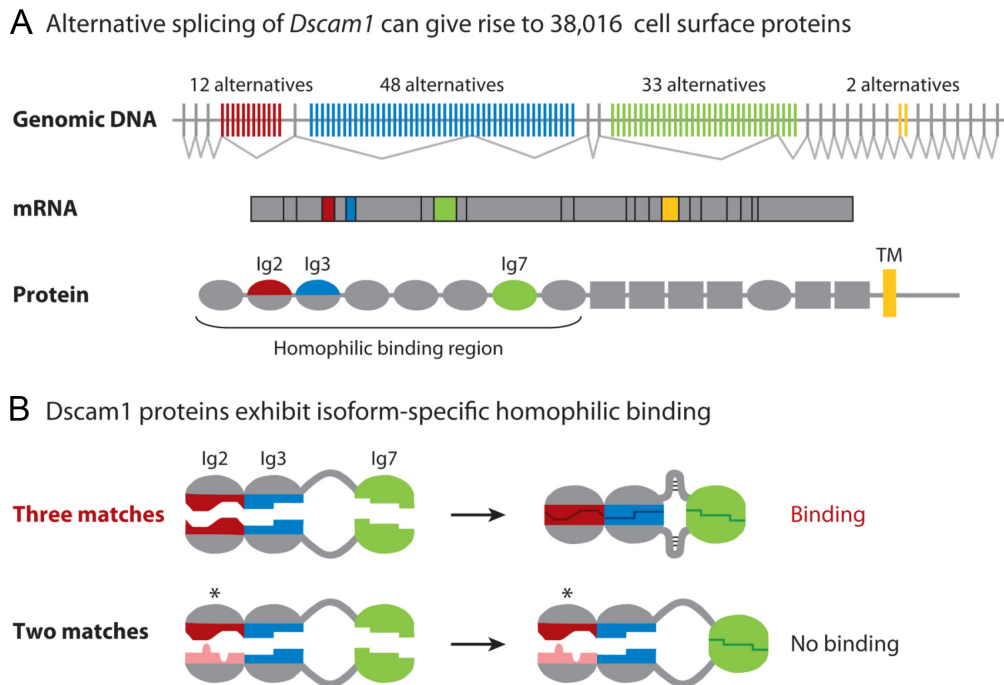


Fig. 8: Isoform diversity and binding specificity of Dscam1.

(A) The *Dscam1* gene locus encodes for 4 blocks of alternative exons that encode 12 different variants for the N-terminal (Amino-terminal) half of Ig2 (*red*), 48 different variants for the N-terminal half of Ig3 (*blue*), 33 different variants for Ig7 (*green*), and two different variants for the TM domain (*yellow*). In total, this variable incorporation of alternative exons leads to 19,008 different ectodomains and hence 38,016 different Dscam1 isoforms. (B) Different Dscam1 isoforms exhibit exquisite isoform-specific recognition, i.e. binding of opposing structures will only occur when all three variable Ig domains match. Modified from Hattori et al., 2008.

Rare exceptions to this exquisite binding rule exist. Heterophilic binding occurs when differing domain-pairs exhibit high amino acid identity (Wojtowicz et al., 2007; Shi and Lee, 2012). Nevertheless, heterophilic binding is always weaker than homophilic binding.

2.2.1.3 Repulsion mechanism

Studies have revealed that the cytoplasmic tail of Dscam1 is required for dendrite repulsion. Expression of chimeric Dscam1-GFP, in which the cytoplasmic domain was substituted with GFP (Green Fluorescent Protein), elicits extensive fasciculation of sister branches in da neurons (Matthews et al., 2007). This argues that, homophilic binding of Dscam1 isoforms on opposing sister dendrites is followed by a repellent response mediated by the cytoplasmic domain (Matthews et al., 2007).

Proteins implicated in the Dscam1 signaling pathway include Dock, an adaptor protein that functions in *Drosophila* axonal guidance and Pak, a serine/threonine kinase (Schmucker et al., 2000). In addition, Dscam1 interacts as counterpart to the netrin-dependent targeting (Matthews and Grueber, 2011). Further interactions of their C-termini with proteins containing PDZ-domains have been described (Yamagata and Sanes, 2010).

2.2.1.4 Structural basis

Detailed analysis of the structural basis behind the Dscam-Dscam interaction was done by Hughes et al. (2007). The results strongly suggest that the N-terminal three Ig domains comprise a region sufficient for homophilic binding *in vivo*. During the binding procedure, each of the three variable domains binds to its identical counterpart in an antiparallel fashion. X-ray crystallography revealed that the ectodomains fold into S shapes so that the variable domains on that side of the molecule are enabled to have interactions to counterparts of opposing molecules (Meijers et al., 2007). These interactions give rise to a double-S homophilic dimer, formed by two homophilic bound monomers. This homophilic dimer buries the homophilic binding area, more than half of which is made up of variable Ig domains. Therefore, small differences between the Ig domains lead to loss of that variable domain surface.

2.2.1.5 Functions in dendritic morphogenesis

Previous studies have numerously demonstrated that sister dendrites which encounter one another during development are recognized by virtue of their shared Dscam1 isoform repertoire (Wang et al., 2002; Zhan et al., 2004; Zhu et al., 2006;

Hattori et al., 2007; Hughes et al., 2007; Matthews et al., 2007; Schmucker, 2007; Soba et al., 2007; Millard and Zipursky, 2008; Zipursky and Grueber, 2013). This mechanism of self-recognition leads to repulsion between sister branches and thus, mediates self versus nonself discrimination (Fig. 9A) (Wojtowicz et al., 2004, 2007; Matthews et al., 2007).

Furthermore, studies of olfactory PNs (Projection Neurons) and da sensory neurons indicate that *Dscam1* plays a key role in dendrite self-avoidance during dendrite morphogenesis in *Drosophila*.

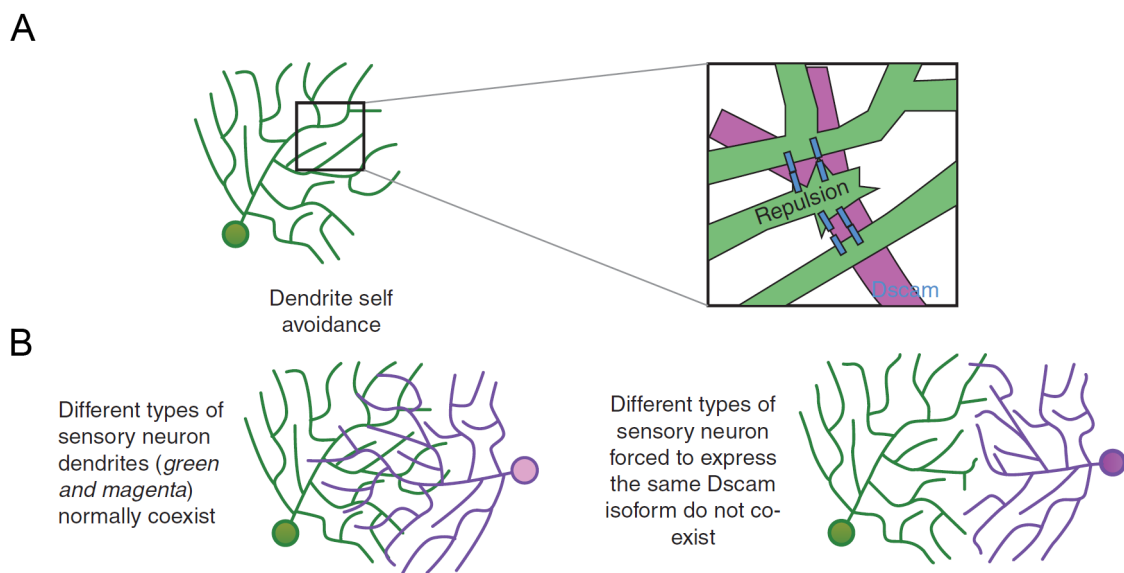


Fig. 9: Dendritic self-avoidance and tiling.

(A) Dendritic self-avoidance is achieved by *Dscam1* mediated repulsion between sister branches. (B) Description see text in figure. Modified from Grueber and Sagasti, 2010.

There are four classes of da neurons, classes I-IV, in the PNS (Peripheral Nervous System) of the fly larva. Genetic studies have established that *Dscam1* is essential for self-avoidance in all four classes of da neurons. In wild-type flies, their dendrites create a two-dimensional meshwork extending across the body wall of the larva. Sister dendrites of da sensory neurons normally do not overlap with each other and thus, self-avoid (Grueber et al., 2002; Sweeney et al., 2002); whereas the dendrites of null mutant show extensive self-crossings. Sister dendrites in da neurons missing *Dscam1* adhere to each other and extend across the body wall in fascicles (Hughes et al., 2007; Matthews et al., 2007; Soba et al., 2007). Rescue experiments by

expressing a single *Dscam1* isoform are able to restore the wild-type morphologies in da neurons independent from the identity of the used isoform. The repulsive mechanism of *Dscam1* is so robust and selective that misexpression of only a single isoform in addition to the normal repertoire of two overlapping da neurons will force them to change their growth cone behavior. These influences in dendritogenesis result in an unusual tiling-like arrangement of da neurons (Fig. 9B) (Hughes et al., 2007; Matthews et al., 2007; Soba et al., 2007; Zipursky and Grueber, 2013).

Genetic studies in adjacent PN neurons further underlined that *Dscam1* is essential for dendritic self-avoidance. In the olfactory system of *Drosophila*, axons of ORNs (Olfactory Receptor Neurons) and dendrites of second-order PNs typically target 1 of ~50 glomeruli. Removal of *Dscam1* selectively from these neurons leads to dendritic agglomerations and major reductions in their dendritic field sizes. Dendritic PN arbors, which are forced to express the same *Dscam1* isoform, show dendritic separation and spreading across larger areas of the antennal lobes (Zhu et al., 2006).

Despite the fact that single *Dscam1* isoforms are sufficient for self-avoidance in dendrites, the molecular diversity of *Dscam1* allows sister branches to selectively recognize and repel each other, while it enables dendritic branches from different neurons to co-stratify (Hattori et al., 2007; Hughes et al., 2007; Matthews et al., 2007; Soba et al., 2007; Zipursky and Grueber, 2013).

A recent study from Hutchinson and coworkers (2014) expanded the view on the function of *Dscam1* in dendritogenesis. They examined the role of *Dscam1* in flight motoneurons. By using targeted expression of RNAi they made a *Dscam1* knockdown specifically in those neurons. The resulting phenotype showed no changes in dendrite spacing but instead, developed supernumerical branches. Additional experiments, in which *Dscam1* was deleted from single motoneurons in an otherwise control background revealed that the lack of *Dscam1* isoforms had no impact on the morphology of mutant cells. These results point to a cell autonomous function of *Dscam1* dendrite growth in motoneurons (Hutchinson et al., 2014).

2.2.1.6 Functions in axonal morphogenesis

Consistent with the role of *Dscam1* in dendritic pattern formation, studies in MB (Mushroom Body) neurons demonstrated that *Dscam1* also plays a crucial role in the segregation of axonal fibers (Wang et al., 2002). During development wild-type MB

cells extend single axons within a nerve bundle called the peduncle. At the base of the peduncle MB axons bifurcate and extend one branch to the medial lobe and the other to the dorsal lobe (Fig. 10A) (Grotewiel et al., 1998). Axons of mutant cells that lack *Dscam1* on their cell surface still bifurcate, but the two sister branches grow in parallel along the same pathway (Wang et al., 2002). This leads to the assumption that *Dscam1* is not required for branch formation itself, but rather for the segregation of the sister branches to different pathways. It is speculated that at the branch point where many different MB axons bifurcate, sister branches selectively recognize each other by homophilic binding of identical or similar *Dscam1* isoforms (self-recognition) and subsequently, repel and extend away from each other along different pathways (self-avoidance). Other studies have pointed out that *Dscam1* mutant axons also affect the projection trajectories of wild-type axons within the same MB. This non-cell autonomous effect provided convincing evidence that the first-born MB neurons play a crucial role in shaping the projection patterns of all later-born MB neurons (Wang et al., 2002).

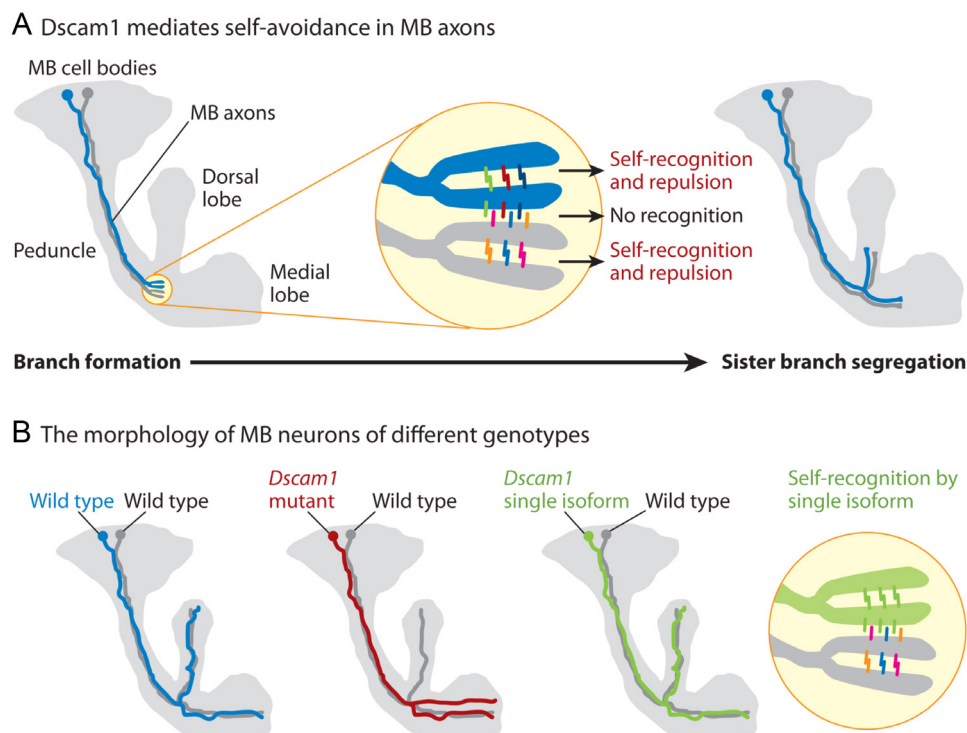


Fig. 10: Axonal morphogenesis of MB neurons.

(A) At the base of the peduncle, MB axons bifurcate and extend one branch to the medial lobe and the other to the dorsal lobe. In wild-type axons sister branches exhibit identical sets of *Dscam1* isoforms

on their surface leading to correct segregation to different pathways. Axons of neighboring MB neurons possess different sets of Dscam1 receptors, and thus are able to co-exist. (B) Axonal branching patterns of MB neurons with different genetic backgrounds. From left to right: Wild-type branching pattern. The axon of a *Dscam1* null mutant cell bifurcates but sister branches often do not segregate. Expression of an arbitrarily chosen single Dscam isoform. Modified from Hattori et al., 2008.

MB axons of *Dscam1*^{single} knock-in mutants, in which all neurons express a single Dscam1 isoform (Hattori et al., 2007), exhibit a loss of segregation phenotype (Fig. 10B). In contrast, when only a single MB neuron expresses *Dscam1*^{single} in an otherwise wild-type background then sister branch segregation remains normal (Fig. 10B) (Hattori et al., 2007). This study convincingly showed that exogenously supplied single Dscam1 isoforms are sufficient to restore sister branch segregation at the single-cell level as long as the isoforms expressed are different from those expressed by neighboring neurons.

2.2.1.7 Reduced *Dscam1* variability

So far studies have clearly established that *Dscam1* is essential for self-recognition and self-avoidance in dendritic as well as in axonal processes of neurons. The question remains how much Dscam1 diversity is required for self-avoidance. One could speculate that different neural tissues need different degrees of diversity. Deletion mutants in whom the Dscam1 ectodomain diversity is reduced from 19,008 to 4,752 maintain self-avoidance in both, the MB (Wang et al., 2004) and the DA systems (Matthews et al., 2007). Thus, it is still unknown how much Dscam1 diversity is required to provide a robust system for self-avoidance in each system.

2.2.1.8 Further functions

Unlike in MB neurons, targeting of MS neurons may involve interactions among a specific set of Dscam1 isoforms present on the axons of MS neurons and also along their trajectories or at their final targets (Chen et al., 2006). In the study from Schmucker and coworkers (Chen et al., 2006) they describe two Dscam1 deletion mutants that are missing 5 of the 12 Ig2 alternative exons, either lack of the exons 4.2-4.6 or 4.4-4.8. Although these deletion lines are still able to express a large number of Dscam1 isoforms (~22,000 per line), individual identified MS neurons in

both mutants show numerous reproducible pathfinding defects (Fig. 11). These defects include an increase in the frequency of branches that usually only occurs at low frequencies in wild-type. Others defects that are not observable in wild-type are presence of ectopic branches, misrouting of branches and absence of certain branches. Intriguingly, both mutants exhibit a differing spectrum of abnormalities. These observations suggest that individual MS neurons may have a unique expression profile of different *Dscam1* isoforms with little animal-to-animal variation. In addition, it has been proposed that *Dscam1* diversity may also play an instructive role in MS neurons. Specific isoforms are supposed to mediate interactions between neurons. The neurites might be guided by adhesive interactions evoked by weak heterophilic interactions with *Dscam1* isoforms which are present along their trajectories. Branching events would then be elicited by homophilic interactions between *Dscam1* isoforms (Bharadwaj and Kolodkin, 2006).

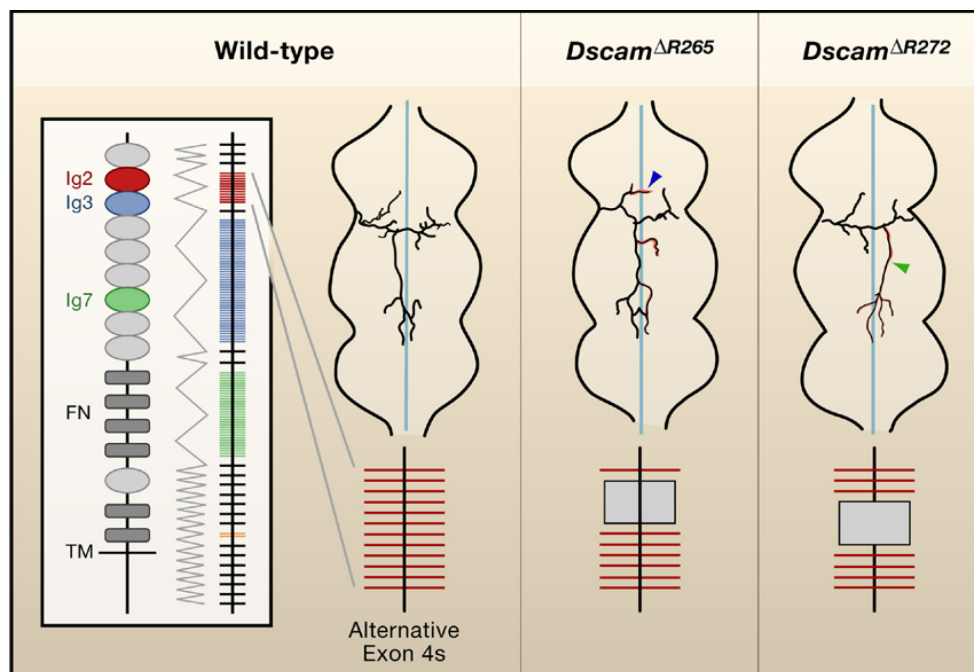


Fig. 11: Axonal morphogenesis of MS neurons.

Schematic drawing of the projections of a MS neuron in wild-type and *Dscam1* deletion mutant flies *Dscam*^{ΔR265} and *Dscam*^{ΔR272} that lack the exons 4.2–4.6 and 4.4–4.8 (grey boxes indicate deletion sites). The blue line denotes the ventral ganglion midline. Blue and green arrowheads point to branches, which are prevalent in either *Dscam1* deletion mutant. In red, ectopic or misrouted branches are highlighted. Modified from Chen et al., 2006.

2.2.2 Tiling and *Dscam2*

Tiling is an efficient way to cover complete but non-redundantly a receptive area by arbors of a functionally related group of neurons (Grueber et al., 2002; Millard and Zipursky, 2008; Wässle et al., 1981). There are two classes of da neurons (class III and class IV neurons), which tile the body wall independently from each other (Grueber et al., 2002). In that case, *Dscam1* appears to be dispensable for tiling in both classes (Hughes et al., 2007; Matthews et al., 2007; Soba et al., 2007) whereas *Dscam2* was found to mediate tiling between processes of L1 neurons in the fly visual system (Fig. 12) (Millard et al., 2007).

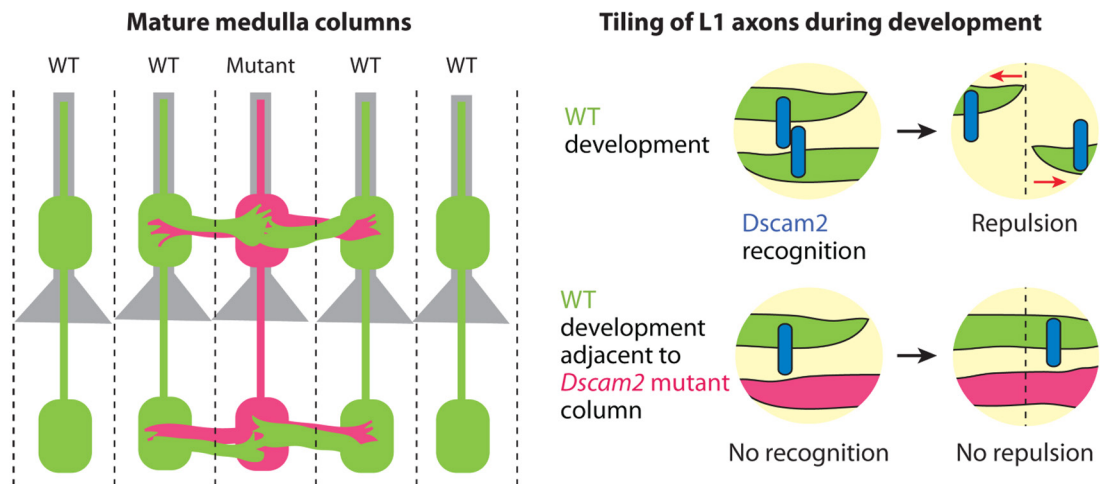


Fig. 12: *Dscam2* mediates tiling in the fly visual system.

In wild-type, the synaptic connections of L1 neurons are restricted to a single column and form at specific layers. Mutant (pink) L1 cell axons that lack *Dscam2* do not interact with wild-type (WT, green) axons during development. Without *Dscam2* homophilic binding, mutant and wild-type L1 cell neurites extend their processes into neighboring columns. Modified from Hattori et al., 2008.

2.2.3 The function of *DSCAM* in mammals

Isoform diversity of *Dscam1* is unique to arthropods however genetic analysis of vertebrate *DSCAM* genes has established an intriguing conservation of molecular functions underlying neural wiring (Schmucker and Chen, 2009). Regulating factors like FMRP were reported to bind to *Dscam* mRNA in mammalian neurons (Brown et

al., 2001; Darnell et al., 2011). However, the functional relevance of the binding needs to be clarified.

In addition, studies have identified a crucial role of *Dscam1* in a subset of amacrine cells (Fuerst et al., 2008). Mice carrying a spontaneous mutation in *DSCAM* showed first, severe disruptions in cell body spacing and second, self-avoidance defects in dopaminergic and bNOS (brain Nitric Oxide Synthase) expressing amacrine cells (Fuerst et al., 2008). In mammals, *DSCAM* does not only function as a mediator of self-avoidance, it has also been proposed to act as an attractive or adhesive cue for synaptic matching (Yamagata and Sanes, 2008), and as a receptor for netrin during axon guidance (Andrews et al., 2008; Ly et al., 2008).

Despite the lack of *DSCAM* isoform variability in mammals, similar strategies to equip neurons with distinct molecular identities and to pattern their arborizations have been found. The group of protocadherins has been demonstrated to play a role in dendritic self-avoidance and self/non-self discrimination (Lefebvre et al., 2012).

Comparatively to the invertebrate *Dscam1* locus, that of protocadherins encodes for several different transmembrane proteins. They are expressed stochastically and combinatorially in single neurons. Some of them exhibit isoform-specific homophilic adhesion. Studies in retinal starburst amacrine cells and cerebellar Purkinje cells demonstrated their function in dendritic-self-avoidance. Further genetic analysis revealed a cell-autonomously acting of protocadherin proteins during development (Lefebvre et al., 2012).

2.3 Genetic tools in *Drosophila*

In *Drosophila melanogaster*, a broad spectrum of elaborated genetic tools and intersectional strategies is available which allows the dissection of neural circuits (Luo et al., 2008). Different approaches based on the Gal4/ UAS (positive regulator of Galactose-induced genes/ Upstream Activating Sequence) system have been developed over the last decades, which allow the restriction of individual Gal4 expression patterns from small cell patches down to single cells. However, in most cases refinements of the tools are still needed. In the following, I will depict several genetic methods, which might help to shed light on the function of LPTCs in behavior and the fly visual system.

2.3.1 The Gal4/ UAS system

Based on the discovery of P-elements, Andrea Brand und Norbert Perrimon were able to introduce a new genetic method called the Gal4/ UAS-system (Brand and Perrimon, 1993) for targeted gene expression that is still one of the most used methods to manipulate the genome in *Drosophila* (Fig. 13).

This two-component system enables a spatial and temporal controlled expression of a certain gene. The Gal4 protein does not have a consensus sequence in *Drosophila* as it is originally derived from the yeast genome. Thus, it will not interfere with any endogenous active sequences in the fly.

The promoter in the P-element is too weak for expressing the Gal4 gene. However, if the insertion happens to be close to an endogenous enhancer region inside the *Drosophila* genome then Gal4 expression will be controlled and regulated through that enhancer (Spradling and Rubin, 1982). Due to that “enhancer trap” method, it has been possible to create a large spectrum of Gal4 lines with variable onsets of gene expression (e.g. Hayashi et al., 2002).

The reporter gene downstream of the UAS sequence is only transcribed when the Gal4 protein binds to the upstreamly located promoter region. The sequence of the UAS-reporter is incorporated into the fly's genome by P-element insertion.

The UAS line thus determines the transgene that is expressed and the Gal4 line where it is expressed. The temporal pattern solely underlies the activity of the promoter- controlled transcription of Gal4.

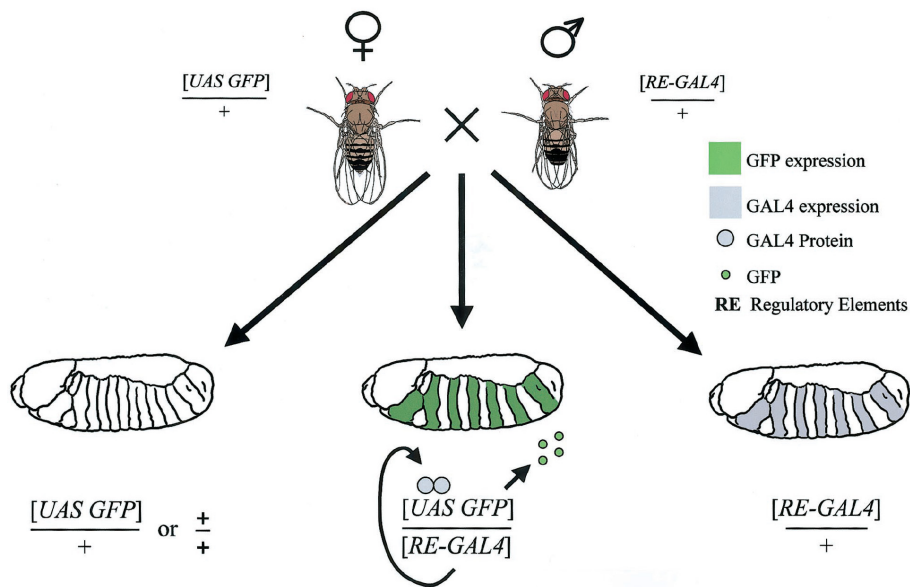


Fig. 13: The Gal4/ UAS-System

In this system, expression of the gene of interest, the responder, is controlled by the presence of the UAS element. This only occurs when the responder line is mated to flies that express Gal4 in a particular pattern, termed the driver. The resulting progeny then expresses the responder in a transcriptional pattern that reflects the Gal4 pattern of the respective driver. Modified from Duffy, 2002.

One disadvantage of the Gal4 system is that most lines do not only show expression in the cells of interest, but also in a variety of other cell types. Therefore, restrictive and intersectional tools are available to narrow down the population of affected cell types.

2.3.1.1 Gal80/ Gal80^{ts}

Gal80 is a repressor protein that blocks Gal4 by binding to its transcriptional activating domain (Lue et al., 1987) (Fig. 14A). Only the cells that are in the Gal4 expression pattern but not expressing Gal80 will have active GAL4, which can then drive the reporter gene. Further temporal control of the Gal4/ UAS system can be achieved by using Gal80^{ts} (temperature sensitive Gal80). At restrictive temperature above 30°C, Gal80^{ts} becomes inactive, thus transgene expression can be activated by subjecting flies to a temperature shift (Zeidler et al., 2004; McGuire et al., 2003).

2.3.1.2 Split-Gal4

A further restrictive method is called the split-Gal4 technique (Luan et al., 2006). Here one fly strain is made to express half of the Gal4 protein, which is inactive by itself. Complementary thereto, another fly strain is made to express the other half of GAL4, also inactive by itself. Therefore, only cells that are covered by the expression pattern of both fly strains possess both halves of the Gal4 protein, which then self-assemble by leucine-zipper (Glick, 2007) into a fully functional protein and thereupon Gal4 is able to activate the reporter gene (Luan et al., 2006).

2.3.1.3 The FRT/ FLP recombination system

A further approach to restrict Gal4 expression patterns is using genetic mosaic techniques. The underlying mechanism is based on FLP (Flippase)-catalyzed intramolecular excision of spacer DNA (Deoxyribonucleic Acid) that is positioned between tandemly oriented FRT (Flippase Recognition Target) sites (Golic and Lindquist, 1989). The spacer includes a transcriptional stop so that prior to the activation of the FLP recombinase (and subsequent FLP-out) the gene downstream of the spacer is not transcribed (Struhl and Basler, 1993). FLP-induced recombination ('FLP-out') leads to both, loss of the marker gene and the termination signals, and expression of the downstream coding sequence. In most applications of this technique, recombination is driven by hs-FLP (heatshock induced FLP activity) with which the timing of the FLP-out and the percentage of cells undergoing recombination depend on the timing and levels of heatshock. Here, the activation of the FLP-out does not require mitosis, and can thus be used to drive gene expression in post mitotic tissues (McGuire et al., 2004).

Temporal refinement can be achieved by introducing a Stop codon flanked by FRT sites in front of the selected transgene (Ro and Rannala, 2004) in combination with flippase activity under control of a heatshock promoter. With that, transcription of the transgene is only enabled when the Stop codon is removed by temperature shift induced flippase activity.

2.3.1.4 MARCM

In the MARCM (Mosaic Analysis with a Repressible Cell Marker) technique, the tub-Gal80 (tubulin driven Gal80 expression) is removed using FRT mediated mitotic

the FRT site on the FRT, Gal80 recombinant chromosome arm. Optionally, there is a mutation distal to the FRT in *trans* but not on the FRT, Gal80 recombinant chromosome arm. Site-specific mitotic recombination at FRT sites (black arrowheads) gives rise to two daughter cells, each of them is homozygous for the chromosome arm distal to the FRT sites. Ubiquitous expression of Gal80 represses Gal4-dependent expression of a UAS-marker (GFP) gene. Loss of Gal80 expression in homozygous mutant cells results in specific expression of GFP. Modified from Wu and Luo, 2006.

2.3.2 Gene knockdown with RNAi

RNAi (RNA interference) is a biological process in which RNA (Ribonucleic Acid) molecules inhibit gene expression (Kennerdell and Carthew, 2000; Hammond et al., 2001; Adams and Sekelsky, 2002). A big advantage in *Drosophila* is the availability of heritable UAS-RNAi fly stocks which provide the ability to interfere with gene function anywhere and anytime during development (Enerly et al., 2002). The RNAi pathway is initiated by the enzyme Dicer, which cleaves long dsRNA (double-stranded RNA) molecules into short siRNAs (small interfering RNA). These double stranded fragments consist of ~20 nucleotides; each of them is unwound into two ssRNAs (single-stranded RNAs): the passenger strand and the guide strand. The passenger strand is degraded, and the guide strand is incorporated into the RISC (RNA-Induced Silencing Complex). The guide strand pairs with a complementary sequence in the mRNA molecule and induces degradation or translation repression (Yang et al., 2000; Zamore et al., 2000; Elbashir et al., 2001). The result is post-transcriptional gene silencing. However, it has been estimated from studying the genomes of *H. sapiens*, *C. elegans*, and *S. pombe* that about 10% of the possible siRNAs will have substantial off-target effects (Qiu et al., 2005). Off-target effects arise when an introduced RNA has a base sequence that can pair and with that diminish the expression of multiple genes at a time. Moreover, RNAi may not totally abolish expression of the gene and hence, this technique is referred as knockdown.

2.3.3 Cell ablation using genetic encoded RicinA

Ricin is organically present in the castor bean (*Ricinus communis*). In nature, the protein is a heterodimeric glycoprotein consisting of an A-chain, which displays a ribosome-inactivating function connected by disulfide bond to a B-chain that is

catalytically inactive but serves to mediate entry of the AB-protein complex into the cytosol. In order to display the cytotoxic function the disulfide bond must be reductively cleaved. In vitro assays demonstrated that the concentration of approximately 5×10^{-10} M is toxic to retinoblastoma cells (Merriam et al., 1984). Since 1992, RicinA has been used as a genetically encoded toxin for targeted cell ablation in *Drosophila* (Moffat et al., 1992). Under control of the UAS/ Gal4 system, it is possible to express RicinA (A-chain of Ricin) in specific tissues and subsets of cells. However, the transcription of RicinA occurred to be leaky, thereby causing unwanted depletion of cells (Kunes and Steller, 1991). Different attempts have been made to control the expression pattern more reliably. One approach was the isolation of temperature-sensitive RicinA mutations. In one study from Basler and Hafen (1989), sevenless-Gal4 is used to drive the expression of RicinA exclusively in R7 photoreceptors. Transgenic RicinA flies are temperature-sensitive and thus RicinA activity can be induced through temperature shift. By doing so, R7 photoreceptors have been completely ablated without affecting neighboring cells.

2.3.4 Genetically encoded calcium indicator TN-XXL

Optical imaging modalities have been proven helpful in the analysis of the neuronal principles underlying visual motion processing in flies. They allow physiological investigation under *in vivo* conditions. Many aspects of dendritic processing in large-field motion-sensitive neurons of *Calliphora* have been investigated by calcium-imaging (Borst and Egelhaaf, 1992; Spalthoff et al., 2010). However, in *Drosophila* electrophysiological techniques can be limited by the small sizes of the cells and their substructures. Here, GECIs (Genetically Encoded Calcium Indicators), such as TN-XXL, are promising alternatives which enable functional studies in cells with lower size limitations (Mank and Griesbeck, 2008). TN-XXL is a ratiometric biosensor that consists of two chromophores YFP (Yellow Fluorescent Protein) and CFP (Cyan Fluorescent Protein) interlinked by the troponin C based calcium binding domain (Mank et al., 2008; Tian et al., 2009). Binding of calcium leads to conformational change that alters the probability of FRET (Fluorescence Resonance Energy Transfer: a mechanism describing energy transfer between the two chromophores); the fluorescence signal of CFP increases whereas that of YFP decreases. Their ratio

can be used as a measure for intracellular calcium concentration (Garaschuk and Griesbeck, 2009). The ratiometric measurement decreases motion artifacts and enables functional studies of columnar neurons in living flies (Reiff et al., 2005).

Unravelling the function of neurons with that method is elegant however, utilizing the Gal4/ UAS system is limited to the expression specificity of the Gal4 promoter. Especially LPTCs with their rich ramifications and overlapping territories are difficult to trace. There are no Gal4 lines, which provide an expression pattern of single LPTCs. The available expression patterns need therefore to be refined.

2.4 Tracing neuronal circuits using viruses

In the past decades, the ability to recover negative-strand RNA viruses entirely from cDNA (complementary DNA) has been established which paved the way for a detailed analysis of molecular genetics and biology of viruses (Conzelmann, 1998). Furthermore, the replication machinery of RNA viruses allows heterologous sequences to be expressed from other species like EGFP (Enhanced GFP) (Tamamaki et al., 2000; Tomioka and Rockland, 2006).

Variations of the viral tropism for particular cell types and their spreading ability can be designed by pseudotyping specific vectors. For example, replacing the envelope G-protein (Glycoprotein) by the encoding sequence for EGFP creates a virus that is not able to infect cells (Fig. 15C) (Mebatsion et al., 1996; Etessami et al., 2000). However, in combination with transgenic animals that deliver the missing transgene, the virus is able to incorporate the protein into its membrane despite the lack of the coding sequence in its own genome. The newly created progeny are trapped within the initial infected cells without the ability to synthesize the G-protein themselves. The result is a high copy number of the viral core and EGFP within single cells allowing anatomical identification in living tissues (Fig. 15A, B) (Wickersham et al., 2007a).

To target the virus specifically to a certain cell type, the EnvA/ TVA (Envelope A/ Avian receptor protein) system is used. EnvA is derived from ASLV-A virus (Avian Sarcoma and Leukosis Virus subgroup A) and it targets exclusively the TVA receptor (Balliet et al., 1999). Studies of brain culture slices derived from the cortex of adult rats plasmids which were co-transfected with plasmids encoding for dsRed (Red fluorescent protein) and TVA have demonstrated that EnvA coated viruses will only target TVA expressing cells resulting in a dual labeling of the infected cells with

dsRed and EGFP (Wickersham et al., 2007b). By providing the G-protein *in trans* the viruses are enabled to spread once. With that, all direct presynaptic neurons are labeled by viral EGFP, allowing an unambiguous identification of initial infected cell population and presynaptic connected ones (Fig. 15D, E).

A major advantage of labeling cells by virus infection is the resulting high intensity of fluorescence in those cells, which can provide detailed information about their anatomical structures even without immunohistochemical amplification (Van Haeften and Wouterlood, 2000).

Viral tracers have been established as powerful tools for the anatomical identification of neuronal circuitries. However, viruses are specialized to specific host species and infection has been shown only in mammalian species. So far, no reports on its function in insect neurons have been published.

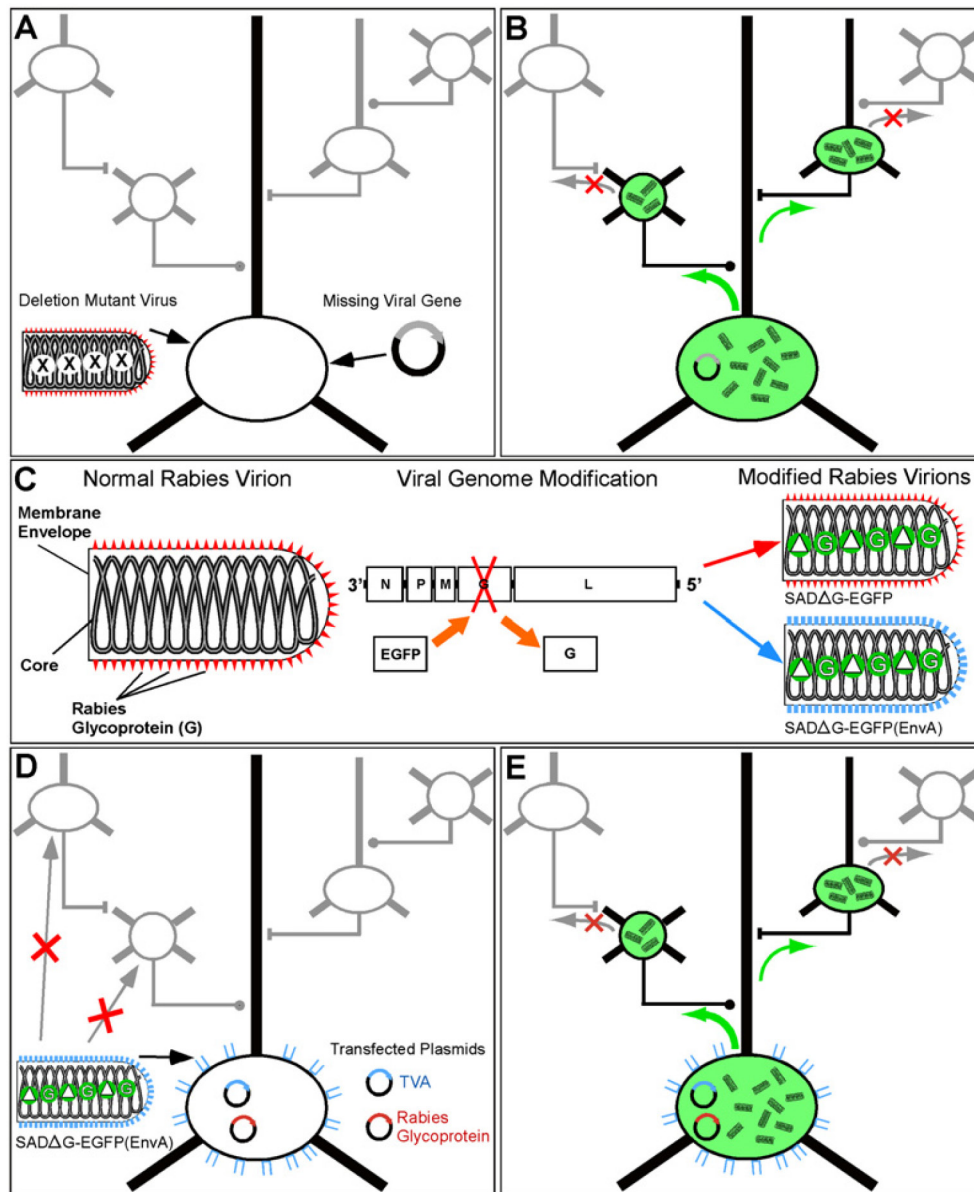


Fig. 15: The EnvA/ TVA system.

(A-B) Here, the Rabies strain: SAD (St. Augustine Decline) is used. A two-component system derived from the ASLV-A virus is used for specific targeting of the virus to the cells of interest. (C) The G-protein deletion mutant virus in which the G-glycoprotein encoding sequence is replaced by EGFP sequence (dG-EGFP) is pseudotyped with EnvA. (D) These SADdG-EGFPs(EnvA) viruses target only host cells, which express the complementary TVA receptor, which is achieved through transfection of the cells with a plasmid encoding for TVA. Co-transfection of the G-glycoprotein encoding plasmid allows the newly created viral progeny to spread normally. However, without the ability to produce the G-glycoprotein by themselves these viruses are trapped within these cells and cannot spread further. Modified from Wickersham et al., 2007b.

2.5 Aims and project outline

Several cellular studies in *Drosophila* have shown that Dscam1 isoforms act as mediators of self- versus nonself-discrimination in numerous fly neurons (Hattori et al., 2008). Whether *Dscam1* constitutes the same role in pattern formation in of LPTC branches has never been investigated before. The major aim of this study is to address the following questions: Is *Dscam1* expressed in LPTCs at all and to which extent may genetic manipulations of the *Dscam1* expression level affect their morphogenesis?

In this thesis I made several approaches to tackle these questions:

Immunolabeling against the intracellular domain of Dscam1 provided a first idea whether any Dscam1 receptors were expressed on the cell surfaces of LPTCs.

Deletion of *Dscam1* from single neurons or entire cell population by using RNAi knockdown, MARCM and FRT/ FLP technique interfered with the endogenous expression in LPTCs. With that, the function of Dscam1 in LPTC morphogenesis should be revealed.

Reduction of the Dscam1 variability in LPTCs gave insight about the necessity of alternative splicing variants of that specific exon for dendritogenesis.

Misexpression of single Dscam1 isoforms in LPTCs provided different gain-of-function phenotypes which were significant for further functional studies.

Generation of single cell clones with the MARCM technique provided additional information whether the misexpression phenotype was cell-autonomous effect or not.

Time-point analysis of the misexpression phenotype by using tub-Gal80^{ts} refined the information when Dscam1 isoforms had an influence on the dendritogenesis of LPTCs.

Besides the Dscam1 project, I also used different genetic tools and protocols to investigate the role of LPTCs in behavior and to study the connectome of the visual system.

Isolation of single LPTCs from a given Gal4 expression pattern was done by using genetically encoded RicinA.

Fly strains were generated which allowed a refined expression pattern of TN-XXL from a given Gal4 expression pattern.

The targeted labeling of LPTCs by viral infection paved the way towards a novel virus based retrograde labeling method in *Drosophila*.

3 Materials and methods

3.1 Materials

3.1.1 Buffers, solutions and media

Name	Recipe
Flyfood	5 l H ₂ O 28 g Agar 110 g Treacle 400 g Maltine 400 g Corn flour 50 g Soy flour 90 g Dry yeast 31.5 ml Nipagin (methyl hydroxybenzoate)
Injection Buffer pH 6.8 10x	0.2 ml 0.5 M NaPi (Sodium Phosphate Symportcarrier) 94.8 ml 1 M KCl (Potassium Chloride) 94.8 ml H ₂ O sterile filtration of 1x solutions
LB (Lysogeny Broth) Medium	5 g/l Yeast extract 10 g/l Trypton 5 g/l NaCl add H ₂ O to 1 l, adjust pH to 7 and autoclave solution
LB Agarplates	1 l LB medium 15 g/l Agar
Lysis Buffer for Western Blot	250 mM Tris-HCl (pH 6.8) 2% SDS (Sodium Dodecyl Sulfate) add H ₂ O to 1 l
PBS 10x (Phosphate Buffered Saline)	1.37 M NaCl (Sodium Chloride) 27 mM KCl 43 mM Na ₂ HPO ₄ (Sodium-Hydroxy-Phosphate) 14.7 mM KH ₂ PO ₄ (Potassium-Hydroxy-Phosphate) add H ₂ O to 1 l
PBT 10x	1 l PBS 10x

	10 ml	100% Triton X-100
Solution A	0.1 M 0.1 M 1% 0.5-1%	Tris-HCl (pH 9) EDTA SDS DEPC (Diethylpyrocarbonate) is added directly before use add H ₂ O to 1 l
Standard brain culture medium	1% 1% 10% 10 µg/ml	Penicillin (10 000 U/ml) Streptomycin (10 mg/ml) Foetal Bovine Serum Insulin mixed into 1l Schneider's <i>Drosophila</i> Medium
TAE Buffer 50x (Tris-Acetate-EDTA)	242 g 57.1 ml 100 ml	Tris (Trisaminomethane) base Glacial acetic acid 0.5 M EDTA (Ethylen-Diamino-Tetra-Acetation) add H ₂ O to 1 l and adjust pH to 8.5
TE Buffer 1x (Tris EDTA)	10 mM 1 mM	Tris-Cl (pH 7.5) EDTA (pH 8) add H ₂ O to 1 l and autoclave solution

3.1.2 Flystocks

Stockname	Chromosome location(s)	Source
Bl/ CyO; UAS-Dscam1 ^{+1.30.30.1} Bl/ CyO; UAS-Dscam1 ^{+7.27.25.1} Bl/ CyO; UAS-Dscam1 ^{+2.9.19.2} Bl/ CyO; UAS-Dscam1 ^{+1.34.30.2} , Dscam1 ^{+1.6..19.2} Bl/ CyO; UAS-Dscam1 ^{+7.6.19.2} Bl/ CyO; UAS-Dscam1 ^{+11.31.25.1} Dscam ^{^23} Dscam ^{^21} / CyO; Exon ^{^6} -FRT FRT40A, Dscam ^{^21} / CyO FRT42D, UAS-Dscam ^{^21} / CyO FRT42D, tub-Gal80/ CyO	2, 3	Dietmar Schmucker
DB331-Gal4	1	Reinhardt Stocker

Dcr2	2	Vienna <i>Drosophila</i> RNAi Center (VDRC)
Dscam RNAi 3115 25622 25623 36233 108835	2 3 3 3 2	Vienna <i>Drosophila</i> RNAi Center (VDRC)
New wild-type		Wild-type Bayreuth; C. Lehner
NP282-Gal4	3	Kei Ito
R27B03-Gal4	3	Gerald Rubin
R42H07 R35F02 R54A03	3	Gerald Rubin
UAS>Stop>RicinA	2	Liqun Luo
UAS-FRT40A	2	Bloomington Stock Center
UAS-GFPcyto	3	Liqun Luo
UAS-hsFLP	1	Liqun Luo
UAS-hsFLP, UAS-mCD8::GFP; UAS-tubGal80, FRT40A/ CyO	2, 3	Bloomington Stock Center
UAS-mCD8::GFP	2	Liqun Luo
UAS-synaptotagmineHA	1	Andreas Prokop
UAS-tub-Gal80ts	3	Ron Davis

3.1.3 Consumables

Consumable	Cat.number	Source
1.5 ml/ 2 ml Eppendorf tubes	0030 125.150	Eppendorf AG
14 ml polypropylene round-bottom tube	352051	Becton Dickinson Biosciences
Agar	A1236	Sigma-Aldrich

Antibiotics		Sigma-Aldrich
Blaugel	9351.1	Carl-Roth GmbH
CIAP/ SAP	EF0651 EF0511	Fermentas GmbH
DPBS	D8537	Sigma Aldrich Co
ExoSAP-IT	78250 40 UL	USB
Falcon Petri dish	351008	Becton Dickinson Biosciences
Femtotips	5242 957.000	Eppendorf AG
Gateway recombination enzymes	BP: 11789013 LR: 11791019	Invitrogen GmbH
Inoculation loop	146051	Greiner Bio-One
iProof High Fidelity Master Mix	172-5310	BioRad
Laminin	610722	BD Biosciences
Microloader	5242 956.003	Eppendorf AG
Micropistill	211-2100	VWR International GmbH
Millicell low height culture plate		M
Mounting medium	50001	Ibidi
Neurobiotin	SP-1120	Vector Labs
PCR tubes	0030 125.215	Eppendorf AG
pDonR221	12536017	Invitrogen
Petri dish	08-757-100A	Falcon
Plasmid extraction kits	Mini Kit: 12123 Midi Kit: 12143 Maxi Kit: 12362	Qiagen GmbH
Primary cell culture dish	353801	Becton Dickinson Biosciences
Primers synthesis		Metabion / MWG
Propidium iodide	P1304MP	Invitrogen (P1304MP)
Proteinase K	EO0491	Thermo scientific
pUAST-Destination		VDRC
Red grape juice	Rio Doro	Aldi Süd

Restriction enzymes		New England Biolabs
Restriction enzymes/ Fast Digest Enzymes		Fermentas GmbH
Schneider's <i>Drosophila</i> Medium	21720-024	GIBCO
Select Agar	30391-023	Life technologies
Silica Gel Orange	T199.1	Carl-Roth GmbH
SOC (Super Optimal Broth with Glucose)	15544-034	Life technologies
T4 DNA ligase	EL0011	Fermentas GmbH
Triton-X 100	X100	Sigma Aldrich Co.
Voltalef 10S	9036-80-0	Labscientific
Voltalef 10S	P24627	VWR
Wizard SV Gel and PCR Clean-Up	A9281	Promega GmbH

3.1.4 Antibodies

Antibody	Cat.	Dilution factor	Source
α -Dlg (mouse)	4F3 anti-discs large	1:200	Hybridoma Bank
α -Dscam1C 357 (rabbit)	gift	1:200 + 4% NGS	Dietmar Schmucker
α -mCD8 (rat)	RM2200	1:200	Invitrogen/Caltag
α -bungarotoxin, Alexa Fluor 647 conjugate	B35450	1:200 + 4% NGS	Molecular Probes
Alexa Fluor 488 goat anti-rat-IgG	A11006	1:200	Molecular Probes
Alexa Fluor 568 goat anti-rabbit-IgG	A11011	1:200	Molecular Probes
Alexa Fluor 594 goat anti-mouse-IgG	A11005	1:200	Molecular Probes
Anti-GFP, rabbit IgG fraction, Alexa Fluor 488	A-21311	1:200	Molecular Probes

conjugate			
NGS (Normal Goat Serum)	G9023	4%	Sigma Aldrich

3.1.5 Electronic equipment

Electronic equipment	Model
Binocular microscopes	Leica MZ6 Leica MZ9
Bright light	Schott FOSTEC LLC
Confocal microscopes	Confocal Leica NT Confocal Leica SP2 Confocal Leica SP2-UV
DNA injector	Eppendorf Femtojet
Fluorescence stereomicroscope	Leica M205 FA
Gel documentation and imaging	BioRad GelDoc2000
Incubator	Binder
PCR cycler	DNA Engine DYAD
Photometer	Eppendorf Biophotometer Plus
Table centrifuge	Eppendorf Centrifuge 5415 D
Thermoshaker	peQ-Lab TS100
UV light	Ebq 100
Vortexer	Scientific industries Vortex Genie-2
Waterbath	Thermo Haake DC10

3.1.6 Primers

Primer	Sequence	Comments
Project: UAS>Stop>TNXXL		
JS1	GTG AGC AAG GGC GAG GAG CT	forward primer pcDNA3-TN-XXL
JS2	CTT AGT CCT CGA TGT TGT GGC	reverse primer pcDNA3-TN-XXL
JS3	GGG GAC CAC TTT GTA CAA GAA AGC	attB2 sequence

	TGG GT	
JS4	GGG GAC CAC TTT GTA CAA GAA AGC TGG GTC TTA GTC CTC GAT GTT GTG GC	reverse primer pcDNA3-TN-XXL with attB2 site
JS5	GTG AGC AAG GGC GAG GAG ATG GTG AGC AAG GGC GAG GAG CT	overlap primer 5'Stop with 3'TN-XXL
JS6	CTC CTC GCC CTT GCT CAC	reverse primer pUAST-Stop-YC3.6
JS7	AGC TCC TCG CCC TTG CTC ACC ATC TCC TCG CCC TTG CTC AC	overlap primer 3'Stop with 5'TN-XXL
JS8	GGT ACC CGG GGA TCT TGA AG	forward primer pUAST-Stop-YC3.6
JS9	GGG GAC AAG TTT GTA CAA AAA AGC AGG CTT CGG TAC CCG GGG ATC TTG AAG	forward primer pUAST-Stop-YC3.6 with attB1 site
JS10	GGG GAC AAG TTT GTA CAA AAA AGC AGG CT	attB1 sequence
JS11	GTG AGC AAG GGC GAG GAG GCC GCC ACC ATG GTG AGC	replacement for JS5
JS12	GCT CAC CAT GGT GGC GGC CTC CTC GCC CTT GCT CAC	replacement for JS7
JS13	CCG TGC GGC CGC CCT CCT CGC CCT TGC TCA C	NotI restriction site JS7
JS14	GGG GAC CAC TTT GTA CAA GAA AGC TGG GTG CCA GTG TGA TGG ATA TCT GCA G	TN-XXL reverse primer new in backbone with attB2 JS4
JS15	CCA AGC TTG GTA CCG AGC TCG G	TN-XXL forward without attB site
JS18	GGG GAC CAC TTT GTA CAA GAA AGC TGG GTG CGG CCG CCT CCT CGC CCT TGC TCA C	attB2-Not-Stop primer

Project: UAS-TVA

JS56	GGG GAC AAG TTT GTA CAA AAA AGC AGG CTT CAT GGC GCG GCT GCT GCC CGC GCT	TVA forward primer attB1
JS57	GGG GAC CAC TTT GTA CAA GAA AGC TGG GTT TAC AGG AAC AGG TGG TGG	TVA reverse primer attB2

	CGG	
JS58	GGG GAC AAG TTT GTA CAA AAA AGC AGG CTT CAT GAA TAT ACC TTG CTT TGC TGT	Mokola-G primer attB1
JS59	GGG GAC CAC TTT GTA CAA GAA AGC TGG GTT CAA GTA CCT GGG AGC CCT TTA	Mokola-G primer attB2
JS60	GGG GAC AAG TTT GTA CAA AAA AGC AGG CTT CAT GAA GTG CCT TTT GTA CTT AGC	VSV-G primer attB1
JS61	GGG GAC CAC TTT GTA CAA GAA AGC TGG GTT TAC TTT CCA AGT CGG TTC ATC	VSV-G primer attB2
JS62	GGG GAC AAG TTT GTA CAA AAA AGC AGG CTT CAT GTT ACT CTC TAC CGC CAT ATT	BH-G primer attB1
JS63	GGG GAC CAC TTT GTA CAA GAA AGC TGG GTT TAT GAC TCA CCA GTG GCC CCC	BH-G primer attB2
JS64	GGG GAC AAG TTT GTA CAA AAA AGC AGG CTT CAT GGT TCC TCA GGC TCT CCT GTT	SAD-G primer attB1
JS65	GGG GAC CAC TTT GTA CAA GAA AGC TGG GTT TAC AGT CTG GTC TCA CCC CCA	SAD-G primer attB2
JS66	GGG GAC AAG TTT GTA CAA AAA AGC AGG CTT CAT GGT TCC TCA GGT TCT TTT GTT TGT A	CVS-G primer attB1
JS67	GGG GAC CAC TTT GTA CAA GAA AGC TGG GTT TAC AGT CTG ATC TCA CCT CCA CTC TT	CVS-G primer attB2
Degenerative PCR		
JS68	GCA GAA GCT TTG CGT ACT CGC	T1BUAS
JS69	ATT CAA ACC CCA CGG ACA TG	T2D

JS30	WGT GNA GWA NCA NAG A	AD3
JS31	AAT CAT ATC GCT GTC TCA CTC A	T2En

3.2 Methods

3.2.1 Molecular biology

3.2.1.1 Plasmid DNA Extraction

For plasmid isolation and purification of DNA for subsequent cloning procedures, the “Plasmid Mini Kit” from QIAGEN was used. From each transformation plate, a single colony was picked with a sterile inoculation loop (Greiner Bio One) and transferred to a 14 ml polypropylene round-bottom tube (Becton) containing 4 ml LB medium with the appropriate selective antibiotic. This primary cell medium was incubated for approximately 8 h at 37°C with vigorous shaking (approx. 300 rpm). Bacterial cells were harvested by centrifugation at 6,000x g for 15 min with an Eppendorf table centrifuge. Therefore, the medium was transferred to 2 ml Eppendorf tubes and twice spun down. The bacterial pellet was resuspended in 0.25 ml of Buffer P1 (provided with the kit) by vortexing them vigorously for several minutes. Afterwards 0.25 ml of Buffer P2 (provided with the kit) was added and mixed thoroughly by inverting the tube 4-6 times. The lysate should appear viscous addition of Buffer P2. Mixing should result in a homogeneously colored suspension. In the next step, 0.35 ml of N3 buffer (provided with the kit) was added and mixed immediately and thoroughly by vigorously inverting 4-6 times. After addition of Buffer N3, a fluffy white material appeared and the lysate became less viscous (“The precipitated material contains genomic DNA, proteins, cell debris, and KDS (Potassium Dodecyl Sulfate)”). The suspension should be mixed until all traces of blue had gone and the suspension was colorless. The final mixture was centrifuged at maximum speed in a table centrifuge for 10 min. The supernatant containing plasmid DNA was transferred to a column with filter and spun down for 1 min. The solution in the column was discarded and the DNA within the filter washed by applying 0.5 ml PE buffer (provided with the kit). The buffer was again centrifuged for 1 min and afterwards discarded. After washing step, the emptied column with filter was centrifuged for another 1 min in order to remove remaining ethanol. For eluting, the DNA 50 µl prewarmed (65°C) EB buffer (provided with the kit) or DNase free H₂O was dropped onto the center of the filter and incubated for 5 min. At the end, the filter was put into a 1.5 ml Eppendorf tube and centrifuged for 1 min at maximum rpm. The final concentration of the DNA should be around 500 ng/µl.

3.2.1.2 Polymerase Chain Reaction

PCR (Poymerase Chain Reaction) allows the amplification of a distinct strand of DNA. Depending on the chosen polymerase, the speed and amplification accuracy varies. In this thesis, I used for all PCRs the “iProof High Fidelity Master Mix” (BioRad). This high-fidelity DNA polymerase offered an extreme enhanced performance rate for all PCR applications by comprising a unique *Pyrococcus*-like proofreading enzyme fused to a DNA binding-protein (Sso7d). This results in a thermostable polymerase that accurately amplifies long products from a variety of DNA templates. The “iProof High Fidelity Master Mix” has already polymerase, nucleotides, included in an optimized reaction buffer. Therefore, no further PCR components were needed. For each 50 µl reaction volume, 1 µl of DNA template was given to 25 µl of 2x Master Mix and filled up with DNase and RNase free water.

Step	Degree (°C)	Time
Denaturation	98	1 min 30 sec
Annealing	98	30 sec
Elongation	Primer Tm	Length of product
End	70	1 min
Cycle	From Annealing till End	40x
Termination	70	10 min
Storage	4	Forever

3.2.1.3 Restriction of DNA vector backbone and insert

Restriction sites are short (~6 bp) DNA palindromic sequences which can be recognized by specific restriction endonucleases. These enzymes break the double stranded DNA sequence in the way that usually a single stranded end (sticky end) is the result; in some cases blunt ends, in which both DNA strands are evenly cut, do also occur. Restriction of the DNA is performed for preparing the vector backbone or PCR product for subsequent cloning procedures or for analyzing the correct introduction of an insert after ligation into a given vector. Control digestion was made with a sample of 1-2 µl of DNA (100-200 ng). For nearly all DNA restriction-procedures, “Fast Digest enzymes” from Fermentas were used.

Components:

2-5 µg DNA

10 U restriction enzyme

8 µl 10x buffer provided with the enzyme

Add H₂O to a total volume of 80 µl

Incubate 1 hour at 37°C

3.2.1.4 Preparation of DNA for ligation

After treatment with restriction enzymes, vector backbones were treated with CIP/CIAP or SAP (Fermentas) for 3 hours in order to dephosphorylate the endings. Neither digestion enzymes nor dephosphorylation enzyme were heat inactivated. Purification of the digestion product was done through gel electrophoresis. Appropriate DNA strand was identified under UV (ultraviolette) light and excised out of the gel.

3.2.1.5 Vector backbone purification

In order to discriminate cut from uncut vector, digested DNA was analyzed via gel electrophoresis. Cut vectors were identified under UV light and excised out of the gel. With “Wizard SV Gel and PCR Clean-Up System” (Promega) the DNA was extracted out of the gel and restriction enzymes were removed. Therefore, the gel slice was put into a 2 ml Eppendorf tube and 10 µl Membrane Binding Solution per 10 mg of gel slice was added into the tube. For PCR purification, the same volume of Membrane Wash Solution was added to the PCR product, respectively. The gel slice was incubated at 50-65°C until it was completely dissolved. For each DNA sample, one SV Minicolumn was inserted into a Collection Tube. Either the dissolved gel mixture or a prepared PCR product was then transferred to the Minicolumn assembly and incubated at RT (room temperature) for 1 min. Then the Minicolumn was centrifuged at 16,000x g for 1 min. The flow through was discarded and Minicolumn reinserted into the Collection Tube. 700 µl Membrane Wash Solution (ethanol added) was added onto the column and centrifuged at 16,000x g for 1 min. Again flow through

was discarded and Minicolumn reinserted into Collection Tube. The washing step was repeated with 500 µl Membrane Wash Solution and centrifugation at 16,000x g for 5 min. The Collection Tube was emptied and the column-assembly re-centrifuged for 1 min with the table centrifuge lid off to allow evaporation of any residual ethanol. The Minicolumn was transferred to a clean 1.5 ml Eppendorf tube and 50 µl of Nuclease-Free Water was added to the Minicolumn. At RT, the water was inoculated for 5 min. For elution of the DNA the assembly was centrifuged for 1 min at 16,000x g. Minicolumn was discarded and the DNA was stored at either 4°C for post-processing within one week or at -20°C.

3.2.1.6 Insert purification

Insertion products were digested with same enzymes as the vector was treated and remaining nucleotides and primers removed through inoculation with ExoSAP-IT (USB). The advantage of ExoSAP-IT is the possibility to remove unused primers and nucleotides with absolutely no sample loss and therefore, it is ideal for small sample volumes. This reaction is an alternative to the common gel purification procedure. It was used for all PCR products, which were used later on for gateway cloning. ExoSAP-IT was directly given to the PCR products and incubated in commonly used PCR buffers.

Components:

20 µl PCR product

2 µl ExoSAP-IT

Incubate 15 min at 37°C

Incubate 15 min at 80°C for inactivation

3.2.1.7 Ligation

A perquisite way to introduce DNA fragments into a vector backbone is to put restriction sites at each end of the desired insert. The treatment of vector and insert with the same set of restriction enzymes enables a directed introduction of the insert into the vector backbone. The molar ratio of vector to insert should be 1:3 or 1:5. The

concentrations were determined apriori via a DNA photometer and ligation was performed after following protocol:

Components:

3 µg PCR product

1 µg of plasmid DNA

0.5 µl of T4 DNA ligase (Fermentas)

1 µl of 10x buffer

H₂O was added to a total reaction volume of 20 µl

Incubation at 16°C overnight

3.2.1.8 Gateway cloning system

The gateway cloning system offers a great alternative to commonly used ligation systems for cloning DNA fragments into appropriate expression vectors. This cloning system is based on “Bacteriophage lambda att site recombination”. In bacteria, there is a stretch of DNA called attB (B stands for bacteria) and in the phage there is a stretch of DNA called attP (P stands for phage). When the phage infects a bacterium, the injected lambda DNA recombines with the corresponding bacterial DNA via the att sites in the presence of integration-specific enzymes. When an attB site recombines with an attP site, the outcome is integration of the phage DNA into the bacterial genome. Once integrated, the hybrid recombination sites are called attL and attR (L stands for left, R stands for right). These recombination reactions (“LR” and “BP”) are the basis of the Gateway Cloning System. The attB × attP reaction is mediated by Gateway BP ClonaseII enzyme mix; the attL × attR reaction is mediated by Gateway LR ClonaseII enzyme mix. ccdB is the F plasmid-encoded gene that inhibits growth of *E. coli*.

BP-reaction

Components:

1-7 µl of attB-PCR product (15-150 ng)

1 µl pDonor 221 vector (150 ng/µl)

TE buffer, pH 8.0 was added to a total volume of 8 μ l
2 μ l of BP Clonase II enzyme was added and mixed by brief vortexing

Incubation at RT overnight

1 μ l of the Proteinase K solution was added to each sample

10 min incubation at 37°C to terminate the reaction

2 μ l of the final mixture was taken for transformation and 50 μ l of transfected cells were spread onto LB agarose plates containing Kanamycin.

LR reaction

For the LR reaction the same procedure was performed. Instead of attB-PCR product, 1-7 μ l of the Entry clone was taken and 2 μ l LR Clonase-II enzyme mix for each reaction. In this step, incubation period was always overnight. Here again, 2 μ l of the final mixture was taken for transformation of chemical competent cells and finally, 50 μ l of the transfected cells were spread onto LB agarose plates containing Ampicillin.

3.2.1.9 Transformation of chemical competent cells

First one aliquot (50 μ l, stored at -80°C) of chemical competent cells (e.g. DH5 α from Invitrogen) was thawed on ice for 15 min. Afterwards, either 150 ng Plasmid or 3 μ l of ligation product per 50 μ l cells were inoculated within the cells on ice for another 30 min. The mixture was then given heatshock at 42°C for 30 sec and chilled on ice for 1.5 min. The cells were incubated in 250 μ l of prewarmed SOC medium or LB medium for 1 hour, at 37°C in a thermoshaker, with 300 rpm. 20 μ l of that suspension were plated onto an agar plate containing the appropriate selective antibiotic. These plates were incubated overnight in 37°C incubator.

3.2.1.10 Rapid small-scale isolation of DNA

With the following protocol it was possible to isolate small-scale DNA samples in a high quality, i.e. very pure and highly concentrated (>1 μ g/ μ l), from adult flies. It can also be used equally well to extract DNA from other developmental stages. DNA

prepared according to that method and used in this thesis majorly for isolation of promoter regions and location of P-element insertions within transgenic flies.

Therefore, flies were first anesthetized with CO₂. 1-20 flies were put in an Eppendorf tube and kept on ice until next step. Solution A was then added into the tube and flies were homogenized with a sterile micropipette (VWR). 100 µl of solution A was applied to extract DNA from 1-5 flies, 200 µl for 6-10 flies and 500 µl for up to 50 flies. The mixture was then incubated for 20-30 min at 70°C. Afterwards, 14 µl of 8 M potassium acetate was added for each 100 µl homogenate and left on ice for 30 min. For DNA extraction 100 µl Phenol-Chloroform (1:3) mixture was added, briefly vortexed and spun 10 min at RT. The supernatant containing DNA was moved to a new tube. Precipitation of DNA was done by adding 0.5 volumes of isopropanol at 16,000x g and spun for 5 min at RT. The pellet was washed carefully with 70% ethanol, respun, dried and redissolved in 10 (1 fly) to 100 (50 flies) µl DNase free H₂O.

3.2.1.11 Degenerative PCR

The degenerative PCR enabled to determine the exact insertion site of the P-element in the genome of transgenic *Drosophilas*. This method was derived from the so-called “nested PCR”. Here, three different primers with specific binding properties were needed for distinguishing the chromosomal location. In the first PCR, one primer had to bind inside of the UAS or Gal4 vector (T1BUAS or T1BGal4). The second one was degenerated (AD3) this means bound at several positions within the genome. The second PCR based on the PCR product of the first one. Here, the first primer was exchanged by another one (T2D) that bound more specifically in the primed out regions. Both primers, T1BUAS and T2D, sat within the 3’P-element site but not within the terminal repeat in the 5’ site whereas, the T1BUAS primer sat with its final 8 nucleotides in the 3’ P-element site thus the rest of the primer was vector specific since T2D sat within the 3’P-element. Therefore, T2D could be used with any P-element. The 2nd PCR was usually checked on gel and subjected to EXOSAP-IT. Primer stock concentration was 10 pmol/ µl. The 3rd PCR with the T2Den Primer was only used if the concentrations after the 2nd PCR were too low.

In the 1st PCR, T1BUAS and AD3 primer were used. The PCR reagent contained:

Components:

0.4 μ l T1BUAS/ T1BGal4

8 μ l AD3

1 μ l DNA template (150 ng)

10 μ l iProof Master Mix

Add H₂O to a total volume of 20 μ l

In the 2nd PCR T2D and the same AD3 primer from the 1st PCR were used.

The PCR reagent contained:

Components:

0.4 μ l T2D

8 μ l AD3

1 μ l DNA from 1st PCR diluted 1:50

10 μ l iProof Master Mix

Add H₂O to a total volume of 20 μ l

Temperature	Time
93°C	1 min
95°C	1 min
94°C	1 min
62°C	1 min
72°C	2 min 30 sec
Cycle to step3 for 4 more times	
94°C	1 min
25°C	3 min
Ramp to 72°C at 0.2°C per sec.	
72°C	2 min 30 sec
94°C	30 sec
68°C	1 min
72°C	2 min 30 sec

94°C	30 sec
68°C	1 min
72°C	2 min 30 sec
94°C	30 sec
44°C	1 min
72°C	2 min 30 sec
Cycle to step10 for 14 more times	
72°C	5 min
4°C	forever
95°C	1 min 30 sec
94°C	30 sec
64°C	1 min
72°C	2 min 30 sec
94°C	30 sec
64°C	1 min
72°C	2 min 30 sec
94°C	30 sec
44°C	1 min
72°C	2 min 30 sec
Cycle to step 2 for 11 more times	
72°C	5 min
4°C	forever
To receive higher concentrations:	
94°C	30 sec
44°C	1 min
73°C	2 min 30 sec
Cycle to step 1 for 30 more times	
72°C	5 min
4°C	forever

3.2.2 Transgenic flies

3.2.2.1 Production of flyfood

Flies were raised on standard corn meal medium supplemented with dry yeast. Soy, corn, and dry yeast were mixed in 1 liter of cold water. Agar was oaked before adding another liter of cold water. 3 liters were heated to 98°C and the agar was added. After 1 hour of heating, malcine and treacle were mixed with boiling water. The solution was then filled up to 5 liters and cooled down to 65°C. Propionic acid was added. The food was filled into plastic vials.

3.2.2.2 Breeding of flies

Breeding fly stocks were kept at 18°C and transferred to fresh vials every 14 days. Experimental flies and crossings were kept at 25°C and were flipped every week. All flies were kept at 70% relative humidity at a 12 hours light/ dark cycle. One development cycle (from egg to adult) takes approximately 7 days at 29°C, 9 days at 25°C, 11 days at 22°C, or 19 days at 18°C (Bloomington stock center). In our incubators this was somewhat slowed down to 11 days at 25°C.

3.2.2.3 Production of egg-laying medium

Grapeagar dishes were prepared for flies to lay eggs on 200 ml red grape juice (Aldi Süd) were warmed up in the microwave for 2 min and mixed with 3 g Select Agar (Life technologies). After reheating, the solution was poured into petri dishes. Fresh plates were prepared on day of injection. After removing all eggs from a plate, it was reused.

3.2.2.4 Generation of transgenic flies

For preparing the DNA injection 6 µg of DNA and 2 µg of transposase $\Delta 2-3$ were diluted in 100 µl DNase and RNase free water and gently mixed by turning the tube 2-3 times. For precipitation $1/10$ volume 3 M Na-Acetate pH 5, 2 µl pellet paint for marking the DNA and 2.5x volume 100% ethanol were added and incubated on ice for 15 min. Afterwards the mixture was spun down at 15,000 rpm, 15 min, 4°C. The

supernatant was removed and afterwards the DNA was washed one time with 70% ethanol and once more with 100% ethanol. The DNA pellet was dried on air for >15 min. The DNA pellet was finally diluted in 20 μ l 1x injection mix. Afterwards the DNA was checked by gel electrophoresis. For P-element mediated germline transfection of *Drosophila*-embryos, 2 days old flies were allowed to lay eggs on grape agar plates for 20-30 min and then flies were transferred to a fresh plate. Eggs were collected, washed in PBT, washed in 50% Klorix for 4.5 min to remove the chorion, rinsed in water and aligned smoothly with a paintbrush side by side on an agar block. Aligned eggs were transferred onto a cover slip coated with glue, such that the posterior end faced the edge of the slip. The slip was then transferred to a drying chamber with Blaugel (Roth) for 14 min. Eggs were fixed to a microscope table, where injections were done using an electrode holder, connected to Femtojet injector. Femtotips were back filled with 3 μ l of injection mix. The electrode tip was gently pushed against the side of the cover slip to widen the tip. Each egg was injected with a small volume of injection mix to its posterior end, where the polar cells formed which set up the germline. Importantly, injections needed to be performed in the syncytial stage of embryos. Cell membranes developed after the 13th nuclear division, at RT approximately 1 h after egg delivery. Polar cells were the first cells to form in the developing embryo. Eggs were then coated with oil (Voltalef 10S) and transferred to a humidified agar plate for embryos to hatch on. The first day the injected eggs were put in an 18°C incubator and later on they were transferred to a 25°C incubator. Embryos were collected during the next 2 days and transferred to fresh yeast vials. Freshly hatched adults were collected and individually crossed to freshly hatched wild-type BT (originally collected in Bayreuth, Germany) flies. Successful transfection was indicated by red-eyed progeny. These again were collected right after hatching and crossed individually to balancer flies (sp/ CyO;TM6/ MKRS), recognizable by the marker phenotypes "curly wings" and "tubby larva". Progeny was collected for red eyes and presence of the balancers, yielding stable lines if insertions hit 2nd or 3rd chromosome. Flies with X chromosomal insertions were backcrossed to yield homozygous stable lines.

3.2.3 Anatomical analysis

3.2.3.1 Fly crossings

Flies were grown on standard corn medium at 25°C, with 12:12 hours dark: light cycle and 60% humidity. In all experiments, flies were kept in 30 ml vials containing 10 ml food. For all crossing experiments, 5-8 female virgin flies were kept together with 3 male flies in one vial and transferred to a fresh one after 5 days.

3.2.3.1.1 Dscam1 project

Immunolabeling experiment

In the immunolabeling experiment, virgin females from the stock R27B03-Gal4 (gift from Gerald Rubin) were crossed to males from the following stock: UAS-mCD8::GFP/ CyO (Bloomington Stock Center). Progenitors were selected after GFP expression.

RNAi knockdown experiment

In the RNAi knockdown experiment, males from the five different UAS-RNAi (3115, 25622, 25623, 36233 and 108835) stocks were crossed to female UAS-mCD8::GFP/ NP282-GAL4 flies and DB331-Gal4; UAS-mCD8::GFP flies. When in addition UAS-Dcr2 (+/ +; UAS-Dcr2; +/ +) was expressed then UAS-RNAi flies were crossed to UAS-mCD8::GFP/ FM7; UAS-Dcr2/ CyO; NP282-GAL4/ TM6.

MARCM experiment

In the MARCM experiment, male flies from the stock: DB331-Gal4/ y; FRT40A/ CyO; UAS-Dscam1^{11.31.25.1}/ TM6 flies were crossed to virgin females of the following stock: UAS-hsFLP, UAS-mCD8::GFP; tub-Gal80, FRT40A/ CyO flies. Flies were transferred to fresh vials hourly. Thus, developmental differences between the offspring varied within that hour. The offspring was kept 24 hours, 48 hours, 72 hours and until late L3 (third instar) larvae were visible in a 25°C incubator before heatshock treatment. L3 larvae were treated differently: 30-40 larvae were collected in an Eppendorf tube with ventilation slits. From earlier experiences, heatshock treatment was much more effective this way. Heatshock was induced by putting vials and Eppendorf tubes, respectively into a waterbath that had a constant temperature of 37°C. The water

covered the vial up to the lid to ensure an even temperature shift of the entire interior. The Eppendorf tubes were put into special water floaters in a way, that the water covered most of the tube. To prevent the larvae to crawl up to the lid, a small tissue was put beneath the lid thereby, keeping the larvae below water level. Temperature shift was induced once for 1 hour. In a second experiment, heatshock was induced twice. The first remained at the same time; the second temperature shift was at L3 stage for 1 hour. After temperature shift, L3 larvae were transferred with a brush to fresh food vials. All larvae were kept at RT until adulthood and analysis.

In the Dscam1^{FLP} MARCM experiment, males from the stock: FRT42D, Dscam1²¹/CyO; UAS-FLP flies were crossed to virgin females of the following stock: DB331-Gal4; FRT42D, tub-Gal80/ CyO; UAS-mCD8::GFP. Crossings were kept in grape-agar plates at 25°C and parental flies discarded after 3 days egg laying. After reaching pupal stage, flies were selected after GFP expression with fluorescence stereomicroscope and transferred to a fresh vial. Flies were kept at RT.

Exon6 deficiency experiment

In the Exon6 deficiency experiment virgin female flies from the stock: Dscam1²³, mCD8::GFP/ CyO; NP282-GAL4, UAS-FLP/ TM6 were crossed to males of the following stock: Dscam1²¹/ CyO_{GB}; Exon⁶-FRT.

Single isoform misexpression experiment

In the misexpression experiment, virgin females from the stock DB331-Gal4; UAS-mCD8::GFP (DB331-Gal4: gift from Reinhardt Stocker) were crossed to males from the Dscam1 single isoform stocks: BI/ CyO; UAS-Dscam1^{+single} (list of all single Dscam1 isoforms: s.3.1.2). Progenitors with following genetic background were taken: DB331-Gal4/ +; UAS-mCD8::GFP/ BI (Dscam misexpression flies). For generating control flies with appropriate wild-type background and balancer Dscam1 misexpression flies were crossed inter se. Flies with the wild-type background of the UAS-Dscam1 stock were kept as control stock: BI/ CyO. With that, I had a stock with the original 2nd chromosome balancer from the Dscam1 stock. Male flies from that stock were crossed to virgin females from the stock DB331-Gal4; UAS-mCD8::GFP. Progenitors with following genetic background: DB331-Gal4/ +; +/- BI; +/- + were taken as control flies in behavior and electrophysiology assays. As wild-type reference flies

from following stock: “*new wild-type*” were compared to control flies in both electrophysiology and behavior assays. No obvious differences occurred.

In the *Dscam1*^{+11.31.25.1} misexpression experiment in T4 and T5 cells, male flies from the following stocks: R42H07, R35F02 and R54A03 were crossed to virgin female flies of the following Stock: UAS-mCD8::GFP. GFP-positive progenies were selected with fluorescence stereomicroscope and subsequently crossed to virgin female flies of following stock: Bl/ CyO; UAS-*Dscam1*^{+11.31.25.1}.

Computer based reconstructions

Reconstructions of HS cells are based on confocal image stacks that were taken from dissected brains after the staining procedure (3.2.3.2). For wild-type HS cell reconstruction, an additional cytosolic GFP marker was added for enhancing the outline of fine structures. Males from the stock UAS-GFPcyto (Bloomington Stock Center) were crossed to virgin females of the following stock: DB331-Gal4; UAS-mCD8::GFP resulting in: DB331-Gal4/ +; UAS-mCD8::GFP/ +; UAS-GFPcyto/ + progenitors of which confocal images were taken.

Time-point analysis experiment

In the time-point analysis, male flies from the stock: tub-Gal80^{ts}/ CyO; UAS-*Dscam1*^{11.31.25.1}/ TM6 were crossed to virgin females of the following stock: DB331-Gal4; UAS-mCD8::GFP/ CyO. For inactivating Gal80^{ts}, the vials containing the experimental flies were shifted to a 30°C heated incubator.

3.2.3.1.2 RicinA project

In the Ricin experiment virgin females from the stock DB331-Gal4; hsFLP/ CyO were crossed to males from the following stock: UAS>Stop>RicinA, UAS-mCD8::GFP/ CyO. Heatshock treatment was made after the developed protocol (s. Ricin methods)

3.2.3.1.3 UAS>Stop>TN-XXL project

For testing the construct, female virgins from the stock UAS>Stop>TN-XXL were crossed to males of the following stock: DB331-Gal4; hsFLP/ CyO. After 48 hours egg laying, adult flies were transferred to another fresh food vial and the egg-

containing vials were given heatshock for 1 hour in a 37°C heated waterbath. Afterwards the vials were kept at RT.

3.2.3.1.4 Virus project

For testing the UAS-TVA-2Alike-dsRed construct, female virgins from the stock DB331-Gal4 were crossed to males of the following stock: UAS-TVA-2Alike-dsRed.

For testing the UAS-G-protein constructs, female virgins from the stock DB331-Gal4 were crossed to males of the UAS-G-protein stocks.

3.2.3.2 Immunohistochemistry

For cell reconstruction, female flies were dissected 3-5 days after eclosion. Flies were anesthetized with CO₂. The head was then removed and placed on a drop of PBS. The head cuticle was first removed using forceps at the frontal part and then the rest was torn off. After discarding the neurolemma, brains were fixed in 4% PFA (Paraformaldehyde) for 30 min at RT. Subsequently, brains were rinsed in PBT. For antibody staining, samples were further incubated in PBT including 4% normal goat serum (Sigma Aldrich) and primary antibodies were added according to their individual dilution factors overnight at 4°C. Antibodies were removed by several washing steps (3 x 20 min in PBT) and secondary antibodies were applied 1:200 overnight at 4°C. Finally, excessive antibodies were removed by a 3 x 20 min washing protocol with PBT. Stained brains were mounted in Ibbidi Mounting Medium (Ibbidi GmbH) and analyzed via confocal microscopy.

The following primary and secondary antibodies were used in the present study. Primary antibodies included: Alexa Fluor 488 conjugate rabbit IgG anti-GFP (Molecular Probes) used in all anti-GFP staining procedures unless otherwise stated, rat anti-mCD8 (Invitrogen Caltag) only used together with rabbit anti-Dscam1-IC (gift from Dietmar Schmucker) in the Dscam1 localization experiment and mouse anti-Dlg (4F3 anti-Discs large; DSHB) used for background staining to visualize shape and borders of the lobula plate.

3.2.3.3 Confocal microscopy

Serial optical sections were taken at 0.3-0.5 µm intervals with 1,024x1,024 pixel resolution and 4 times frame average using confocal microscopes (Leica NT and

Leica SP2) and oil-immersion 40x (n.a. 1.25) for cell reconstruction images and 63x (n.a. 1.4) Plan-Apochromat objectives. The individual confocal stacks were analyzed in Amira 5 (Zuse Institute Berlin) software.

3.2.3.4 Image post-processing

The size, contrast, and brightness of the resulting images were adjusted in Photoshop CS3 (Adobe Systems). Separation of HS and VS cells from the expression pattern of DB331-Gal4 was done in Amira.

3.2.3.5 Cell reconstructions

All cell reconstructions were done by Friedrich Förstner. The confocal image stacks taken were transferred to Matlab (Mathworks, Natick, MA) and all reconstruction analysis was performed there in a custom written software in combination with the “TREES” software (Cuntz et. al, 2008). Based on 2-dimensional images cylinder models of the main branching structures were obtained in a semi-automated way: interactive software allowed switched viewing of either Z-projection or an individual slice of an image stack. Z-values were attributed to each cylinder directly from the depth-map according to their 2-dimensional location. Quick tracing results (30 min) were achievable. Working corrections based on individual slices were necessary in all reconstruction steps. Jumps in the Z-axis were smoothed by use of linear interpolation. With that procedure, the hull-areas of HS cell dendrites were calculated. In order to obtain a measure for the convexity of dendrites, the convex hull was drawn around all dendrite nodes. The surface ratio between the dendritic spanning field and this convex hull was chosen as a characteristic spanning field parameter, the convexity index.

3.2.4 RicinA project

3.2.4.1 Development of LPTCs

Flies from the stock DB331-Gal4; UAS-mCD8::GFP were screened for GFP expression in LPTCs at several developmental stages. The number of cell bodies at late larval stage L3 was less than the number of LPTCs present in the adult stage, leading to the assumption that there was a successive development of different LPTCs.

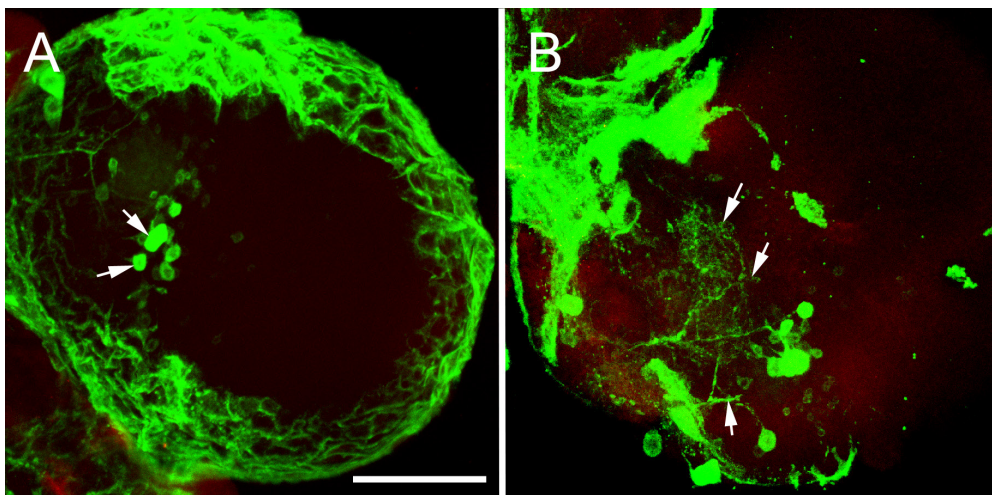


Fig. 16: Neurite outgrowth of LPTCs.

(A) In the late L3 larvae, the cell bodies of LPTCs emerged for the first time. (B) Later, in the white pupa stage, first rudimentary outgrowing neurites could be detected. Neurites of outgrowing LPTCs were depicted in A and B with arrows. Confocal image stacks were taken with a z-increment of 0.2 μm , a 63x objective and minimized pinhole. Composite images were generated by collapsing ~ 60 images. Scale bar 50 μm .

3.2.4.2 Heatshock protocol

I separated the progenies of the RicinA crossings with a brush when they reached the developmental stage of late L3. This was recognizable when the larvae crawled out of the food source and stucked to the wall of the vials. 20-30 larvae were collected into one eppendorf tube which was prepared with respiration slits. Next, I put a small piece of wet paper towel on the top of the larvae in order to prevent the larvae to accumulate at the lid of the tube and for an even heatshock. Following, the

tube was put into a 37°C waterbath for 2 hours. After heatshock, larvae were transferred with a brush into a new food vial and kept at RT.

3.2.4.3 Cell vitality test

After the brains were excised according to the previously described protocol, I incubated them immediately in PI (Propidium Iodide) solution (1:3000) for 1 min without fixation. After several washing steps with PBS, confocal images were taken. PI was thereby excited with a 488 nm argon-ion laser light and detected by a 562-588 nm band pass filter. In all tested brains (n=7), no overlap of red labeling PI with GFP positive LPTCs could be detected. This experiment demonstrated that remaining neurons were not affected by RicinA expression in neighboring neurons.

3.2.5 TN-XXL project

The scheme shows the cloning strategy for generating the UAS>Stop>TN-XXL vector. Using common cloning strategies did not work in the past. Gateway Cloning Technology was therefore used to create the plasmid.

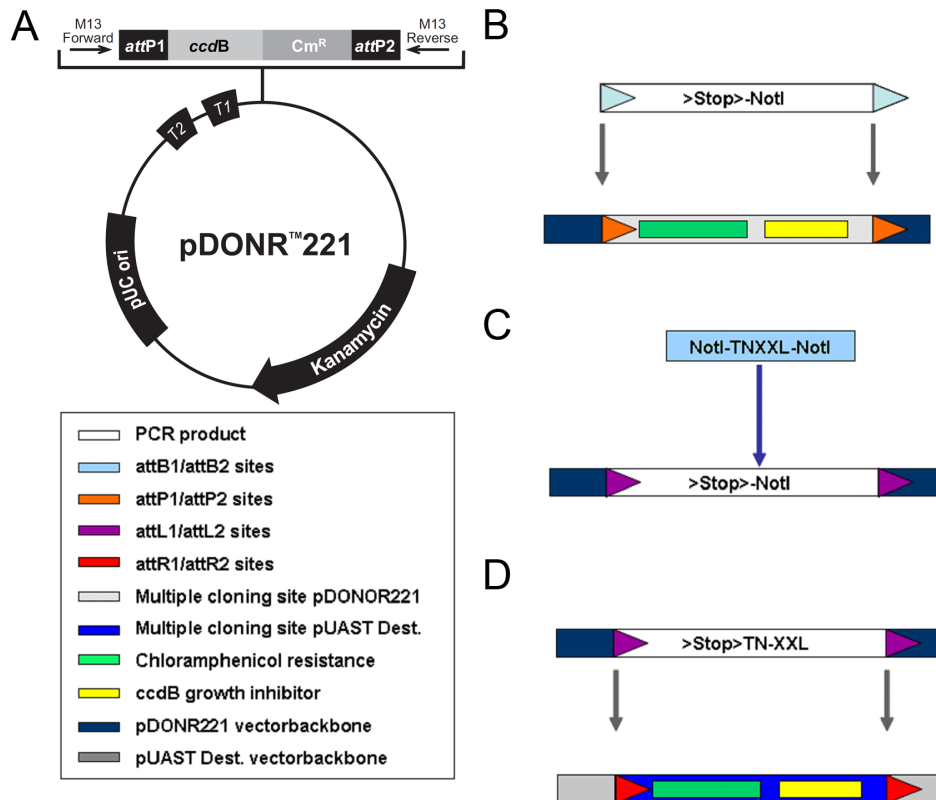


Fig. 17: The UAS>Stop>TNXXL plasmid.

(A) The first cloning steps were performed within the pDONR221 (modified from Invitrogen). (B) First, the FRT-flanked Stop sequence (>Stop>) with a NotI restriction site at the C-terminus was recombined into the pDONR vector via BP reaction. (C) Subsequently, TN-XXL was inserted via the NotI restriction site. (D) Finally, the completed insert was recombined into the pUAST vector via LR reaction.

3.2.6 Virus project

3.2.6.1 Brain culture

All manipulations were performed in a clean environment using disinfected equipment (forceps, pipettes, PCR tubes, etc.) in order to prevent bacterial or fungal contamination.

Excised *Drosophila* brains were placed onto Millicell low height culture plate inserts (Milipore) which were placed in a sterile Petri dish (Falcon) containing 1 ml of sterile DPBS (Dulbecco's PBS; Sigma Aldrich). On top of the membrane a freshly prepared coating, solution of Laminin (3.3 µg/ mL; BD Biosciences) and Polylysine (33.3 µg/ mL; BD Biosciences) in sterile DPBS was added. The culture plate inserts were incubated overnight at 37°C. The next day they were washed extensively with sterile DPBS and were stored at 4°C for up to three weeks. Just before use, the coated inserts were transferred to an empty sterile Petri dish. For making the brain explants, adult female flies of the desired genotype were collected within 4 days after eclosion. After CO₂ anesthesia, the flies were placed in a 1.5 ml centrifuge tube on ice, keeping them alive but immobile. Before dissection, flies were washed in 70% Ethanol for a few seconds and placed into a sterile Petri dish containing ice-cold Schneider's *Drosophila* Medium (GIBCO). Fly brains were quickly dissected within that medium (<3 min). Parts of the eyes and lamina were left attached when they were difficult to remove. Damage to the brain or delay in the speed of the dissection reduced the quality of the brain culture and therefore, I discarded all damaged brains. The dissected brains were collected in a steril PCR tube containing Schneider's *Drosophila* Medium on ice and then washed with ice-cold dissection medium. Afterwards, brains were placed in a drop of medium on the membrane of the culture plate insert, using a pipette. For this step, the pipette tip was cut a bit open with a scissor and rinsed with Schneider's *Drosophila* Medium. This prevented the brain to be stuck at the inner wall of the pipette tip. Up to five brains were transferred from the PCR tube onto the same insert. When all brains were in place, their antero-posterior orientation was verified and corrected if necessary. Exceeding medium was removed using a pipette, leaving only a thin film of medium covering each brain. 1.1 ml of culture medium was then added to the Petri dish containing the insert. The culture

dishes with the explants were kept in a plastic box in a cell culture incubator at 25°C. The culture medium was refreshed every 2 days.

To test this method, I first cultured fluorescent brains of DB331-Gal4; UAS-mCD8:GFP flies and checked strength of the expression under fluorescence binocular and the morphology of LPTCs by confocal imaging. Within 10 days, the expression level and cell morphology appeared to be stable.

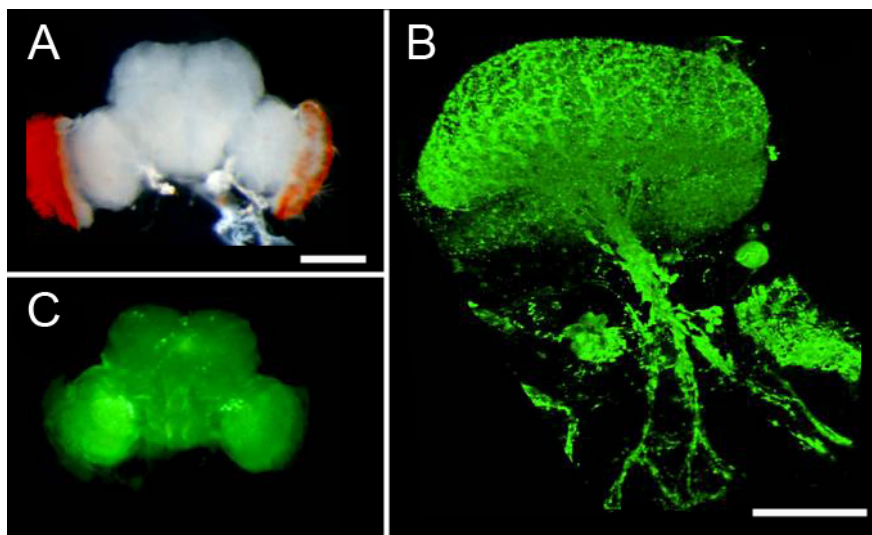


Fig. 18: Ex vivo fly brain culture.

(A) Bright field image shows a dissected brain from a DB331-Gal4; UAS-mCD8::GFP fly after a total incubation time of 7 days. The brain does not undergo any visible morphological changes or degradation during incubation time besides flattening of the entire brain. (B) Fluorescence image reveals remaining GFP expression pattern observable under fluorescence stereomicroscope. (C) Confocal image of one 7 days-old cultured brain reveals an intact LPTC morphology in both dendritic and axonal parts. Stereomicroscope images were taken with a Leica M205 FA and full apochromatic zoom. Confocal image stacks were taken with a z-increment of 0.5 μm , a 63x objective and minimized pinhole. Composite images were generated by collapsing ~ 60 images. Scale bars 50 μm .

3.2.6.2 The UAS-TVA-2Alike-dsRed construct

The sequence of the TVA-2Alike-dsRed construct was integrated into the pUAST-vector with the gateway cloning system. The insert was kindly provided by Alexander Ghanem and Klaus Conzelmann.

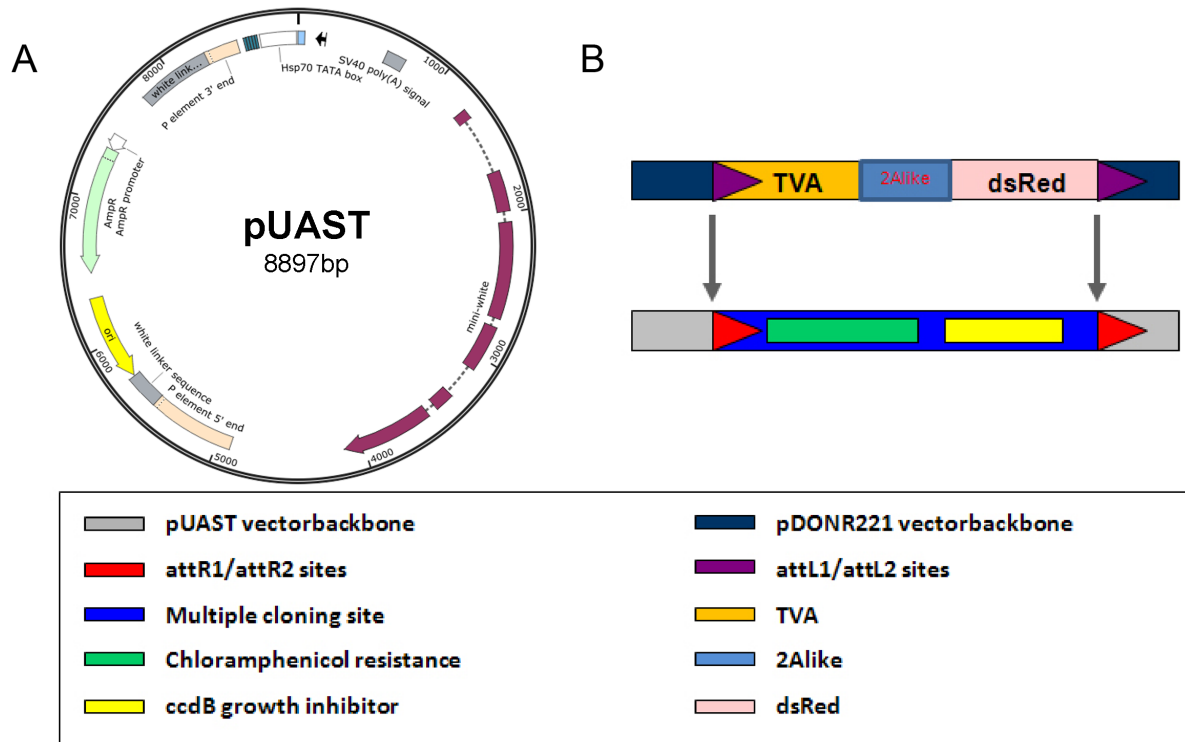


Fig. 19: The UAS-TVA-2Alike-dsRed plasmid.

(A) The pUAST destination vector (modified from snappene) has attR1/ attR2 recombination sites which allow the integration of the (B) TVA-2Alike-dsRed sequence that is flanked with attL1/ attL2 recombination sites via enzymatic reaction.

3.2.6.3 The UAS-G-protein constructs

The sequences of the G-protein constructs were integrated into the pUAST-vectors with the gateway cloning system.

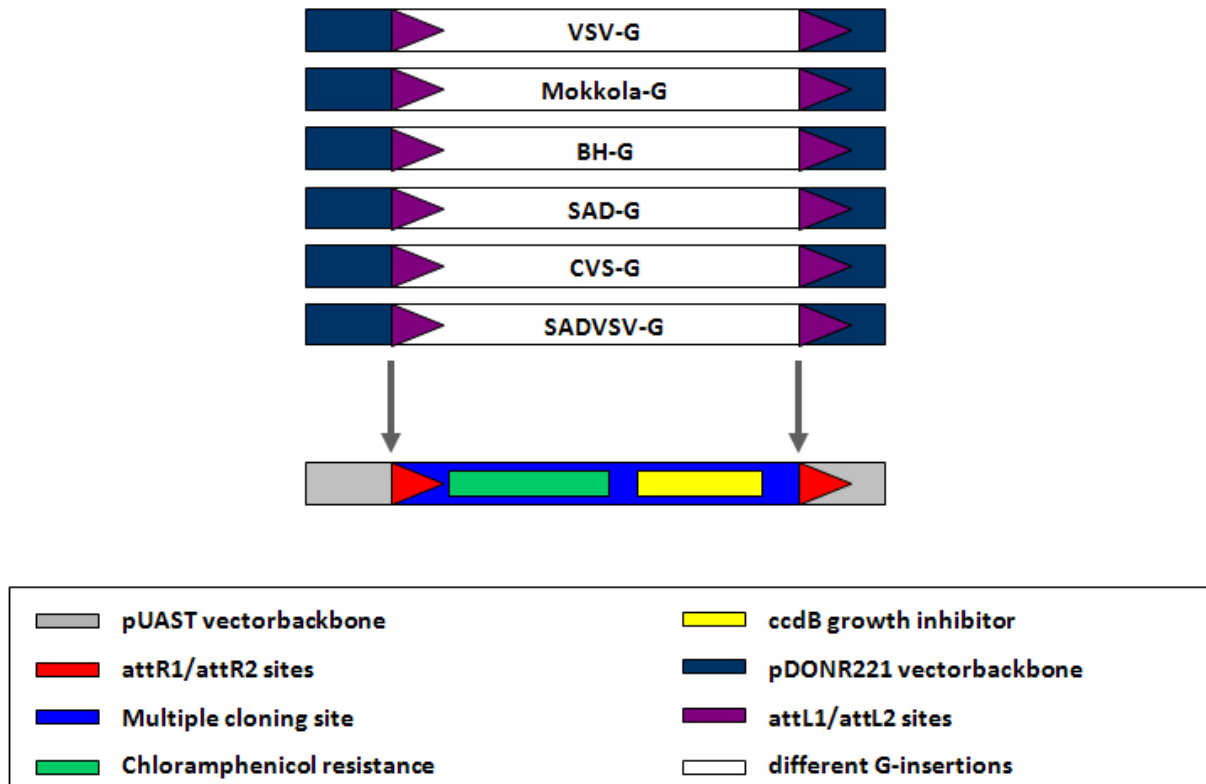


Fig. 20: The UAS-G-protein plasmids.

The pUAST destination vector possesses attR1/ attR2 recombination sites, which allowed the integration of the G-protein sequences, flanked with attL1/ attL2 recombination sites, through an enzyme-mediated process (s. 3.2.1.8). Original inserts were kindly provided by Alexander Ghanem.

4 Results

4.1 Manipulations of the *Dscam1* expression in LPTCs

4.1.1 Immunolabeling against *Dscam1*

To investigate the presence of *Dscam1* in HS and VS cells, I expressed GFP in these cells in addition to the immunolabeling with *Dscam1*-IC antibody raised against the intracellular domain. I used three different driver lines: DB331-Gal4 (Joesch et al., 2008), NP282-Gal4 (Schnell et al., 2010) and R27B03-Gal4 (Seelig et al., 2010) (s. 3.1.2) to express membrane-tagged GFP (UAS-mCD8::GFP) in LPTCs. DB331-Gal4 drove expression in 3 HS and 6 VS cells (Fig. 21A+B). R27B03-Gal4 was a highly specific driver for all 3 HS cells (Fig. 21C+E) in the lobula plate and drove additionally expression in the central brain. The large, overlapping dendritic branches of HS cells covered constant areas along the dorso-ventral area of the lobula plate; the dendrites of VS cells run along the proximal-distal axis of the lobula plate. Their dendrites covered the entire neuropile of both lobula plate layers up to the outer border (Fig. 21A-E). As HS and VS cells had only few overlapping branches in the dorsal area of the lobula plate, it was possible to carry out a software-based separation of VS cells from the expression pattern of DB331-Gal4 (Fig. 21D).

In accordance to previous studies (Wang et al., 2004; Hummel et al., 2003), *Dscam1* is broadly expressed in the optical lobe and the central brain (Fig. 21A). Notably, horizontal sections showed that *Dscam1* was located in all four lobula plate layers (Buchner et al., 1984; Fischbach and Dittrich, 1989) (Fig. 21E). GFP expression in HS and VS cells clearly co-localized with *Dscam1*-IC immunolabeling (Fig. 21B+E) which was further corroborated by magnified single confocal sections of the dendrites, soma and axon terminals (Fig. 21F-J). Same results were obtained with all tested Gal4-driver lines.

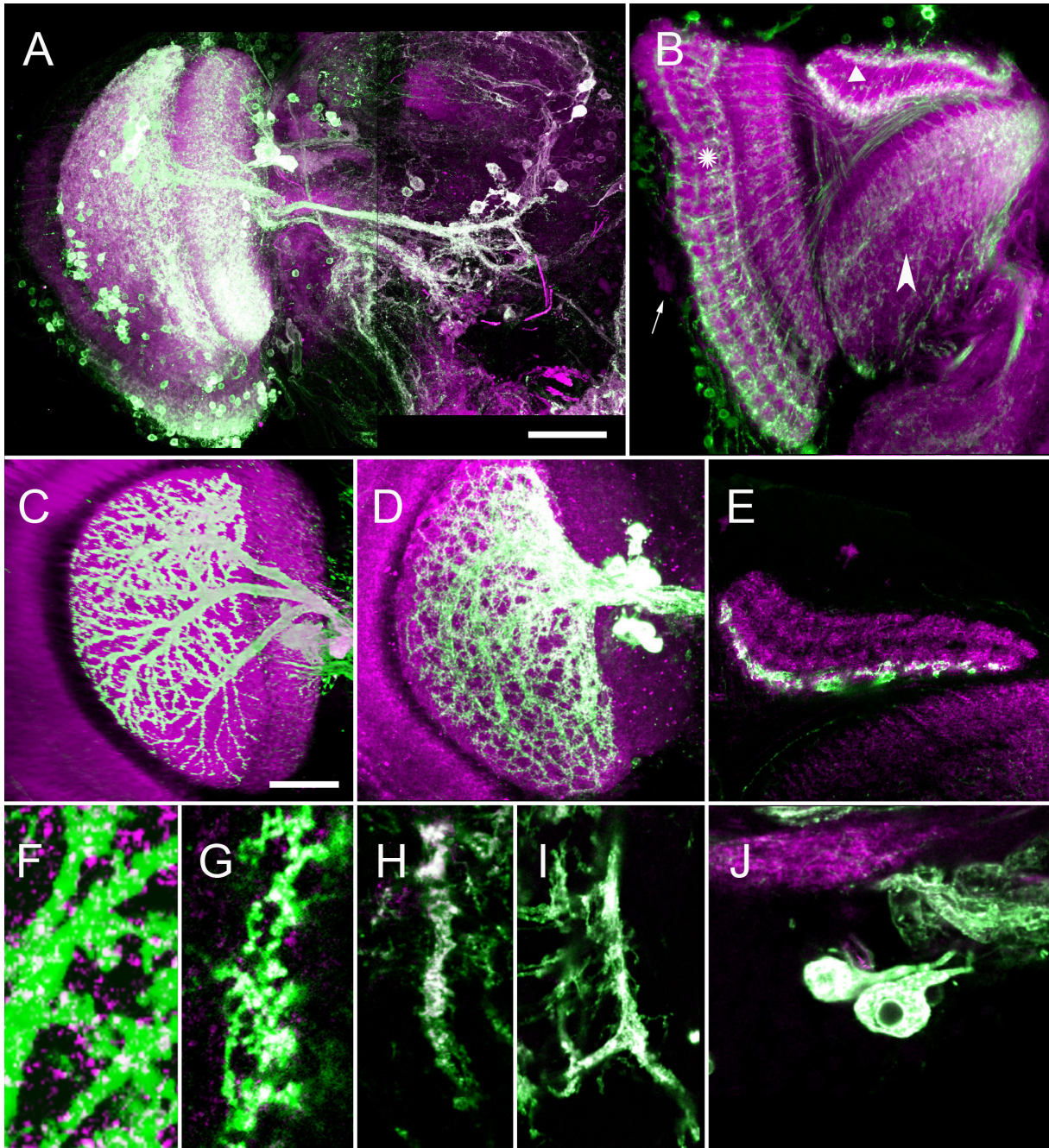


Fig. 21: *Dscam1* expression in the optical lobe.

(A) Double immunolabelings of *Dscam1* (magenta) and GFP (green) show *Dscam1* expression in all neuropils of the fly visual system (DB331-Gal4; UAS-mCD8::GFP). (B) Horizontal section view. Immunolabeling with *Dscam1*-IC highlights columns and layers in the lamina (arrow), medulla (asterisk), lobula (arrowhead), and the lobula plate (triangle) of the fly visual system. (C) The large overlapping dendrites of HS cells are stacked along the dorsal-ventral axis and cover the entire lobula plate where they co-localize with *Dscam1* immunolabeling (UAS-mCD8::GFP; R27B03-Gal4). (D) The overlapping dendrites of VS cells (separated from the DB331-Gal4 expression pattern) are located along the proximal-distal axis of the lobula plate and co-localize with *Dscam1*. (E) Horizontal section (UAS-mCD8::GFP; R27B03-Gal4). The dendritic arborizations of HS cells are restricted to the thin,

most-anterior layer of the lobula plate and the distribution of *Dscam1* in all four layers of the lobula plate (UAS-mCD8::GFP; R27B03-Gal4). Close up single sections of the distal lobula plate region reveal in detail the colocalizations of GFP and the antibody in (F) HS and in (G) VS cell dendrites. Colocalizations could also be found in the axons of (H) HS cells and (I) VS cells and in their (J) somata. Confocal image stacks were taken with a z-increment of 0.3 μm , a 63x objective and minimized pinhole. Composite images in (A-E) were generated by collapsing 40-150 images; (F-J) are single confocal images. Scale bars 50 μm . Magnifications in E: 165% of A; F+G: 370%, H+I: 250%, J: 170% of C.

4.1.2 Reduced *Dscam1* expression level

For studying the functional role of *Dscam1* in HS cells, I used different genetic approaches to remove endogenous *Dscam1*. First, I tried a gene knockdown by expressing RNAi under control of the Gal4/ UAS system. Second, I tried to obtain single HS cell clones in which *Dscam1* is deleted with the MARCM technique. Third, I used the MARCM technique to remove *Dscam1* in the entire Gal4 expression pattern.

4.1.2.1 Silencing *Dscam1* with RNAi

Using RNAi (Enerly et al., 2002) under control of the Gal4/ UAS system (Brand and Perrimon, 1993) provides the possibility to silence *Dscam1* function in HS cells during development. To investigate whether expression of UAS-*Dscam1*-RNAi has an effect on dendritogenesis of LPTCs, I co-expressed GFP in these cells and immunolabeling was performed. I started with DB331-Gal4 that provided an expression in 3 HS cells and 6 VS cells. I tested five different UAS-RNAi lines targeting against *Dscam1* mRNA (s. 3.1.2). As control, I took flies from the same crossings without RNAi expression (DB331-Gal4; UAS-mCD8::GFP/ CyO; (NP282-Gal4)/ Tm6: with curly wings and tubby) (Fig. 22A+E+I). RNAi flies driven with DB331-Gal4 showed an overgrowth phenotype in the dendrites of HS cells (Fig. 22C) and VS cells (Fig. 22G). Close up images of the distal regions of RNAi expressing HS (Fig. 22D) and VS (Fig. 22H) cells underline the increase in the number of small branches compared to that of control cells (Fig. 22B+F). Although, I was able to separate VS and HS cells from the DB331-Gal4 expression pattern, it was impossible for me to track single branches throughout the dense dendritic ramification pattern. Therefore, I continued the experiment with NP282-Gal4 that gave a restricted expression pattern in only HSN

and HSE cells (Fig. 22I). RNAi flies (n=10 for each RNAi line) showed a different phenotype than that when DB331-Gal4 was used as driver line. Notably, most flies were showing no mutant phenotype in the HS cell dendrites at all. In some flies, I detected defects in the pattern formation of HSE cells (Fig. 22J-K). The defects included elongation of single side branches (Fig. 22J+K arrows) and lack of branches in the distal lobula plate area (Fig. 22J asterisk). In most cases, the dendritic morphology of HSN cells was not affected by RNAi expression.

For investigation of the dendritic receptor distributions, I performed immunolabeling with fluorescent α -bungarotoxin-Alexa 647 in order to visualize nAChRs. This peptide is extracted from the venom of *Bungarus multicinctus* and binds with high affinity to the α -subunits of the nAChR in the brain. Studies from Raghu et al. (2007, 2009) showed that HS and VS cell dendrites possess a high number of GABA and nAChRs, whose density increases with higher-order branches. The staining revealed in single section images an even distribution of nAChRs on the remaining HS cell dendrites (Fig. 22N) that resembled the pattern in wild-type cells. Taken together, the observed RNAi phenotypes were rather subtle and not constant when driven with NP282-Gal4. Additional immunolabeling with Dscam1-IC antibody confirmed the assumption that remaining *Dscam1* expression was present in HSN and HSE (Fig. 22L+M). Detailed analysis of the DB331-Gal4 driven RNAi phenotype was not carried out due to the very complex and highly variable branching pattern of the HS cell dendrites. Using additional UAS-Dicer2 did not enhance the phenotype or its frequency. Here, I concluded that using RNAi did not knockdown entirely *Dscam1* in the HS cells. One of the underlying reasons, which need to be discussed, might be the presence of redundancy among *Dscam1* exon-alternatives (Wang et al., 2004).

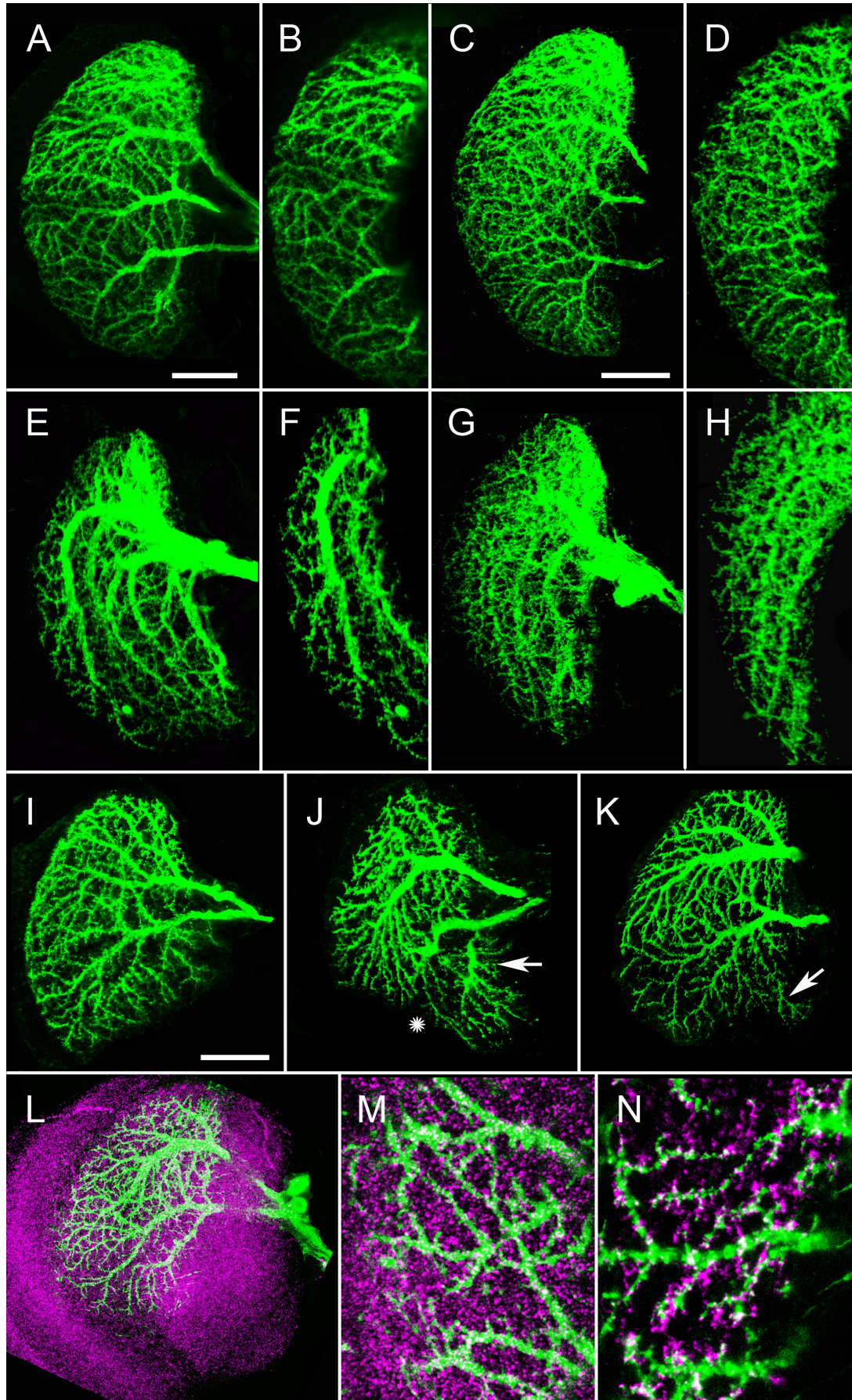


Fig. 22: *Dscam1* knockdown with RNAi.

Flies expressing UAS-RNAi targeted against *Dscam1* (DB331)/ +; UAS-mCD8::GFP/ UAS RNAi; NP282-Gal4/+). (A) Control HS cells (DB331-Gal4; UAS-mCD8::GFP) separated from the expression pattern of DB331-Gal4. (B) Close up image from control HS cells at the distal area of the lobula plate. (C) HS cells in RNAi 3115 expressing flies (DB331/ +; UAS-mCD8::GFP/ UAS RNAi) show an overgrowth phenotype with increased number of terminal branches. (D) Close up image from RNAi expressing VS cells at the distal area of the lobula plate. (E) Control VS cells extracted from the expression pattern of DB331-Gal4. (F) Close up image from control VS cells at the distal area of the lobula plate. (G) VS cells in RNAi 3115 expressing flies (DB331/ +; UAS-mCD8::GFP/ UAS RNAi) show an overgrowth phenotype with increased number of terminal branches. (H) Close up image from RNAi expressing VS cells at the distal area of the lobula plate. (I) Control HS cells (UAS-mCD8::GFP/ +; NP282-Gal4/ +) from the expression pattern of NP282-Gal4. (J+K) RNAi expression driven with NP282-Gal4. Flies show defects in dendritic patterning of HSE cells. In some cases, dendritic sidebranches are stretching beyond the territorial area of the cell (arrows); in others, single ramifications do not reach to the lateral territorial border (asterisk). (L) Immunolabeling with *Dscam1*-IC antibody (magenta) reveals remaining *Dscam1* expression in HS cells. (M) Close up single section image of the dendritic tips visualizes the co-localization of GFP expressing cells (green) with *Dscam1*-IC-antibody. (N) Single section image. Immunolabeling with α -Btx (alpha-Bungarotoxin) shows the distribution of nAChRs at the dendritic tips of RNAi expressing HS cells. Confocal image stacks were taken with a z-increment of 0.2 μ m, a 63x objective and minimized pinhole. Composite images were generated by collapsing 20-80 images. Scale bars 50 μ m. Magnifications in B, D, F, H: 115%, M+N: 320% according to the scale bar in I.

4.1.2.2 MARCM

As *Dscam1* homozygous loss-of-function alleles are embryonic lethal (Hummel et al., 2003), I tried to apply the MARCM technique (Lee and Luo, 1999) to assess the function of *Dscam1* in single LPTC clones. I used DB331-Gal4 to drive expression of GFP and flippase activity in LPTCs. *Dscam1* null cells had following genetic background: DB331-Gal4/ hs-FLP; FRT42D, tub-Gal80/ FRT42D, *Dscam1*^{LOF}; UAS-mCD8::GFP. The genetic design of the transgenic flies ensured that only homozygous cells lacking Gal80 were *Dscam1* null and GFP labeled. The rest of the fly still possessed the intact *Dscam1* code and Gal80 and thus, did not express the marker gene. This method has been successfully implemented before for selective labeling of *Dscam1* null cells (Chen et al., 2006; Zhu et al., 2006; Zhan et al., 2004). As recombination is driven by hs-FLP, the timing of the FLP-out and the percentage of cells undergoing recombination depend on the timing and levels of heatshock (s. 3.2.3.1). I varied successively both parameters and screened several hundreds of flies but unfortunately, I did not receive any LPTCs with that technique.

Instead, MARCM analysis revealed couples of lobula plate intrinsic neurons, trans-lobula plate neurons, trans-medulla neurons. Whether these neurons were interacting with LPTCs has yet to be investigated.

4.1.2.3 MARCM with residual flippase activity

Here, I used UAS-FLP instead of heatshock induced flippase activity. Flies had following genetic background: DB331-Gal4; FRT42D, tub-Gal80/ FRT42D, *Dscam1*^{LOF}; UAS-mCD8::GFP/ UAS-FLP. Despite the fact that Gal80 should prohibit flippase activity, those flies (*Dscam1*^{FLP}) revealed a strong and constant overgrowth phenotype that qualitatively resembled the one detected in the RNAi experiment yet by far outperformed it in reproducibility. This was also the reason why I recognized the genetic contradiction at the very end of the study. The *Dscam1*^{FLP} phenotype is likely based on residual flippase expression and it is unclear whether LPTCs were completely missing *Dscam1* in those flies. Control flies (Fig. 23A-C) without *Dscam1*^{LOF} (*Dscam1* loss-of-function) allele displayed a normal dendritic branching pattern in HS (Fig. 23B) and VS cells (Fig. 23C). Their axonal terminals (Fig. 23M) resembled also those of wild-type cells. In this experiment, I separated VS and HS cells from the expression pattern of DB331-Gal4 with software based methods.

HS and VS cells with *Dscam1*^{FLP} showed a strong constant overgrowth phenotype with dendritic (Fig. 23D-F) and axonal disorders (Fig. 23N). The relative positions of HS cell dendrites within the lobula plate and their covering areas were indifferent from wild-type LPTCs, whereas secondary branches gave rise to a larger number of tertiary branches and so on. Sister dendrites of the same neuron were crossing each other in a very high frequency (Fig. 23I+L). The overgrowth phenotype could also be observed in VS cells (Fig. 23F). Secondary branches ramified to tertiary branches in much shorter distances and more frequently (Fig. 23K) than in control cells (Fig. 23J). In collaboration with Friedrich Förstner the *Dscam1*^{FLP} overgrowth phenotype was corroborated by reconstructions of the HS cell dendrites. He used the open source software package “TREES toolbox” (Cuntz et al., 2010) for the manipulation and analysis of confocal image stacks. The resulting morphological reconstructions of the HSN cell (Fig. 24A+B) visualize and corroborate the lack of self-avoidance mechanism in the dendritic branches.

By using DB331-Gal4 as driver line, the axons of HS and VS cells could be traced along their entire pathway from the lobula plate to the central brain region. In control flies, the axons terminated in two separate destination areas in the central complex (Fig. 23M): The VS cell axons were located slightly above the esophagus and HS cell axons ventral to the esophagus. In the expression pattern of DB331-Gal4, a third axonbundle from yet unidentified cells descended from the lobula plate terminating dorsal to the esophagus. The axonbundles of HS and VS cells were forming characteristic branching patterns at the terminal areas in the central brain. The axons of HS cells did not ramify but terminated bundled in the central brain whereas, the axonbundle of VS cells first splitted up in two arbors along the dorsal-ventral axis before their terminals stratified at the area above the esophagus. In *Dscam1^{FLP}* flies, VS and HS cells showed an increased degree of ramifications in the central brain area (Fig. 23N). In some cases, I could observe single axon fibers of HS cells separating from the main bundle before reaching their target area. The same phenotype was found in VS cell axons. Single fibers were still entering the central brain in a single bundle. The bifurcation was also present. However, at the terminal area the separation from the main bundles appeared stronger than in control cells. Inspired by previous studies in the MB that showed that *Dscam1* mutant axons could alter the projections of neighboring wild-type axons (Wang et al., 2002), I wanted to investigate whether non-cell-autonomous effects were also present in *Dscam1^{FLP}* flies. Preliminary experiment was done in collaboration with Bettina Schnell. *Dscam1^{FLP}* cells were GFP labeled whereas surrounding wild-type neurons did not possess a fluorescent marker. The fluorescent dye (Alexa-Fluor 569/ Invitrogen) was injected into a wild-type cell. The chosen neuron was located close to those of HS cells in order to raise the possibility of interactions between both cell types. The wild-type cell might be the Lpt2 (Lobula plate tangential 2) neuron described in the study from Fischbach and Dittrich (1989). This cell displayed indeed one location where two sister branches were crossing each other (Fig. 23O+P, arrow) whereas the rest of the neuronal ramifications strictly avoided self-crossings. This spatially restricted lack of self-avoidance might be caused by interactions between this cell with *Dscam1^{FLP}* expressing cells or missing interactions with *Dscam1^{FLP}* cells. Functional studies have been carried out and the results are described in the discussion.

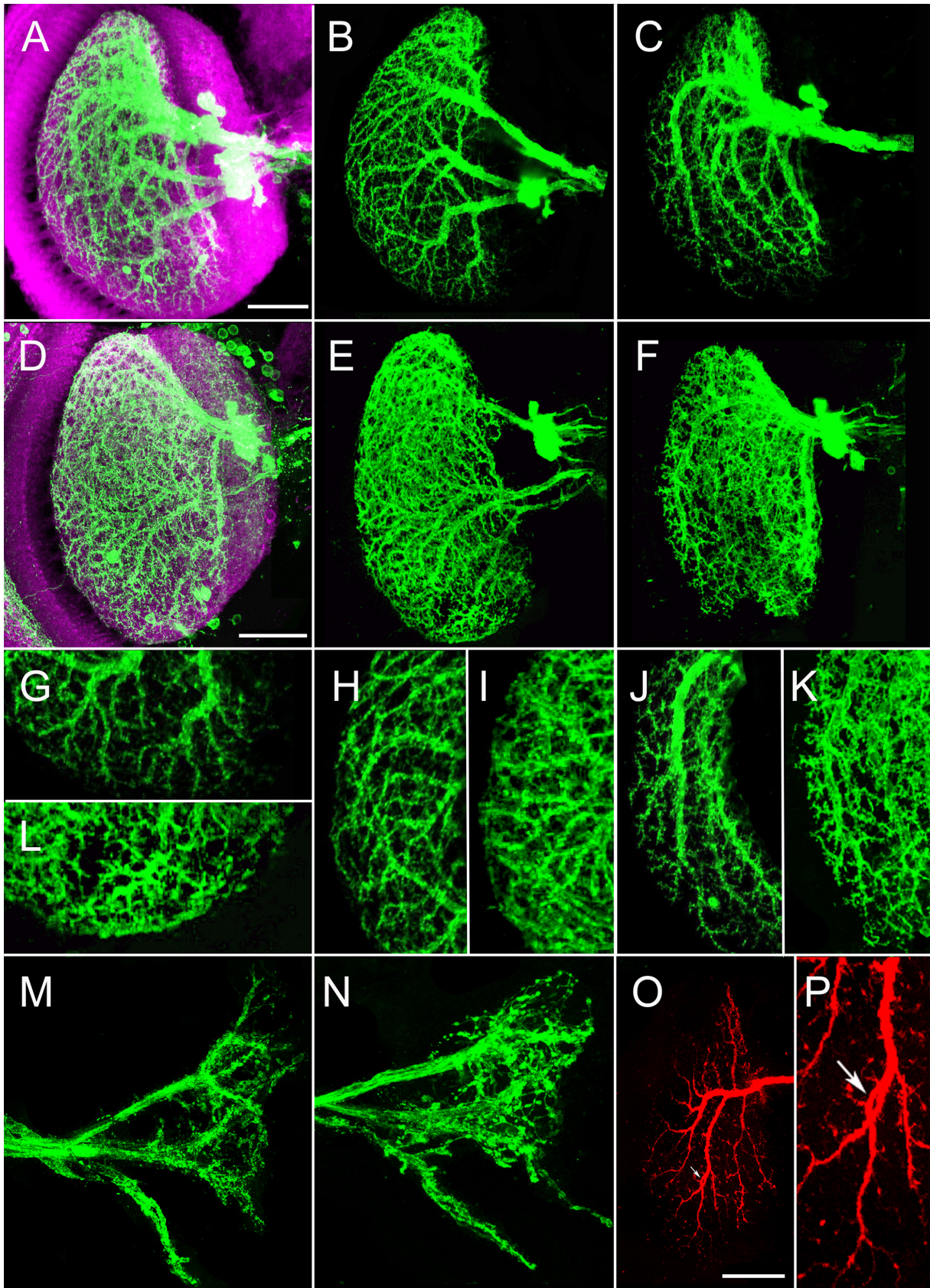


Fig. 23: The effects of $Dscam1^{FLP}$ on lobula plate cells.

Flies with residual flippase expression (DB331-Gal4; FRT42D, tub-Gal80/ FRT42D, Dscam1^{Δ21}; UAS-mCD8::GFP/ UAS-FLP) show an overgrowth of dendritic and axonal branches in HS and VS cells. Double immunolabelings of Dlg (Discs large: magenta) and GFP (green) visualize the anatomy of LPTCs and the borders of the lobula plate. (A-C) Control cells (DB331-Gal4; FRT42D, tub-Gal80/ FRT42D, Dscam1^{Δ21}; UAS-mCD8::GFP/ +). (B) HS and (C) VS cells can be separated from the expression pattern of DB331-Gal4 (A) by using software based methods. (D-F) The expression pattern in Dscam1^{FLP} flies reveals a high increase of terminal dendritic structures in (E) HS and (F) VS cells. (G-L) Close up images of the (G+L) southern and (H+I) distal regions of HS cell dendrites and the (J+K) distal regions of VS cell dendrites in (G, H, J) control and (I, K, L) Dscam1^{FLP} flies underline the overgrowth phenotype. (M+N) Comparison of the LPTC axons in (M) control and (N) Dscam1^{FLP} flies shows the presence of overgrowth also in the axonal terminals. (O) One neighboring wild-type cell (Lpt2) was highlighted by a blind injection of a fluorescent dye into the cell body of a neuron. (P) Close up image of the Lpt2 neuron. A single crossing event of sister branches could be detected in the dendrites of the Lpt2 cell. Close up images of the axon terminals of VS cells. Confocal image stacks were taken with a z-increment of 0.3 μm, a 63x objective and minimized pinhole. Composite images were generated by collapsing 10-150 images. Scale bar 50 μm. Magnifications in G-K: 200%, in P: 310% according to the scale bars in A+D.

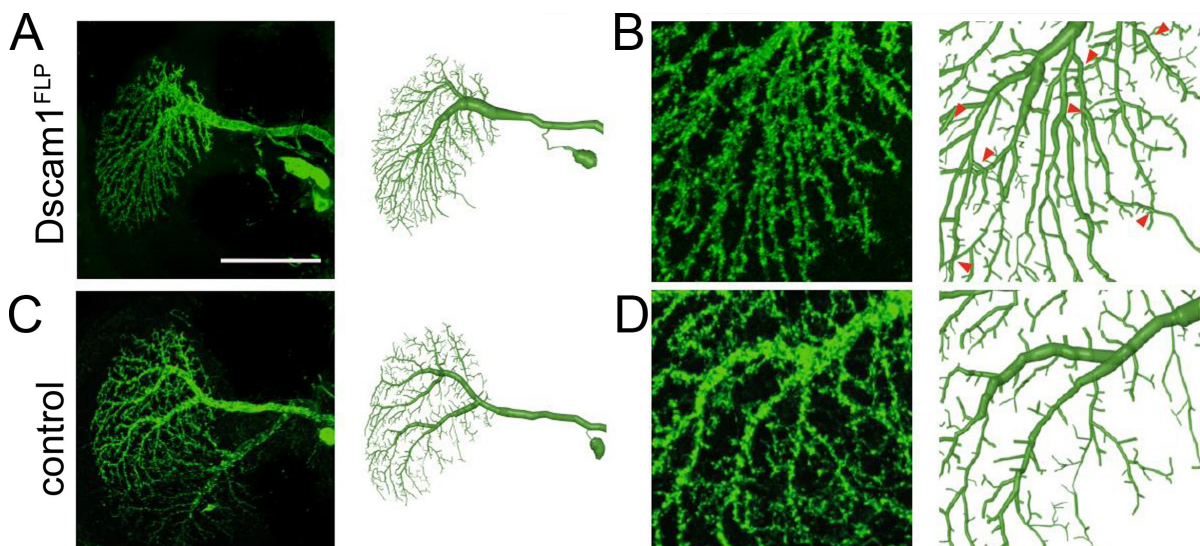


Fig. 24: Computer based reconstructions.

Image data taken for reconstruction are shown on the left sides. Corresponding reconstructions are illustrated on the right sides. Overviews of the reconstructed HSN cell dendrites from (A) Dscam1^{FLP} flies (DB331-Gal4; FRT42D, tub-Gal80/ FRT42D, Dscam1^{Δ21}; UAS-mCD8::GFP/ UAS-FLP) and (C) control (UAS-mCD8::GFP; NP282-Gal4). (B) Close up image of the reconstructed Dscam1^{FLP} cell depicts several crossing events of sister branches which are caused by lack of self-avoidance mechanism (red arrowheads). (D) Close up image of the reconstructed wild-type cell shows that in wild-type cells self-avoidance mechanisms prohibit crossing of sister branches. Confocal image stacks

were taken with a z-increment of 0.2 μm , a 63x objective and minimized pinhole. Composite images were generated by collapsing ~150 images. Scale bar 50 μm (A+C) and 15 μm (B+D). Reconstruction data was kindly provided by Friedrich Förstner.

4.1.3 Reduced *Dscam1* diversity

Previous studies in the MB and the da system showed that reduction of *Dscam1* ectodomain diversity from 19,008 to 4,752 potential isoforms did not interrupt the self-avoidance mechanism in MB (Wang et al., 2004) and da neurons (Matthews et al., 2007). I set out to analyze if full isoform diversity is required for proper dendritic growth and development. Exon-cluster 6 diversity was eliminated using flies with following genetic background: *Dscam1*^{Δ23}, mCD8::GFP/ *Dscam1*^{Δ21}; NP282-Gal4, UAS-FLP/ Exon^{Δ6}. Here, I used a *Dscam1* deletion mutant that lacks Exon6 variability (generously provided by Dietmar Schmucker) and thus, resulted in a reduction of *Dscam1* diversity from 19,008 to 1,584 potential isoforms in the affected cells (Fig. 25). Parental fly stocks were in addition heterozygous *Dscam1* null, each carrying a loss-of-function allele: *Dscam1*^{Δ21}/ *Dscam1*^{Δ23} (Hummel et al., 2003; Zhu et al., 2006; Zhan et al., 2004). I used NP282-Gal4 to drive expression in HSN and HSE cells. Exon6 deletion mutants were homozygous *Dscam1* null (*Dscam1*^{Δ21}/ *Dscam1*^{Δ23}) that was rescued by a heterozygous *Dscam1* allele, in which Exon6 is flanked by FRT sites (Exon^{Δ6}). By flippase activity, the FRT flanked sequence was removed from the rescue-allele, thereby resulting in a deletion of Exon6 variability (Fig. 25) within the expression pattern of NP282-Gal4. As control, I took flies without flippase activity: *Dscam1*^{Δ23}, mCD8::GFP/ *Dscam1*^{Δ21}; NP282-Gal4, CyO/ Exon^{Δ6}. I also controlled that *Dscam1* null flies without rescue allele (*Dscam1*^{Δ23}, mCD8::GFP/ *Dscam1*^{Δ21}; NP282-Gal4, UAS-FLP/ TM6) were indeed not viable; They did not reach the larval stage.

In control flies, the dendritic branching pattern of HSN and HSE resembled wild-type morphology (Fig. 26A-C). The dendrites covered the entire neuropile of the lobula plate up to the distal border and no unusual crossings of sister branches were detectable leading to the assumption that the *Dscam1* allele of Exon^{Δ6} completely rescued *Dscam1* null.

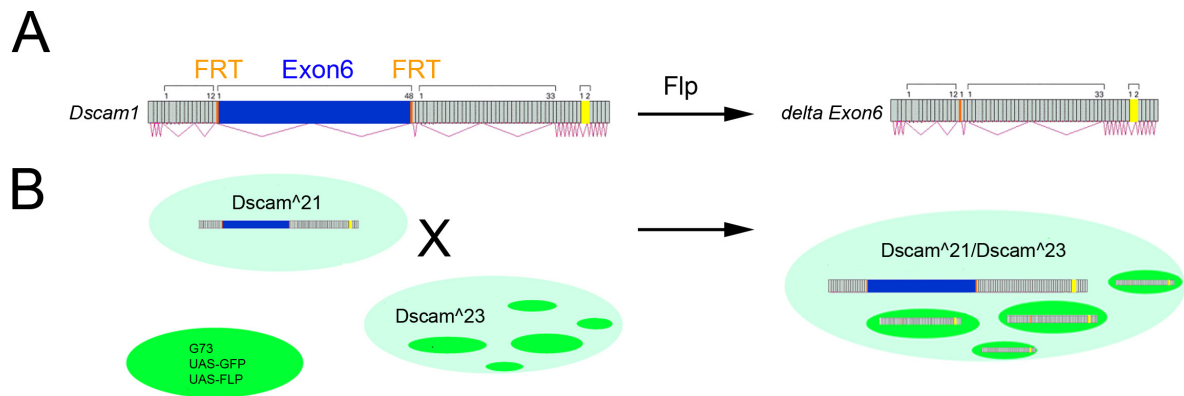


Fig. 25: Schematic description of Exon6 deletion.

(A) The Exon6 deletion mutant carries the entire *Dscam1* gene sequence in which Exon6 is flanked by FRT sites. This allows the excision of Exon6 by flippase activity. (B) Crossing flies, one carrying *Dscam1*²¹ and Exon⁶ with the other, carrying *Dscam1*²³, NP282-Gal4, UAS-FLP and UAS-mCD8::GFP, results in progenies with a lethal *Dscam1* null background (*Dscam1*^{21/23}). *Dscam1* null is rescued by the Exon⁶ construct. GFP-labeled cells driven by NP282-Gal4 possess FLP activity which leads to excision of Exon6 sequences from the *Dscam1* allele. This reduces the hypervariability of Exon6 from 18 down to 1.

The excision of Exon6 caused highly variable phenotypes (Fig. 26D+G). Here, I analyzed the phenotype in more than ten different animals. In all animals, the branching pattern of the HS cells dendrites appeared unusual compared to control or wild-type cells. Dendritic branches of HSE cells ran parallel to the dendritic border (Fig. 26E+H: arrows), some branches extended beyond their dendritic territorial area, others stopped before reaching the distal lobula plate border and sister branches were crossing each other, speaking for a lack of self-avoidance mechanism (Fig. 26E+H: red arrowheads). In HSN cells the later phenotype could also be observed (Fig. 26F+I). The branching density of HS cell dendrites, however, seemed not to be affected in *Dscam1* deficient animals. Notably, the observed phenotypes did not constantly occur altogether but varied in combination and frequency.

From the results, I could conclude that Exon6 diversity is most probably required to provide a robust system for self-avoidance in HS cell dendrites. One reason for the phenotype variability might be the developmental onset of the used Gal4 line and thereby relying FRT/ FLP activity. This will be discussed later on.

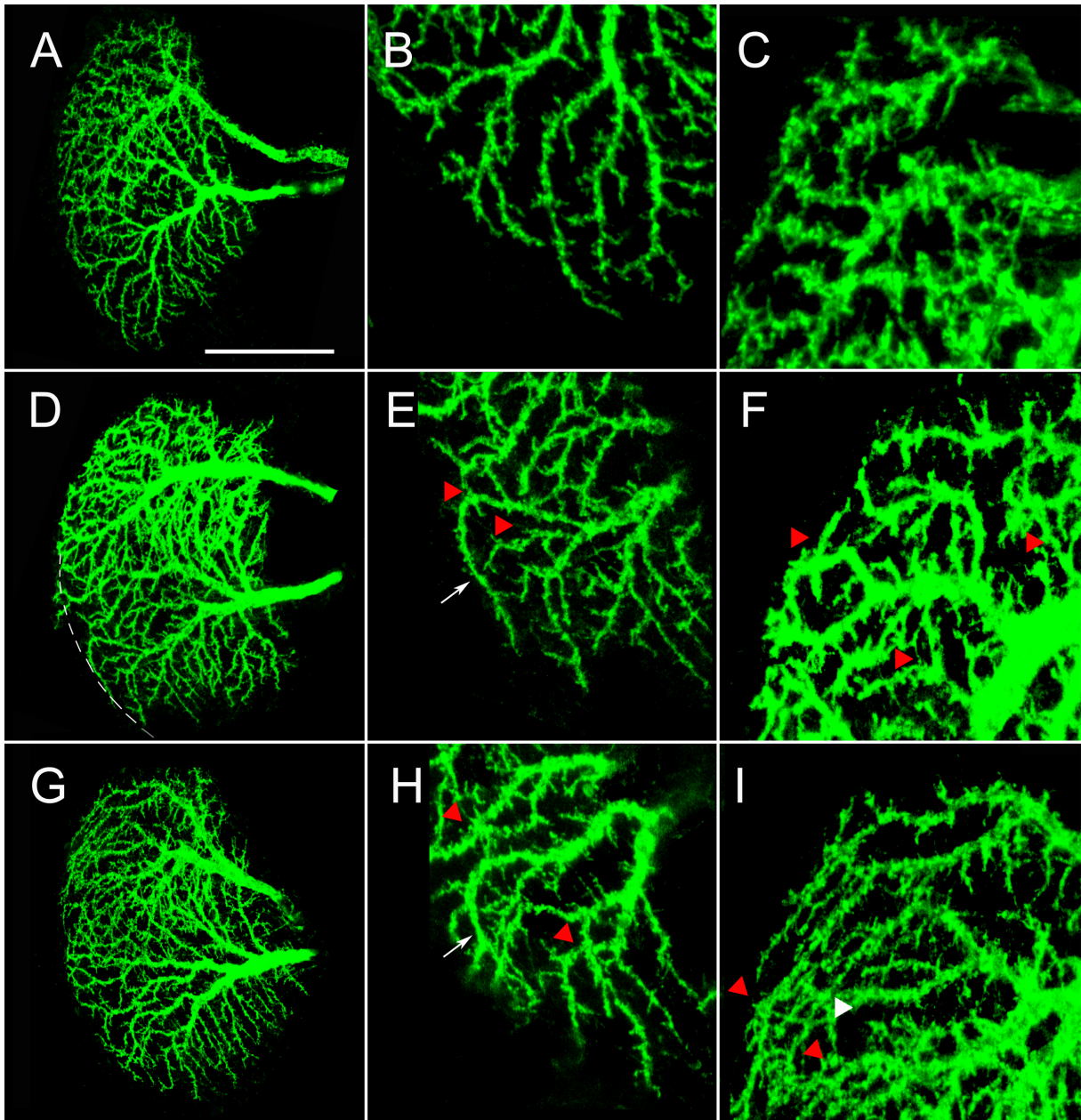


Fig. 26: Reduction of Exon6 variability.

(A) Control flies ($Dscam1^{23}$, $UAS-mCD8::GFP/ Dscam1^{21}$; $NP282-Gal4/ Exon6$) without FLP activity display a normal dendritic arborization pattern in HSE (B) and HSN (C), indifferent from wild-type ones. (D+G) Reduction of $Dscam1$ variability ($Dscam1^{23}$, $UAS-mCD8::GFP/ Dscam1^{21}$; $NP282-Gal4$, $UAS-FLP/ Exon6$) changes the dendritic branching pattern of HS cells. (D) HSE cells dendrites do not reach or exceed the distal lobula plate border (dashed line shows the border of the lobula plate). (E+H) Close up images of the distal regions of HSE cells reveal the presence of aberrant growth pathways (arrows) and self-crossings (red arrowheads). (F+I) Close up images reveal the same lack of self-avoidance in HSN cells (arrowhead). Confocal image stacks were taken with a z-increment of $0.2 \mu m$, a 63x objective and minimized pinhole. Composite images were generated by collapsing ~ 150 images; Close up images ~ 10 . Scale bar $50 \mu m$. Magnifications: 300% according to the scale bar in A.

4.1.4 Misexpression of single Dscam1 isoforms

Next, I used the the Gal4/ UAS system to perform gain-of-function experiments by misexpressing single Dscam1 isoforms in LPTCs. I used two different driver lines, NP282-Gal4 and DB331-Gal4 to express mCD8::GFP in LPTCs. All brain samples were immunolabeled with an antibody against GFP. This enhanced the expressed GFP signal, thus the fine terminal dendritic structures of HS cells were better visualized.

In a first series of experiments, I misexpressed six randomly chosen Dscam1 single isoforms in the expression pattern of NP282-Gal4: 1.30.30.1, 7.27.25.1, 2.9.19.2, 7.6.19.2, 11.31.25.1 and 1.34.30.2 + 1.6.19.2. The coding of single Dscam1 isoforms is built up of 6 constant domains and 4 different hypervariable exon domains that are individually spliced and assembled. The four numbers stand for the IG domains 2, 3, 7 and TM which are encoded by the corresponding exon clusters ectodomains and the last one that of the transmembrane domain. By visual inspection of the confocal images, only the misexpression of Dscam1 7.6.19.2 (Dscam1^{+7.6.19.2}) and Dscam1 11.31.25.1 (Dscam1^{+11.31.25.1}) resulted in severe alterations of the dendritic branching pattern of LPTCs. A major reduction in arborization density was present in Dscam1^{+7.6.19.2} cells leading to the assumption that higher order branches were missing (Fig. 27). Dscam1^{+11.31.25.1} cells were partially lacking the entire lateral areas of their dendritic fields (Fig. 28).

4.1.4.1 Dscam1^{+7.6.19.2}

Notably, when NP282-Gal4 was used as driver line (UAS-mCD8::GFP/ +; NP282-Gal4/ Dscam1^{+7.6.19.2}) the reproducibility of the gain-of-function phenotype was not constant but varied from animal to animal. In comparison to control flies (UAS-mCD8::GFP; NP282-Gal4), the misexpression phenotypes of Dscam1^{+7.6.19.2} cells ranged from wild-type branching pattern to “fishbone”-like dendritic tree with a very sparse branching pattern, in which secondary branches gave rise to only a very small number of higher order branches (Fig. 27B-D). Immunolabeling with α -Btx visualized the presence of nAChRs on the HS cell dendrites in control HS cells (Fig. 27M) and misexpression cell (Fig. 27N). In Dscam1^{+7.6.19.2} HS cells with a strong misexpression phenotype the receptor density seemed to be significantly reduced in the entire distal

area consistent with the lack of higher order branches. Whether remaining HS cell branches still possessed their functionality was tested with functional methods (s. discussion).

When DB331-Gal4 was used to misexpress $Dscam1^{+7.6.19.2}$ in LPTCs (Fig. 27F+H), then the penetrance of the phenotype grew from 20 to 80% (Fig. 27F) rose from 20% to 80%. Software based separation of VS and HS cells was applied to improve the visualization of the misexpression phenotypes. By using DB331-Gal4 (DB331-Gal4/ +; UAS-mCD8::GFP/ +; $Dscam1^{+7.6.19.2}$ / +) also provided the advantage to allow misexpression of $Dscam1^{+7.6.19.2}$ in VS cells and the observation of axonal trajectories (Fig. 27J). The misexpression showed the same effects in VS cells (Fig. 27H): Main and secondary branches were much thinner than in control flies (Fig. 27G+K), giving rise to only a small number of terminal branches (Fig. 27L). In comparison to control cells (Fig. 27I) the axonal pathways of VS and HS cells appeared not to be affected by $Dscam1^{+7.6.19.2}$ misexpression (Fig. 27J). Both axon bundles were reaching their destination areas in the central complex without showing any obvious projection errors.

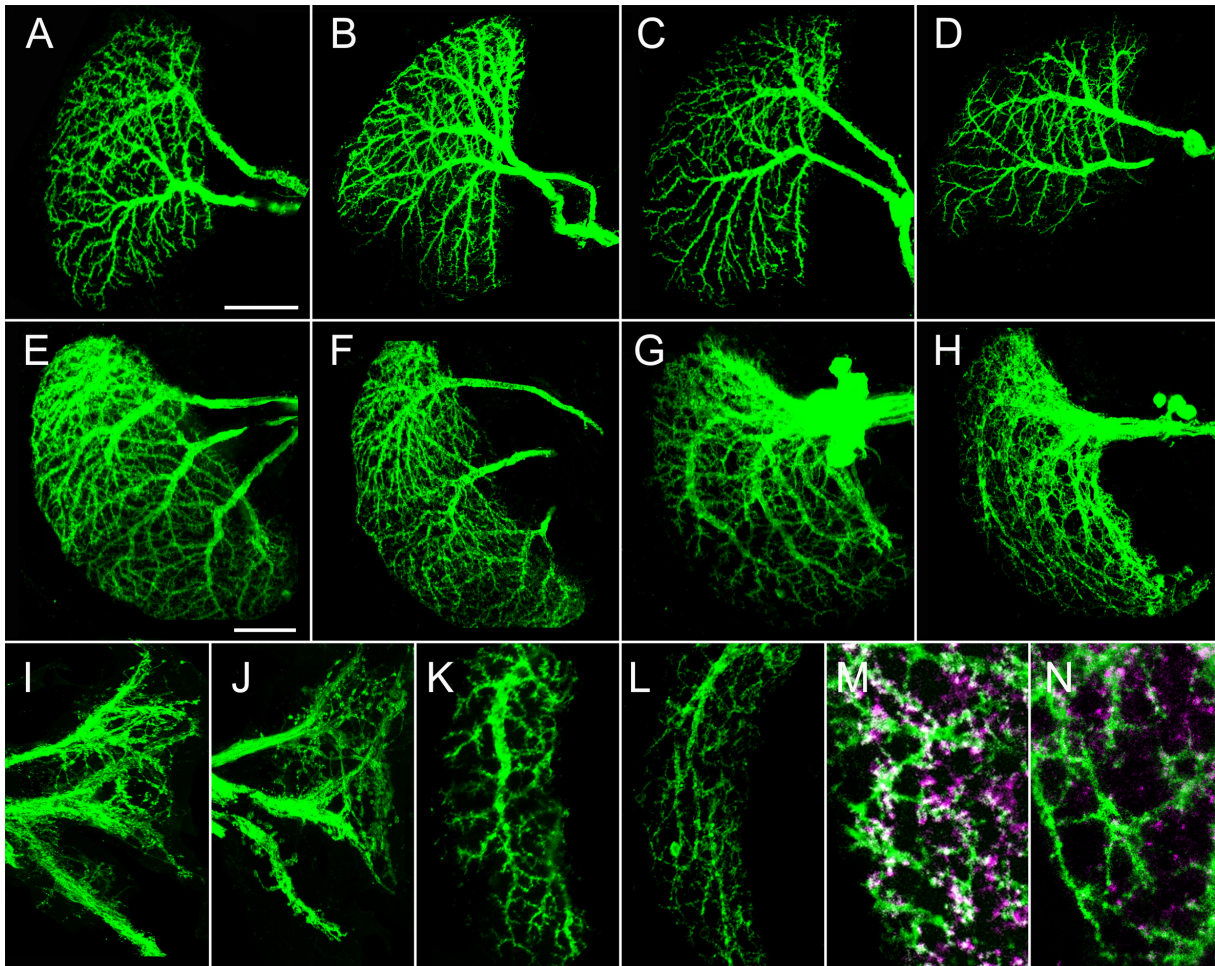


Fig. 27: Misexpression of $Dscam1^{+7.6.19.2}$.

(A) Control flies with GFP expression in HSN and HSE (UAS-mCD8::GFP; NP282-Gal4). (B-D) Misexpression of $Dscam1^{+7.6.19.2}$ (UAS-mCD8::GFP/ +; NP282-Gal4/ $Dscam1^{+7.6.19.2}$) reduces the branching density of HS cells. The number of missing branches strongly varies. The range goes from wild-type branching density to total lack of terminal branches. (E) Control HS cells separated from the expression pattern of DB331-Gal4. (F) DB331-Gal4 (DB331-Gal4/ +; UAS-mCD8::GFP/ +)(BI), $Dscam1^{+7.6.19.2}$ / +) increases the reproducibility of HS cells with severe reductions of higher order branches. (G) Control VS cells separated from the expression pattern of DB331-Gal4. (H) VS cells miexpressing $Dscam1^{+7.6.19.2}$ (separated from the DB331-Gal4 pattern) show the same phenotype as HS cells. (I) Control LPTC axons project to the peri-esophageal region of the central brain. (J) The axonal trajectories of the $Dscam1^{+7.6.19.2}$ LPTCs are not affected by the misexpression. (K+L) Close up images of VS dendrites of (K) control and (L) $Dscam1^{+7.6.19.2}$ cells. (M+N) Single section images of HS dendrites of (K) control and (L) $Dscam1^{+7.6.19.2}$ cells. (M+N) Immunolabeling with α -Btx visualizes the distribution of the remaining nAChRs in (M) control and (N) $Dscam1^{+7.6.19.2}$ HS cell dendrites (driver line: NP282-Gal4). Here, the distal regions of the HS cells are chosen for the comparison of the receptor densities. Confocal image stacks were taken with a z-increment of 0.2 μ m, a 63x objective and minimized pinhole. Composite images were generated by collapsing 10-150 images. Scale bars 50 μ m. Magnifications K+L: 200%, M+N: 300% according to the scale bar in E.

4.1.4.2 Dscam1^{+11.31.25.1}

Next, I wanted to analyze the misexpression phenotype of Dscam1^{+11.31.25.1}. When NP282-Gal4 was used as driver line then around 80% of flies (UAS-mCD8::GFP/ +; NP282-Gal4/ Dscam1^{+11.31.25.1}) had HS cell dendrites with missing terminal branches. Sometimes only rudimentary HSE dendrites remained. Notably, Dscam1^{+11.31.25.1} misexpression with NP282-Gal4 rarely affected both cells simultaneously, i.e. either HSN or HSE showed disorders in their dendritic branching pattern. By using DB331-Gal4 as driver line I obtained a constant misexpression phenotype in which all HS cells were affected (Fig. 28).

Immunolabeling with Dlg allowed me to visualize the borders of the neuropils in the fly visual system (background staining) and to evaluate the topological structure of dendritic arborization. In addition, my colleague Friedrich Förstner was supporting me by reconstructing the dendrites of HSN and HSE (Fig. 29). In control flies, cytosolic GFP was co-expressed additionally to the membrane tagged GFP (DB331-Gal4/ +; UAS-mCD8::GFP/ +; UAS-GFP_{cyto}/ +). This dual labeling resulted in a clearer outline of the dendritic arbors that enabled tracing of the fine dendritic processes. In Dscam1^{+11.31.25.1} flies, expression of membrane tagged GFP was sufficient as the HS cell dendrites appeared to be less dense than in wild-type flies. Based on the reconstructions of 10 HSN-HSE pairs of control animals and 8 HSN-HSE pairs of Dscam1^{+11.31.25.1} flies (Fig. 29A), we analyzed the branching pattern, position along the dorsal-ventral axis, laminar position, and coverage of HSN and HSE dendrites. The dendrites of wild-type HSN and HSE showed several characteristic branching features (Fig. 28A, Fig. 29A control). First, individual HS cell dendrites and dendritic branches strictly avoided self-crossing and occupied their territory in the lobula plate in the most efficient way. Second, their dendritic branching patterns were extraordinarily complex, and the consecutions of main, higher order and terminal branches densely covered the occupied territory reaching the outermost border of the lobula plate. Third, the dendrites of HSN and HSE did not tile the occupied territory of the lobula plate. They showed massive overlap: 90% of the territory was shared by HSN and HSE dendrites (Schnell et al., 2010). Despite a high frequency of crossing events between both cells, they strictly avoided fasciculation. Fourth, the dendritic arborizations of HS cells were restricted to the most-anterior layer of the lobula plate. The HS cell dendrites in Dscam1^{+11.31.25.1} flies (Fig. 28D) covered a far smaller territory in the lobula plate than in control flies (Fig. 28A). In particular, the small and

terminal branches were missing (Fig. 28I). This caused a reduction of their dendritic spanning fields (Fig. 29B) and overlap areas (Fig. 29C). Spanning fields of HSN dendrites were reduced from 38% to 25% coverage of the lobula plate. Spanning fields of HSE dendrites were reduced from 60% to 35% coverage of the lobula plate. The dendritic overlapping area was significantly reduced from 2,695 μm^2 to 936 μm^2 . The loss of mostly terminal branches resulted in a gap in the coverage of the lateral lobula plate whereas the medial area was still occupied by the dendrites.

Similar observations could be done in VS cells (Fig. 28E). Their dendrites covered far smaller areas of the lobula plate. The distal area of the lobula plate was totally missing VS cell dendrites. Close up images of VS1 revealed the reduction of terminal branches (Fig. 28H).

In accordance with previous observations, the dendritic branching phenotype varied from animal to animal and between each hemisphere. Immunolabeling with α -Btx revealed clusters of nAChRs at the dendritic terminals (Fig. 28J), which might point to local accumulations of presynaptic input elements.

In contrast to $Dscam1^{+7.6.19.2}$, misexpression of $Dscam1^{+11.31.25.1}$ (DB331-Gal4/ +; UAS-mCD8::GFP/ +; $Dscam1^{+11.31.25.1}$ / +) severely disrupted the axonal trajectories (Fig. 28F+G). In some animals, the HS cell axons displayed a large number of single fibers which separated from the main axon bundle before they reached their destination area in the central brain (Fig. 28G arrows). In addition, some axon bundles innervated wrong areas inside the central complex; others did not run directly to their destination areas but showed aberrant trajectories. The axonal phenotypes occurred were highly reproducible (n=10 each stock).

Here, I concluded that the misexpression of the two depicted $Dscam1$ isoforms had different influences on axonal projections and dendritic branching pattern. In which way the TM domain had influences on the phenotype needs to be discussed. Functional studies have been carried out and the results are described in the discussion.

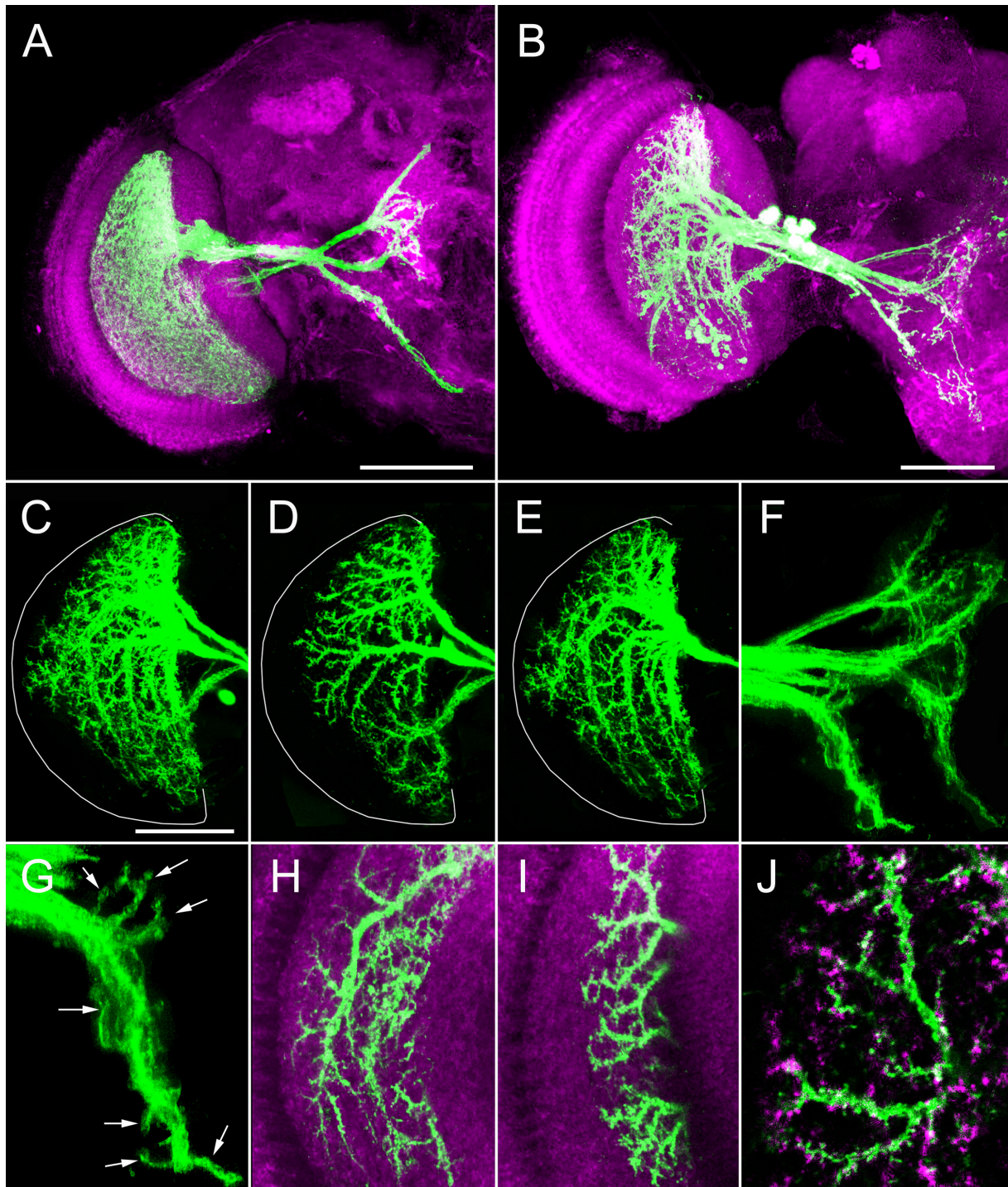


Fig. 28: Misexpression of $Dscam1^{+11.31.25.1}$.

Determination of dendritic branching pattern of $Dscam1^{+11.31.25.1}$ LPTCs. The neuromuscular system is visualized by immunolabeling of Dlg (magenta). HS and VS cells express membrane tagged GFP (green). Overview images of (A) control LPTCs (DB331-Gal4/+; UAS-mCD8::GFP/+) and (B) $Dscam1^{+11.31.25.1}$ LPTCs. (C) Misexpression of $Dscam1^{+11.31.25.1}$ driven with DB331-Gal4 (DB331-Gal4/+; UAS-mCD8::GFP/+; $Dscam1^{+11.31.25.1}/+$). (D) HS cells and (E) VS cells separated from the DB331-Gal4 expression pattern. Both cell types show a decrease in dendritic branching complexity and missing lateral branches. The distal area of the lobula plate is not covered anymore by their branches. (F) LPTC

axons in *Dscam1*^{+11.31.25.1} misexpression flies. (G) Close up image of the HS axon bundle points to single axon fibers separating from the main axon bundle before they reach their destination area in the central brain (arrows). Close up images of the distal lobula plate regions visualize the lack of lateral (H) HS and (I) VS cell dendrites. The higher order and terminal dendritic branches are completely. (J) Immunolabeling with α -Btx shows the distribution of nAChRs on the remaining HS cell dendrites. The antibody staining reveals clusters of nAChRs on the dendritic tips. Confocal image stacks were taken with a z-increment of 0.2 μ m, a 63x objective and minimized pinhole. Composite images were generated by collapsing 30-150 images. Scale bars 100 μ m. Magnifications G-I: 170%, J: 300% according to the scale bar in C.

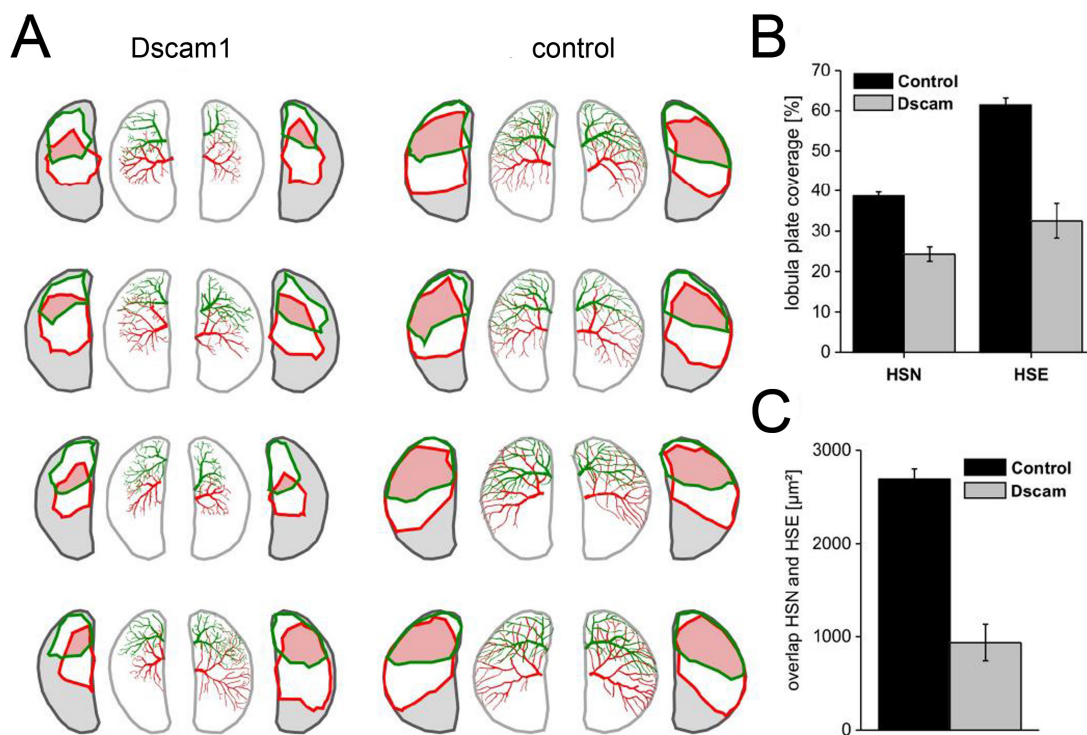


Fig. 29: Computer based analysis of the *Dscam1*^{+11.31.25.1} phenotype.

(A) 8 pairs of HSN (green) and HSE (red) main dendritic branches were reconstructed from 10 control flies (DB331 Gal4/ +; UAS-mCD8::GFP/ +; UAS-GPFcyto/ +) and *Dscam1*^{+11.31.25.1} flies (DB331-Gal4; UAS-mCD8::GFP/ Bl; *Dscam1*^{+11.31.25.1} / +). The lobula plate borders are illustrated in grey. The approximated coverage areas in the lobula plate are shown in green for HSN and in red for HSE cell dendrites. The overlap areas in which outlines of HSN and HSE cell dendrites share a common territory are marked in red. In those overlap areas heteroneuronal interactions between both cell dendrites might take place. (B) Analysis of lobula plate coverage areas demonstrates that misexpression of *Dscam1*^{+11.31.25.1} causes a reduction of about 35% in HSN cell dendrites (from 38% to 25%) and in HSE cell dendrites of about 42% (from 60% to 35%). (C) Analysis of the overlap areas of HSN and HSE cell dendrites reveal expected results. In control flies, both dendrites overlap in an area of 2,695 μ m² that is more than 90% of the entire dendritic area of the cell. In *Dscam1*^{+11.31.25.1} flies, this

overlap area is strongly reduced to a value of $936 \mu\text{m}^2$. Reconstruction data and analysis were kindly provided by Friedrich Förstner.

4.1.4.2.1 Horizontal connectivity

In addition to the dendritic processing of retinotopically organized input from presynaptic elementary motion detectors HS cells are coupled via gap junctions (Schnell et al., 2010). Misexpression of $\text{Dscam1}^{+11.31.25.1}$ caused a strong reduction of dendritic fields in HS cells and with that also their overlapping territories where the horizontal information flow might happen. As it is still elusive where exactly HS cells connect to each other, we wanted to observe whether this connectivity was still present in $\text{Dscam1}^{+11.31.25.1}$ cells. We used NP282-Gal4 as driver line to drive expression in HSN and HSE cells in the lobula plate. Following experiment was then carried out by Bettina Schnell. She injected neurobiotin, a dye that passes gap junctions, with a sharp electrode into the cellbody of a HS cell. The dye revealed that all 3 HS cells were still connected via gap junctions in $\text{Dscam1}^{+11.31.25.1}$ flies (Fig. 30) despite the decreased dendritic field of the HSE cell.

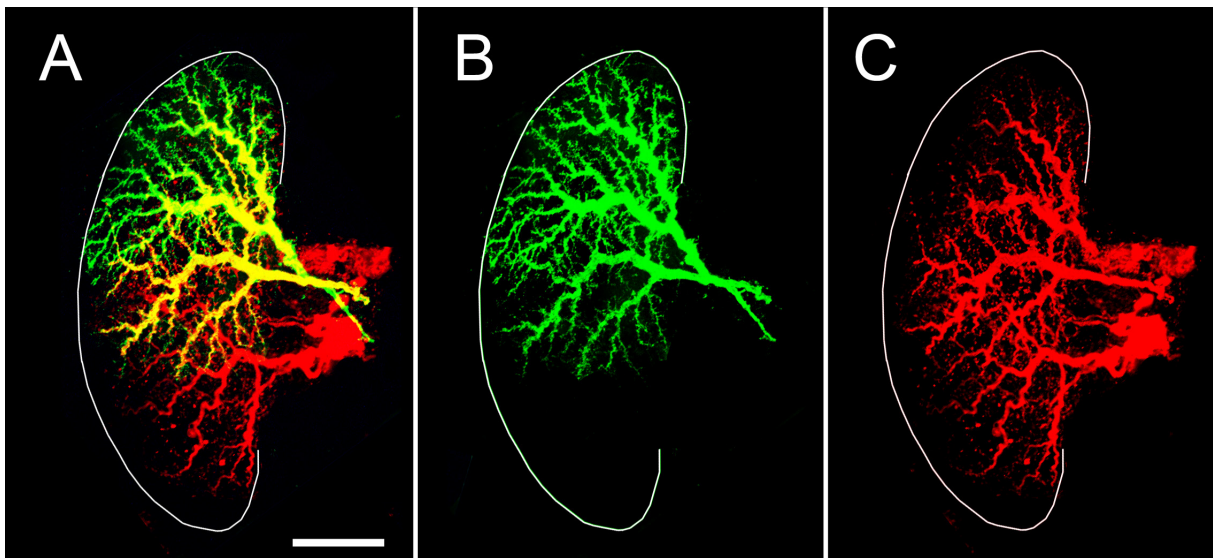


Fig. 30: Electric coupling between $\text{Dscam1}^{+11.31.25.1}$ HS cells.

(A) HSN neuron was filled by a sharp electrode with neurobiotin (red) in $\text{UAS-mCD8::GFP; NP282-Gal4/ Dscam1}^{+11.31.25.1}$ flies. (B) GFP labeled HSN and HSE neurons are illustrated in green. The HSE cell dendrite has a decreased dendritic field whereas the dendrites of the HSN cell reach the distal border of the lobula plate (dashed line). (C) Neurobiotin was spreading from the initial injected cell into neighboring HS cells thereby revealing an intact electrical coupling between them. Confocal image

stacks were taken with a z-increment of 0.2 μm , a 63x objective and minimized pinhole. Composite images were generated by collapsing ~ 100 images. Scale bar 50 μm .

4.1.4.2.2 MARCM analysis

In the following, I wanted to observe whether the gain-of-function phenotype was promoted by heteroneuronal Dscam1 interactions between HSN and HSE cells, between HS cells and columnar neurons or by cell autonomous effects between sister branches. If Dscam1^{+11.31.25.1} acted cell autonomously in HS cells then single cell clones should show a Dscam1^{+11.31.25.1} phenotype independent from the wild-type surrounding. Alternatively, if single Dscam1^{+11.31.25.1} cells did not show an aberrant phenotype, then this would suggest that the Dscam1^{+11.31.25.1} mediated phenotype results from repulsive interaction between different HS neurons or between HS neuron and yet unidentified cells.

Here, I applied the MARCM technique in order to drive misexpression in single cells in a otherwise control background. Immunolabeling with Dlg allowed me to visualize the outline and the size of the lobula plate and to evaluate the topological structure of dendritic arborization. The HSN cell with Dscam1^{+11.31.25.1} misexpression did not show the characteristic lack of distal arborizations (Fig. 31). The dendritic morphology resembled that of wild-type HSN cells: The terminal branches of the dendritic tree reached up to the distal border of the lobula plate, the branches were evenly tiling the northern territory of the lobula plate and also the degree of ramifications resembled that of wild-type cells (Fig. 31B). The axons appeared also to be normal in their trajectory and targeting area (Fig. 31C). This result can be explained by the fact that sister branches of HS cells never cross each other and thus, misexpressed isoforms could not affect their dendritogenesis. In line with that result are studies in the MB, which reported that expression of single Dscam1 isoforms in a cohort of MB neurons is able to induce dominant phenotypes, while expression of a single isoform in a single cell cannot (Zhan et al., 2004).

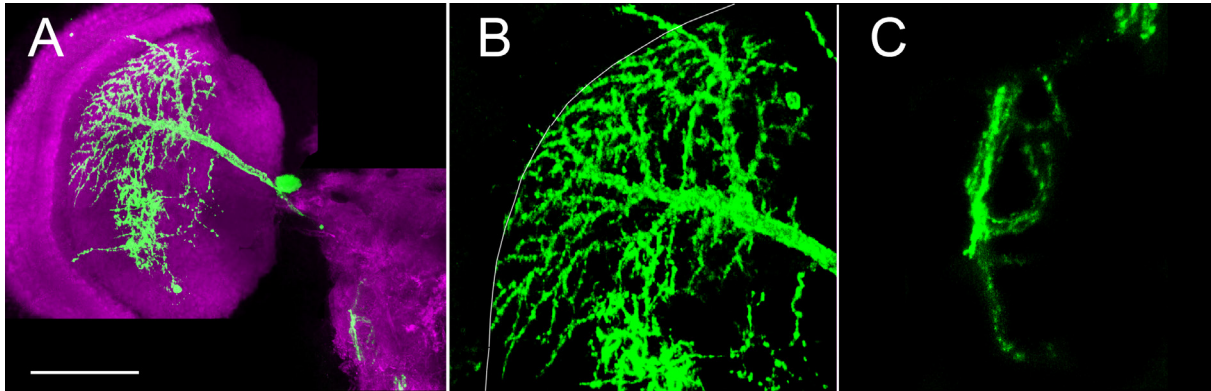


Fig. 31: Misexpression of $Dscam1^{+11.31.25.1}$ in a single HSN cell.

(A) Overview image of single GFP labeled HSN cell with $Dscam1^{+11.31.25.1}$ misexpression (green) shows no morphological changes neither in the dendritic arborization pattern (B) nor in the axonal pathway (C). DB331-Gal4 was used as driver line and mCD8::GFP to label cells. The neuropile is visualized by immunolabeling of Dlg (magenta). The border of the lobula plate is depicted with the line in B. Confocal image stacks were taken with a z-increment of 0.2 μm , a 63x objective and minimized pinhole. Composite images were generated by collapsing ~150 images. Scale bar 100 μm . Magnifications in B+C: 220% according to the scale bar in A.

4.1.4.2.3 Time-point analysis

So far, only little is known about the mechanisms for promoting dendritic organization of LPTCs. Based on previous studies, LPTCs are known to arise in L3 larvae (Scott et al., 2002). I started to observe the morphological dendritogenesis of wild-type LPTCs at three distinct developmental timepoints: L3, P35 (35 hours after puparium formation) and P50 (50 hours after puparium formation). Based on the localization within the lobula plate and cell body diameter (Geiger and Nässel, 1981) I could identify the LPTCs. At L3, I observed fluorescently labeled cells with short diversely oriented neurites. There was a central cluster of cell bodies present from which neurites were outgrowing. At P35, secondary branches appeared, however the overall dendritic trees of LPTCs were relatively sparse. At P50, the main branches reached the distal layers of the lobula plate and thus covering their final territories. In addition, the branching pattern occurred much denser.

Here, I hypothesized that HS cells possess different $Dscam1$ isoforms regulating the pathway finding of LPTC dendrites. Therefore, misexpression of single $Dscam1$ isoforms should only affect dendritic growth before P50 but not at later time-points when refinement of the branching pattern occurs.

To observe the developmental timepoints when $Dscam1^{+11.31.25.1}$ has an influence on the dendritic outgrowth and pathway finding in HS cells, following transgenic flies were generated: DB331-Gal4/ +; tub-Gal80^{ts}/ UAS-mCD8::GFP; $Dscam1^{+11.31.25.1}$ / TM6. Here, temperature sensitive tub-Gal80 (tub-Gal80^{ts}) was used to control Gal4 activity. As long as the flies were kept at 18°C, Gal80^{ts} inhibited Gal4. Therefore, flies were developing under wild-type conditions at 18°C. By shifting the temperature to 30°C, Gal80^{ts} became inactivated and Gal4 activated. With that, the onset of $Dscam1^{+11.31.25.1}$ misexpression was triggered to different developmental stages of the fly. The temperature shift was implemented at L3, ~P35, and ~P50; Flies were observed in adulthood. If different $Dscam1$ isoforms were regulating pathway finding during the dendritogenesis of HS cells, then the phenotype depends on the temporal onset of $Dscam1^{+11.31.25.1}$ misexpression.

The characteristic $Dscam1^{+11.31.25.1}$ phenotype in LPTCs could be found when the misexpression was induced at L3 (Fig. 32A+B) and ~P35 (Fig. 32E+F). However, when the timepoint of misexpression was shifted to P50 or later, then the dendrites retained the wild-type morphology (Fig. 32I+J). Control flies (DB331-Gal4/ +; UAS-mCD8::GFP/ CyO; +/- TM6) were accordingly heatshock treated at L3 (Fig. 32C+D), P35 (Fig. 32G+H) and P50 (Fig. 32K+L). The morphologies of LPTCs resembled those of wild-type cells. Intriguingly, misexpression induced at P35 elicited a stronger phenotype with increased reductions of the lateral dendritic arbors than at L3 stage. These observations led to the conclusion that $Dscam1^{+11.31.25.1}$ misexpression was not able to process neurite repulsion once the main branches established their final patterning.

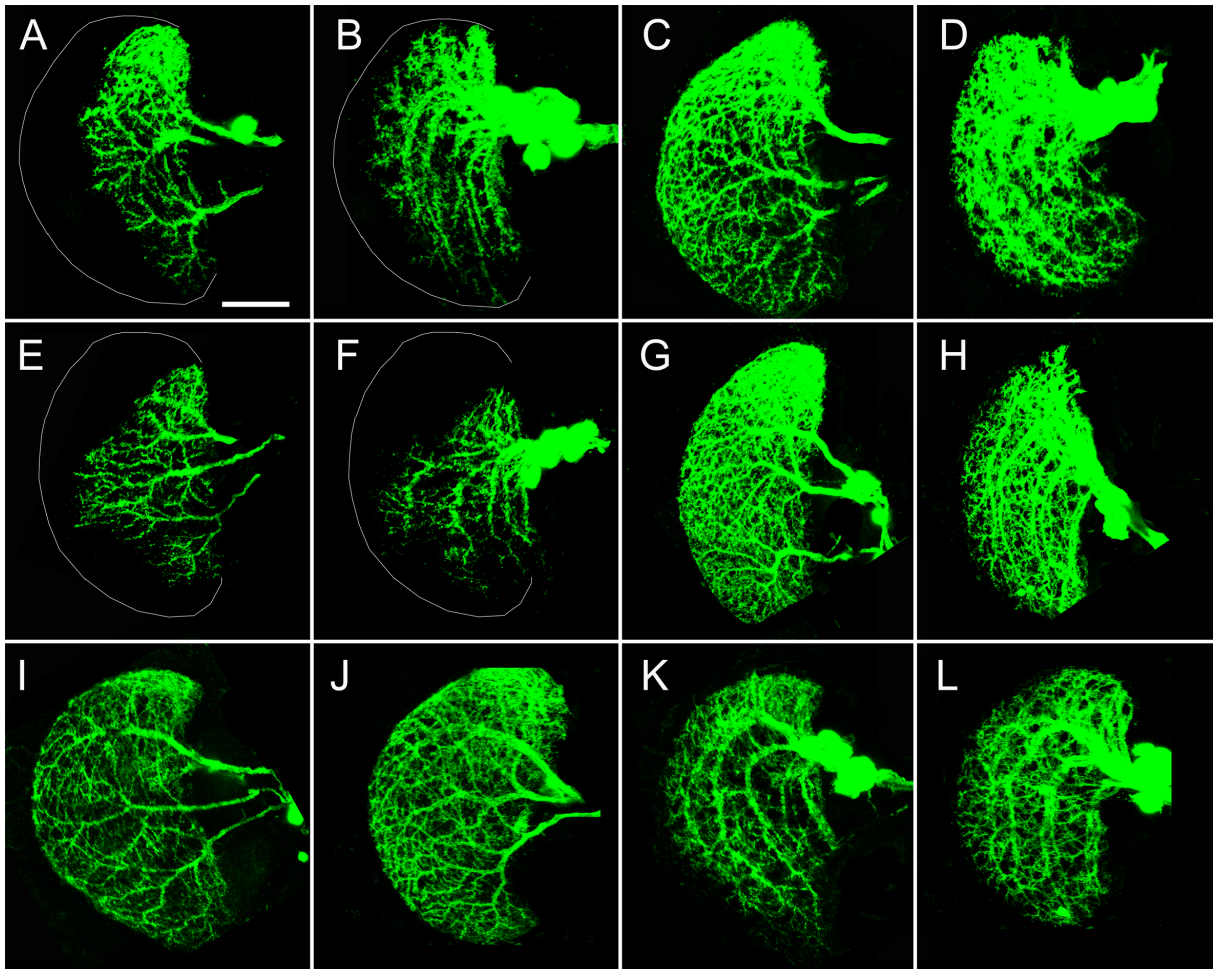


Fig. 32: Time-point analysis of the $Dscam1^{+11.31.25.1}$ phenotype.

By using temperature sensitive $Gal80^{ts}$ activity, the onset of $Dscam1^{+11.31.25.1}$ misexpression was triggered to different developmental stages of the fly (DB331-Gal4/ +; tub-Gal80^{ts}/ UAS-mCD8::GFP; $Dscam1^{+11.31.25.1}$ / TM6). Temperature shift to 30°C was implemented at 3 different developmental stages: (A-D) at L3, (E-H) at ~P35 and (I-L) at ~P50. (C+D; G+H; K+L) Control animals (DB331-Gal4/ +; UAS-mCD8::GFP/ CyO; +/- TM6) were treated accordingly. The expression patterns of $Dscam1^{+11.31.25.1}$ and control cells were analyzed from adult flies. (A+E) HS and (B+F) VS cells display the characteristic misexpression phenotype: Their dendritic fields are much smaller compared to (C+G) HS and (D+H) VS cells in control flies. The lobula plate borders are depicted with lines. (I+J) However, when the onset of misexpression is triggered to P50 and later then the terminal branches of HS and VS cell dendrites extend to the lateral border of the lobula plate just like the LPTCs from (K+L) control animals. Confocal image stacks were taken with a z-increment of 0.2 μm , a 63x objective and minimized pinhole. Composite images were generated by collapsing ~150 images. Scale bar 25 μm .

4.1.4.2.4 Misexpression in T4/ T5 cells

HS cells with *Dscam1*^{+11.31.25.1} misexpression had reduced dendritic fields but did not tile at the overlapping areas. One reason could be that the phenotype was not caused by *Dscam1* interactions between HS-HS cells but interactions between HS-T4/ T5 cells. Here, I wanted to observe the morphological changes when *Dscam1*^{+11.31.25.1} was misexpressed in both, LPTCs and columnar T4/ T5 cells. I suspected that if *Dscam1* contributes to the formation of neuronal connectivity between both cell groups then *Dscam1*^{+11.31.25.1} misexpression might elicit a stronger dendritic phenotype in HS cells, while axon terminals of T4/ T5 might avoid synapsing on remaining dendrites.

I used R54A03-Gal4 as a driver line and GFP as cell marker. R54A03-Gal4 provides a highly specific expression pattern of only T4/ T5 cells and LPTCs. Immunolabeling with Dlg allowed me to visualize the outline of the neuropils in the fly visual system.

In order to highlight presynaptic terminals of T4 and T5, I co-expressed a presynaptic marker synaptotagmine-HA (generously provided by Andreas Prokop), a calcium sensor that regulates neurotransmitter release in axon terminals which has been engineered to express human influenza hemagglutinin (HA) (*UAS-synaptotagmine-HA/+; UAS-mCD:8-GFP/+; R54A03/+*). The HA-tag has never been reported to interfere with the bioactivity or the biodistribution of the recombinant protein but facilitates its detection. Fluorescent labeling was done with anti-HA conjugated with Alexa Fluor 568. In accordance with previous descriptions (Fischbach and Dittrich, 1989; Bausenwein et al., 1992), the dendrites of T4 occupied the most proximal layer of the medulla (Fig. 33A-C asterisk) and those of T5 cells the posterior layer of the lobula (Fig. 33A-C arrow). Their axonal projections terminated in all four neuropile layers of the lobula plate and thus, co-located with the dendrites of VS and HS cells. Close up images from horizontal sections as well as frontal sections show overlap areas between GFP-labeled LPTC dendrites in green and synaptotagmine-labeled T4/ T5 axon terminals in magenta (Fig. 33C).

In the next step, I used R54A03-Gal4 to misexpress *Dscam1*^{+11.31.25.1} in T4/ T5 and LPTCs (*UAS-mCD:8-GFP/+; R47H07-Gal4/ Dscam1*^{+11.31.25.1}). The dendritic branches of HS cells showed a similar phenotype as observed in previously described misexpression experiments. HS cell dendrites had smaller dendritic fields with a gap towards the distal lobula plate border, reduced branching density, and

decreased overlapping territories (Fig. 33D). To validate this observation, I repeated this misexpression experiment with a further driver line: R35F02-Gal4. Repeatedly I observed the same phenotype in HS cells.

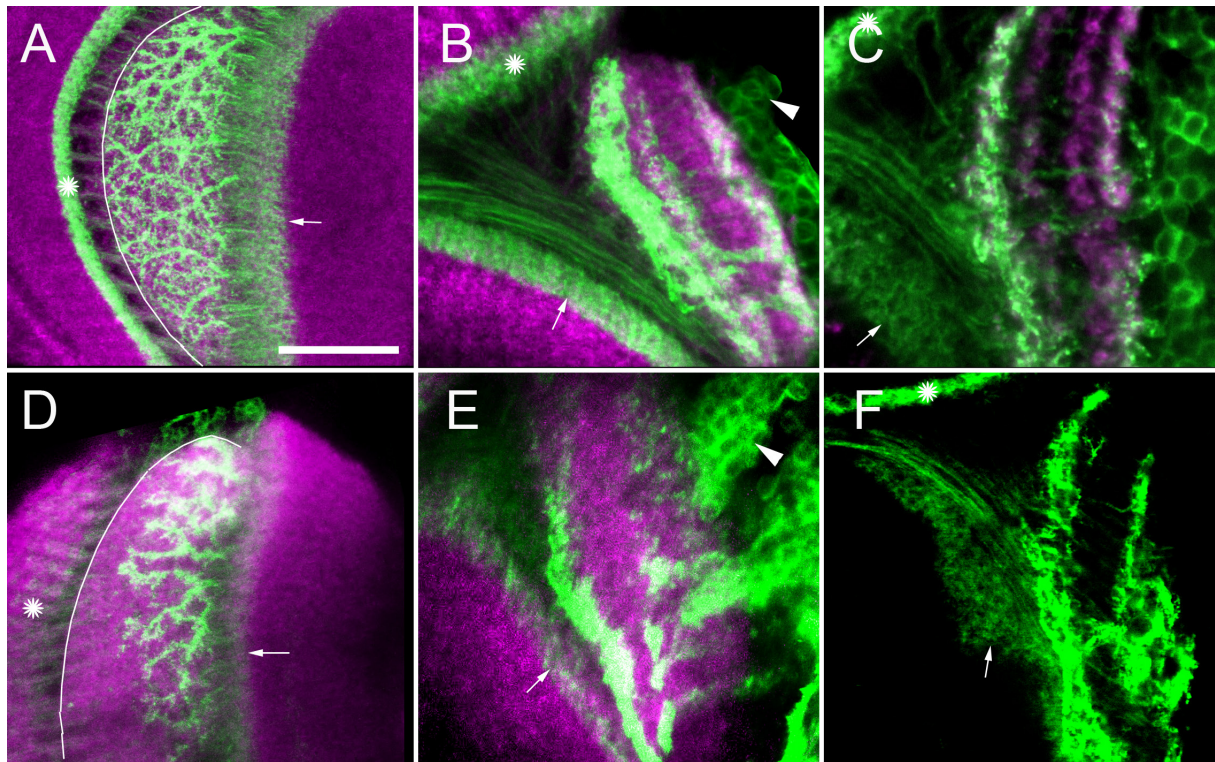


Fig. 33: Misexpression of $Dscam1^{+11.31.25.1}$ in T4/ T5 cells.

(A-C) Control cells (UAS-mCD:8-GFP/+; R54A03-Gal4/+). The neuropiles are visualized by immunolabeling of Dlg (magenta). (A) Frontal section shows the ramification areas of T4/ T5 cells in the medulla (asterisk), the lobula, where they overlap with the dendrites of LPTCs, and the lobula (arrow). (B+C) Horizontal sections. The soma of T4 and T5 neurons are evenly distributed next to the lobula plate (arrowhead). The axons of T4/ T5 cells ramify in the medulla layer 10, in the superficial most lobula layer and in all four layers of the lobula plate, thereby exhibiting potential interactions to LPTCs. (C) The axon terminals of T4/ T5 cells are highlighted in magenta by expressing an additional presynaptic marker, synaptotagmine-HA (UAS-synaptotagmine-HA/+; UAS-mCD:8-GFP/+; R54A03-Gal4/+) and immunolabeling with a secondary fluorescent antibody. (D-F) Misexpression of $Dscam1^{+11.31.25.1}$ in LPTCs and T4/ T5 cells (UAS-mCD:8-GFP/+; R54H03-Gal4/ $Dscam1^{+11.31.25.1}$). (D) Frontal section reveals that misexpression of $Dscam1^{+11.31.25.1}$ leads to reduced arbor sizes in HS cell dendrites and disruptions in axonal targeting in T4 and T5 cells. The border of the lobula plate is depicted with a line. (E) T4/ T5 cell axons do not terminate in an ordered fashion within defined layers of the medulla (asterisk), lobula (arrow) and lobula plate. Moreover, the cellbodies of T4 and T5 cells are forming clusters (arrowhead). Confocal image stacks were taken with a z-increment of 0.2 μm , a 63x objective and minimized pinhole. Composite images were generated by collapsing ~ 20 images. Scale bar 20 μm .

Misexpression of $Dscam1^{+11.31.25.1}$ elicited in T4 and T5 neurons severe axonal misprojections. The four target layers in the lobula plate were not innervated in a structured way but randomly whereas the ramifications in the lobula and medulla were only partially mislocated (Fig. 33D-F asterisk and arrow). Intriguingly, the cellbodies of T4 and T5 were forming clusters (Fig. 33E arrowhead). For unknown reason it was not possible to co-express synaptotagmine-HA with $Dscam1^{+11.31.25.1}$ in both cell groups. Due to the lack of a specific Gal4 driver line that gives an expression only in T4 and T5 cells, I was not able to misexpress $Dscam1^{+11.31.25.1}$ restrictively in those columnar cells. Whether the $Dscam1^{+11.31.25.1}$ phenotype in T4/T5 cells was a result from interactions within columnar neurons or with LPTCs remains to be elucidated.

4.2 RicinA induced ablation of LPTCs

LPTCs are speculated to be part of the optomotor pathways in flies. So far, studies were done on mutant flies missing the entire subgroups of LPTCs (Heisenberg, 1971; Heisenberg and Götz, 1975; Heisenberg and Buchner, 1977; Heisenberg et al., 1978; Warzecha et al., 1993). Photoablation of single LPTCs was done in the blowfly thereby unraveling individual cell functions, cell-cell connectivities and underlying mechanisms of optomotor responses (Kalb et al., 2006; Warzecha et al., 1993; Farrow et al., 2005). However, due to the small size of *Drosophila* neurons ablation by illumination is not feasible. Here, I used an available fly line in which RicinA is genetically encoded (UAS>Stop>RicinA: generously provided by L. Luo). A Stop codon flanked by FRT sites is in front of the transgene. Temporal control was therefore achievable by using hs-FLP, whose activity was induced by temperature shift. My aim was to establish a heatshock protocol to specifically ablate single LPTCs in RicinA flies. Here, DB331-Gal4 was chosen to drive expression in LPTCs (DB331/ +; hsFLP/ UAS>Stop>RicinA, UAS-mCD8::GFP) and thus, to label surviving neurons. The remaining expression pattern was then compared to that of control flies (DB331-Gal4/ +; UAS-mCD8::GFP/ CyO) which were heatshock treated the same way like RicinA flies. The morphology of control cells remained unaffected.

Due to the early onset of the DB331-Gal4, it was possible to observe GFP expression in all larval stages. Hence, the probability was high that the expression time of the driver line coincides with the developmental onset of LPTC progenitor cells. In the first step, I determined the exact time point when the progenitor cells of LPTCs became detectable during development. For that, flies of the stock DB331-Gal4; UAS-mCD8::GFP were analyzed via confocal imaging at different developmental stages. By looking at the localizations within the lobula plate, I could identify the LPTCs. In late L3, the cell bodies of LPTCs were detectable for the first time. However, the number of the observed cell bodies was less than in the adult stages, leading to the assumption that there was a successive development of different LPTCs. Flies in the white pupal stage have already developed rudimentary LPTC neurites (s. 3.2.4.1). The branches of HS cells were particularly identifiable in later stages.

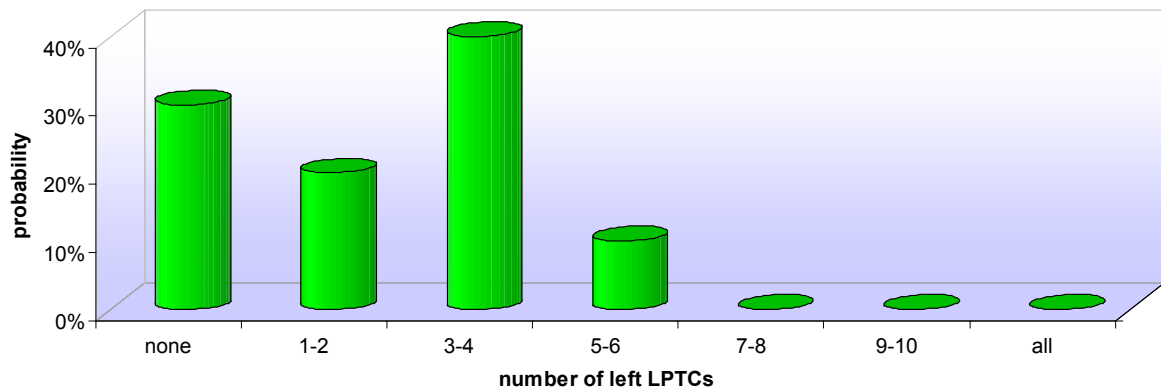


Fig. 34: Statistical analysis of the ablation rate.

The scheme depicts the statistical distribution of the number of ablated LPTCs. In the examined flies, more than 40% of the examined flies showed a reduction of LPTCs down to 3-4 remaining LPTCs, around 20% possessed 1 or 2 and around 10% 5 or 6 remaining LPTCs. Around 30% had a total loss of LPTCs. None of the flies had more than 7 remaining LPTCs.

Based on these results, I developed a heatshock protocol to trigger RicinA expression in single LPTCs (s. methods 3.2.4). In accordance with the previous experiment, I experienced that the best time point for the temperature shift was at late L3 stage. Notably, when heatshock was induced in L3 then the ablation efficiency rate rose to 100%. For further analysis of the ablation efficiency, confocal images were taken in adult stages and the numbers of remaining LPTCs counted for each optical lobe. There were no flies lacking less than 50% of LPTCs. Mostly 3-4 remaining LPTCs were detectable. Furthermore, in 30% of all analyzed optical lobes, no LPTCs were left at all (Fig. 34). The number and the types of remaining LPTCs varied from animal to animal (Fig. 35 C-G). Intriguingly, there were also differences in the remaining expression pattern between left and right hemisphere of the same fly (Fig. 35 E+F).

Heatshock treatment in later pupal stages and in adult flies, resulted in no ablation of LPTCs. These experiments demonstrated that the flip-out did not work in post-mitotic cells.

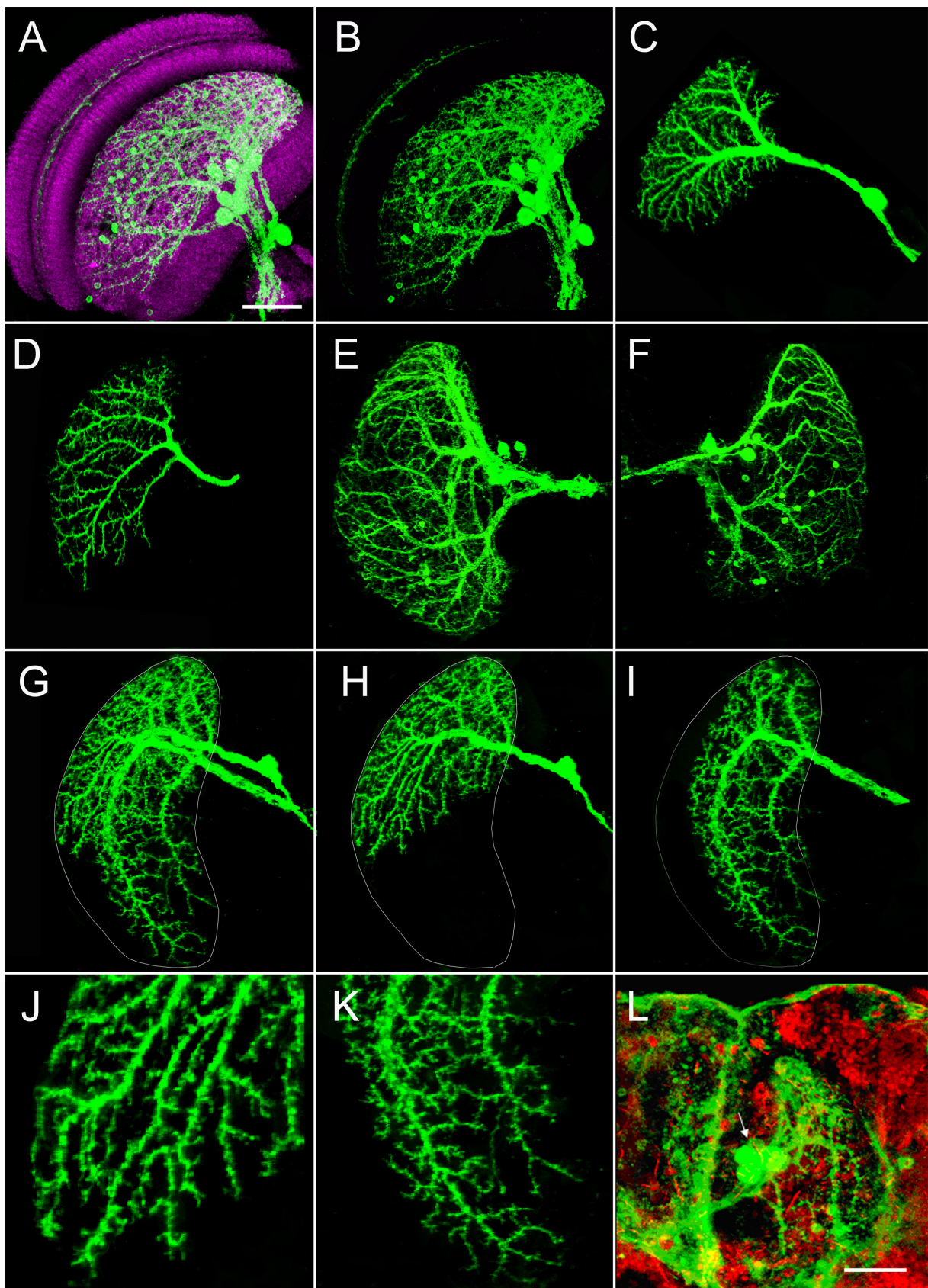


Fig. 35: Expression patterns after RicinA induced ablation.

The images demonstrate the efficiency of RicinA ablation in LPTCs with the developed heatshock protocol. Depending on the cell type, progenitor cell or non-mitotic cell, in which RicinA is initially

induced, the number of surviving LPTCs decreases to a single LPTC. The driver line DB331-Gal4 is used to label the LPTCs with mCD8::GFP (green). (A+B) Control cells (DB331-Gal4/ +; UAS-mCD8::GFP/ CyO). The neuropiles are visualized by immunolabeling of Dlg (magenta). (C-G) Heatshock treated RicinA flies (DB331/ +; hsFLP/ UAS>Stop>RicinA, UAS-mCD8::GFP). The neurons are displayed in the relative position within the brain, i.e. left and right hemispheres are not oriented in the same direction. Only (C) HSN cell and (D) Lpt1 cell escaped from RicinA ablation. (E+F) There differences in cell ablation efficiency between both hemispheres within one RicinA fly. The left hemisphere has less remaining LPTCs than the right one. (G) A small subset of LPTCs escaped from RicinA ablation. Software based separation of HS and VS cell layer reveals the identity of the remaining cells: (H) HSN and (I) VS5. The border of the lobula plate is depicted with a line. (J+K) Close up images of the dendritic branches show that their detailed anatomies are indifferent from those described in literature. (L) Cell vitality test with PI (red) proves that the remaining LPTCs of the DB331-Gal4 expression pattern are healthy. The dye is not able to perfuse into the healthy cell soma (arrow) and thus, reveals intact cell membranes. Confocal image stacks were taken with a z-increment of 0.2 μm , a 63x objective and minimized pinhole. Composite images were generated by collapsing ~ 60 images. Scale bar in A-I 50 μm and in L 100 μm . Magnifications in J+K: 290% according to the scale bar in A.

By visual inspection, the remaining LPTCs showed wild-type morphologies consistent with the descriptions from previous studies (Fischbach and Dittrich, 1989; Joesch et al., 2008). Nevertheless, in order to prove this assumption, a cell vitality test was performed. Here, PI was used as a fluorescent, intercalating agent for DNA staining (s. 3.2.4.3). In viable cells, PI could not pass the cell membrane whereas, in dead cells or non-vital cells, the protein synthesis was interrupted and with that, PI could pass through the porous membrane. In all tested brains, no overlap of PI with GFP positive LPTCs was detectable (Fig. 35L arrow), proving that the remaining neurons were not affected by RicinA expression in neighboring neurons.

In this study, I showed that genetically encoded RicinA was a powerful tool to ablate subgroups of cells in *Drosophila* without affecting cell vitality of neighboring neurons. The elaborated heatshock protocol paves the way for future behavioral studies in which the function and importance of individual LPTCs for optomotor response can be investigated. Preliminary functional studies have been carried out and the results are described in the discussion.

4.3 Refined expression pattern of TN-XXL

TN-XXL represents an efficient tool for the analysis of activities in neurons (Mank and Griesbeck, 2008). However, using this indicator under the control of the UAS system requires Gal4 driver lines with a highly restricted expression pattern in order to recognize the cell region from which the recording was made. I tried to solve this problem by generating fly strains carrying a construct with a FRT flanked Stop sequence for spatial restriction of TN-XXL expression (Ro and Rannala, 2004). The Stop sequence prohibited translation of the downstream-located TN-XXL sequence. Here, flippase activity induced site-directed recombination of FRT sites leading to removal of the Stop sequence. I combined classical cloning tools with the gateway cloning system (s. 3.2.1.8) for the integration of DNA sequences into the pUAST vector.

Transgenic flies were tested with DB331-Gal4; hs-FLP/ CyO. Heatshock treatment was induced at various developmental time points starting 48 hours after egg deposition until late L3 stage. The resulting number of TN-XXL highlighted LPTCs varied from single cells over small subgroups (Fig. 36B+C) to the complete number of LPTCs covered by the DB331-Gal4 expression pattern (Fig. 36A). This indicated that the construct was enabling restrictive expression in the way it was intended, i.e. the Stop cassette was able to prohibit completely the transcription of TN-XXL and was efficiently removed by heatshock-induced flippase activity. The confocal images were taken directly after dissection and without fixation or further immunostaining in order to show the strength of TN-XXL expression within these neurons.

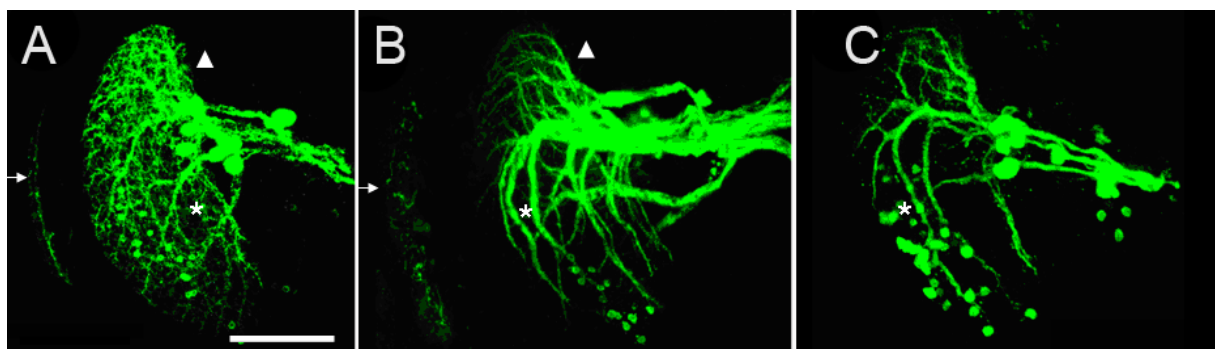


Fig. 36: Restricted expression patterns of TN-XXL expressing LPTCs.

UAS>Stop>TN-XXL flies were crossed with DB331-Gal4,hs-FLP flies; L2 (2nd instar) and L3 larvae were given heatshock treatment for 2 hours. The TN-XXL expression in green was observable within 24 hours under a fluorescent stereomicroscope. Adult brains were dissected for detailed analysis. Compared to control flies (A) with mCD8::GFP expression, a decreased number of LPTCs and general reduction of the expression pattern was observed (B). Depending on the timing of heatshock treatment, different subsets of neurons within the DB331-Gal4 expression pattern were labeled by TN-XXL. (B) The first TN-XXL sample shows expression in the medulla (arrow) as well as VS (asterisk) and HS cells (triangle) whereas the second sample (C) expresses TN-XXL only in VS cells (asterisk). All images show the optical lobes in full projection. Confocal image stacks were taken with a z-increment of 0.2 μm , a 63x objective and minimized pinhole. Composite images were generated by collapsing ~100 images. Scale bar 100 μm

Here, I demonstrated that the generated UAS>Stop>TN-XXL transgenic flies were indeed working for inducing TN-XXL transcription restrictively in subsets of LPTCs. In order to target specific single LPTC subgroups, further refinement of the heatshock protocol is needed. The strength of TN-XXL expression appeared to be strong however, only calcium imaging would provide a clear conclusion.

4.4 Viral labeling of LPTCs

Recent studies have demonstrated the manifold ways in which viruses for the transsynaptic retrograde labeling can be used to highlight the morphology of cells (Tamamaki et al., 2000; Tomioka and Rockland, 2006; Conzelmann, 1998) and to trace neural connectivities (Wickersham et al., 2007a; Ugolini, 1995; Mebatsion et al., 1996; Etessami et al., 2000). So far, the use of viral abilities has only been demonstrated in the mammalian model system. The aim of this study was to make the first step in applying viral techniques in *Drosophila melanogaster*. The experiments were carried out in collaboration with Alexander Ghanem and Klaus Conzelmann who generously supported me with their expertise and provided all viral stocks for the following experiments.

We wanted to target viral infection to the neurons of interest by using the TVA/ EnvA system (Balliet et al., 1999; Wickersham et al., 2007b). Transgenic flies were generated encoding a TVA-2Alike-dsRed sequence under control of the UAS promoter. The construct was additionally encoding for fluorescent protein dsRed to visualize the expression of the TVA receptor. Both sequences were separated by a ribosomal skip mechanism caused by a "2A like" linker (Tang et al., 2009; Szymczak

et al., 2004). The expression of UAS-TVA-2Alike-dsRed flies was tested by crossing them with DB331-Gal4. Throughout all developmental stages the expression of dsRed was detectable with a fluorescence stereomicroscope (Fig. 37). Confocal images of adult brains confirmed the expression of dsRed in LPTCs (Fig. 37C). Here, the main branches were strongly labeled whereas higher order branches were merely visible due to the cytoplasmic localization of the marker protein. This observation points to a separated translation of dsRed and TVA translation through the 2Alike sequence.

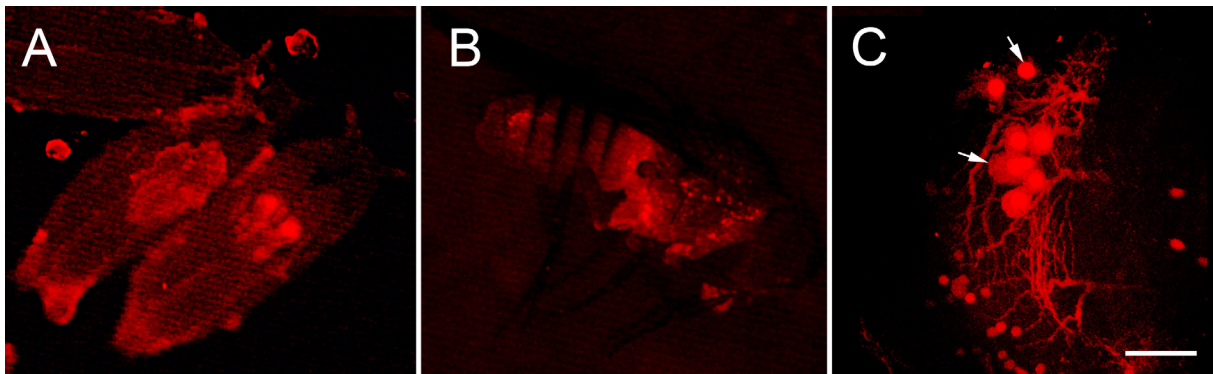


Fig. 37: TVA expression in flies

Expression of dsRed is detected with a fluorescence stereomicroscope in larvae (not shown), (A) pupae, throughout the entire development and (B) in adult flies. A strong expression level of dsRed was observable. (C) Confocal images reveal dsRed expression in cell structures like soma (arrows) and dendritic ramifications. Here, images were taken immediately after fixation. The confocal stack was taken with a z-increment of 0.5 μm , a 63x objective and minimized pinhole. Composite images were generated by collapsing ~ 30 images. Scale bar in C 50 μm .

Next, we infected TVA/ dsRed expressing brains (DB331-Gal4/ UAS-TVA-2Alike-dsRed) in culture with VSV (VSV DG EGFP-EnvA): mutant Vesicular Stomatitis Viruses carrying EnvA, the complementary component, and EGFP as a marker. Mutant viruses were lacking the G-protein encoding sequence and thus, were not able to spread from the initial infected cells (Mebatsion et al., 1996; Etessami et al., 2000). After 24 hours incubation time, the first neurons were EGFP labeled by viral infection. Visual identification was done with a fluorescence stereomicroscope. Some of the labeled neurons could be identified as VS neurons (Fig. 38). EGFP was only detectable in neurons expressing dsRed. This allows the conclusion that specific targeting of VSV viruses to the neurons of interest can be achieved through the EnvA/ TVA system in fly brain cultures.

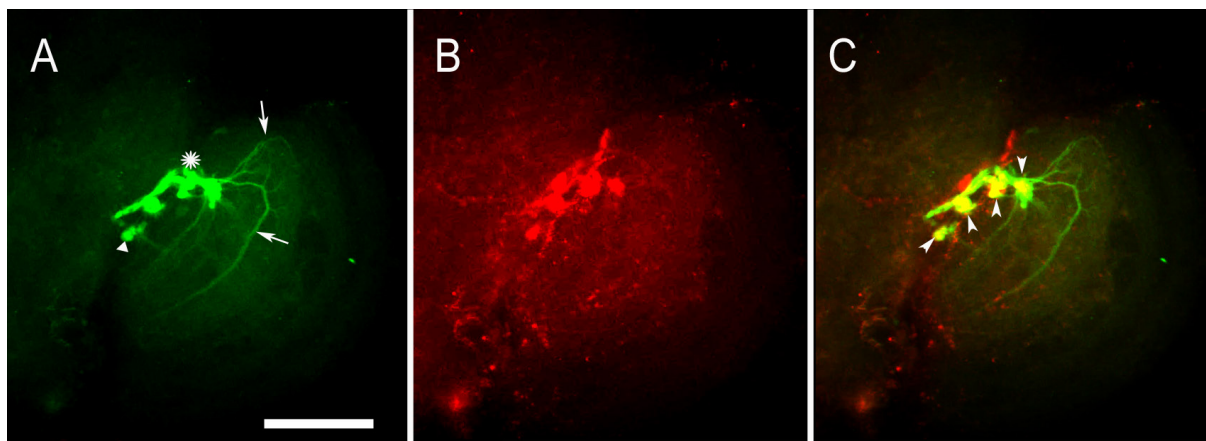


Fig. 38: Viral labeling of LPTCs.

The images taken by a fluorescence stereomicroscope show one-half of a fly's brain in culture. Here, TVA receptors were expressed under control of DB331-Gal4 (DB331-Gal4/ UAS-TVA-2Alike-dsRed). The viruses carry the EnvA component and specifically target TVA expressing cells. (A) Here, several neurons in the lobula plate (asterisk) are GFP labeled (triangle, arrows) through the virus infection and anatomically identifiable as VS cells (arrows), whereas (B) dsRed expression shows the endogenous expression pattern of DB331-Gal4. GFP expression coincides with dsRed labeled cells (C: arrowheads) revealing the efficiency of that system. Single image was taken from fluorescence stereomicroscope. Scale bar 100 μ m.

To enable the identification of direct synaptically connected cells from the initial infected cell population the G-protein needs to be provided *in trans* (Wickersham et al., 2007b). For that, we put G-proteins from different viruses under control of the UAS promoter (s. methods 3.2.6.3), which would allow a co-expression with the TVA receptor. Unfortunately, first experiments made in brain culture were inconclusive. Western Blot analysis (not shown) done by Alexander Gharnem showed that ubiquitin-driven expression of pCVS-G vector in S2 (*Drosophila* Schneider 2) cells were positive, thereby revealing that *Drosophila* cells were able to synthesize viral G-proteins. Here, further studies are needed to elucidate first, the expression levels of the different G-proteins in flies and second, which G-protein works for transsynaptic spreading of VSV viruses.

In this study, we made the first steps towards a new tool for transsynaptic labeling with VSV viruses in *Drosophila*. However, further studies are needed to learn more about the mechanisms of viral infection and spreading in flies.

5 Discussion

5.1 *Dscam1* manipulation in LPTCs

The dendritic branches of different HS cells overlap to a large degree. Yet, sister-branches of the same cell never fasciculate or cross each other (Fig. 24C+D). Such anatomical characteristics are in line with numerous previous reports in which surface interactions between the ectodomain of identical *Dscam1* isoforms (Wojtowicz et al., 2004, 2007) induce a repulsive signal that establishes a self-avoidance mechanism (Matthews et al., 2007; Hughes et al., 2007; Zhan et al., 2004; Soba et al., 2007; Zirpursky and Grueber, 2013). This signal, mediated via the cytoplasmatic domain of *Dscam1*, causes cells to retract their neurites during development (Matthews et al., 2007; Matthews and Grueber, 2011). Similarly, dendrites of closely related cells that express the same set of *Dscam1* isoforms are engaged in homophilic repulsion (Matthews et al., 2007).

5.1.1 Anatomical changes and underlying mechanisms

5.1.1.1 Reduced *Dscam1* expression level

In this study, I was able to provide first evidences that LPTCs might possess an endogenous *Dscam1* code. Immunolabeling against the intracellular domain of *Dscam1* revealed a broad expression in the entire optical lobe, including HS and VS cells (Fig. 21). This result is corroborated by *Dscam1* loss-of-function (Fig. 23) and knock-down (Fig. 22) experiments.

Assuming that residual flippase activity erased *Dscam1* activity in HS cells, the observed crossings of sister dendrites (Fig. 24B) were likely caused by loss of *Dscam1* mediated self-avoidance during neuronal morphogenesis.

Dscam1 interactions are supposed to regulate neurite guidance and targeting (Zhan et al., 2004; Zhu et al., 2006; Zipursky and Grueber, 2013). Dendritic and axonal growth has been shown to be regulated by different subsets of *Dscam1* isoforms. Depending on the identity of the transmembrane, isoforms are sorted to different neuronal compartments (Wang et al., 2004). TM1-containing isoforms have been shown to locate in dendrites whereas TM2-containing ones specifically target axonal regions.

An increase of small branches was observed in the dendrites and axons of HS and VS cells in *Dscam1*^{FLP} flies (Fig. 23D-F). Furthermore, sister branches were crossing each other in a high frequency (Fig. 24A+B) which points to a lack of self-avoidance mechanism in *Dscam1*^{FLP} cells. However, the dendritic overgrowth phenotype did not include fasciculations or any evident impacts on the coverage areas in the lobula plate (Fig. 24A+B). These findings speak for a function of *Dscam1* in dendritic branching but not in dendritic spacing of LPTCs.

Dscam1 has been shown to interact with netrins and other proteins which are known to be involved in neurite development (Matthews and Grueber, 2011; Yamagata and Sanes, 2010). Here, the growth of higher order branches might be regulated by two signaling pathways which have opposing effects on dendritic growth. Netrins have been described to enhance neurite outgrowth whereas *Dscam1* isoforms have been shown to restrict netrin elicited growth by repulsive interactions (Matthews and Grueber, 2011). The lack of repulsive signals would then explain the development of additional small branches in *Dscam1*^{FLP} flies. Just recently the similar growth functions of *Dscam1* have been described for flight motoneurons (Hutchinson et al., 2014).

Injection of neurobiotin revealed that the wild-type Lpt2 neuron had a local defect in its self-avoidance mechanism (Fig. 23O+P). This effect has already been described in the MB where single *Dscam1* mutant axons can alter the projections of neighboring wild-type axons (Wang et al., 2004; Zhan et al., 2004). This observation is also very interesting regarding the connectome of the fly visual system. The influences on wild-type Lpt2 points to a *Dscam1* mediated interaction with LPTCs.

5.1.1.2 Reduced *Dscam1* expression diversity

It has been reported that removal of various subsets of *Dscam1* exon-alternatives does not affect MB neuronal morphogenesis. This might point to redundancy among some exon alternatives (Wang et al., 2004). The attempt to silence the expression of *Dscam1* by using RNAi lines failed when using NP282-Gal4. Morphological changes of the shape in HS cell dendrites could be detected but were not reproducible (Fig. 22J+K). The underlying reason could be that RNAi activity was not strong enough for an overall knockdown when using NP282-Gal4. Instead, there might be only few alternative exons silenced (Wang et al., 2004). With that, some dendritic ramifications would develop normal whereas others might lack *Dscam1* isoforms which were

important to restrict dendritic growth. Further explanation of the high variability observed in RNAi knock-down cells is provided by the study from Mirura and coworkers (2013), in which they demonstrated that alternative splicing of *Dscam1* exons not only differs from cell to cell but also changes during development. Uncomplete RNAi knock-down would then have different effects on HSN and HSE depending on the *Dscam1* repertoire that was endogenously present at that time-point of development.

This also explains the phenotype when DB331-Gal4 was used to express RNAi in LPTCs. DB331-Gal4 has an earlier expression onset and stronger expression level than NP282-Gal4. Here, I received a constant phenotype in LPTCs, which resembled that in *Dscam1*^{FLP} flies. However, in this case immunohistochemical validations are still needed.

It has been shown that thousands of isoforms are essential to provide neurons with a robust discrimination mechanism to distinguish between self and non-self neurites (Hattori et al., 2009). In this study, deletion of Exon6 reduced *Dscam1* ectodomain diversity from 19,008 to 1,584 potential isoforms. Reduction of Exon6 variability impaired dendritogenesis of HS cells. Self-crossing events and pathfinding defects could be detected in their dendritic regions (Fig. 26). The reason why some branches were affected and others were not could be explained by the stochastic yet biased expression mechanism of *Dscam1* isoforms in single HS cells. It has been demonstrated that neurons largely express a nonspecific set of isoforms but some isoforms are needed for correct targeting and self-avoidance (Matthews et al., 2007; Zipursky and Grueber 2013; Shi and Lee, 2012; Miura et al., 2013). Comparable to the RNAi knock-down scenario, single processes of HS cells which normally selectively express the deleted isoforms, might lose *Dscam1* expression altogether and thus, were rendered null mutants. Missing *Dscam1* interactions between either sister dendrites of the same HS cell or single dendritic branches and columnar neurons would then explain why self-crossings and misprojections appeared in the entire dendritic tree but only at single branches.

NP282-Gal4 has a late developmental onset and a relatively weak expression level. Hence, flippase activity might induce the deletion of Exon6 variants at a relatively late developmental time-point or was too weak to cause mitotic recombination in the entire cell. Therefore, the repetition of this deletion experiment with DB331-Gal4

might be interesting in future studies. Nevertheless, underlined with the immunolabeling results, this experiment not only confirmed the presence of *Dscam1* in LPTCs but also demonstrated its functional role in constituting dendritic self-avoidance.

Unfortunately, the attempt to generate single *Dscam1* null LPTC clones with MARCM has not been successful, yet. Other experiments (s. RicinA study), in which the same Gal4 line was used, showed a high probability to induce mitotic recombination in LPTCs by following the elaborated temperature shift protocol. Therefore, it is most likely that the used flippase was too weak and should be replaced in future studies.

5.1.1.3 Misexpression of single *Dscam1* isoforms

Misexpression of *Dscam1*^{+7.6.19.2} caused a reduced branching complexity leading to a minor coverage density of lobula plate by the HS cell dendrites (Fig. 27). Misexpression of *Dscam1*^{+11.31.25.1} in LPTCs caused reduction in dendritic branching and dendritic field (Fig. 28). The phenotype comprised missing HS and VS cell dendrites at the lateral part of the retinotopically organized lobula plate and reduction in the overlap between two neighboring cells. Several interaction possibilities could account for both misexpression phenotypes.

First hypothesis is that the repulsion signal could be mediated by the misexpression of the same *Dscam1* isoform on the overlapping surface of two neighboring HS or VS cells. Second hypothesis is that functionally different neuronal populations might interact via *Dscam1* expression (Chen et al., 2006). T4 and T5 cells have been shown to provide input to LPTCs (Buchner et al., 1984; Shinomiya et al., 2014; Schnell et al., 2012; Maisak et al., 2013; Mauss et al., 2014).

Speaking in favor for the first hypothesis is the observation that misexpression of *Dscam1*^{+11.31.25.1} in a single HS cell did not affect its morphogenesis (Fig. 31). However, in case of MARCM, differences in expression levels intrinsic to the method are present which could lead to a weak phenotype comparable to the scenario when NP282-Gal4 was used to drive the misexpression.

Ectopic expression of single *Dscam1* isoforms did not force HS cell dendrites to tile the lobula plate or to induce mosaic spacing. This result is in line with previous studies which have shown that *Dscam1* is dispensable for tiling (Hughes et al., 2007;

Matthews et al., 2007; Soba et al., 2007) and is mediated by *Dscam2* (Millard et al., 2007;). Misexpression of further isoforms or combinatorial misexpression might provide further insights into the role of *Dscam1* in the morphogenesis of LPTCs.

Previous studies have reported that the *Dscam1* splicing pattern can change during morphogenesis (Miura et al., 2013). Depending on the developmental stage of dendritogenesis the splicing pattern of *Dscam1* might therefore be different. This would explain the onset-dependent differences of the misexpression phenotype (Fig. 32). The phenotype of *Dscam1*^{+7.6.19.2} misexpression could either point to repulsive interactions at later developmental stages when the main dendritic branches of HS cells were already established or a specific localization of this isoform at the terminal dendritic branches.

Speaking in favor for the second hypothesis is the phenotype when *Dscam1*^{+11.31.25.1} was misexpressed in both, LPTCs and T4/ T5 cells (Fig. 33D-F). The highly structured innervation of the lobula plate was completely abolished whereas the layers in medulla and lobula were still specifically targeted by T4/ T5 axons. In this case, repulsive signals elicited by the misexpression of *Dscam1*^{+11.31.25.1} on pre- and postsynaptical sides led to a complete avoidance of T4/ T5 axons to innervate the lobula plate. Flies with those severe disruptions within the visual circuitry should be motion-blind. This needs to be tested in future functional studies.

In the axons of HS and VS cells, misexpression of *Dscam1*^{+11.31.25.1} caused projection errors of single axon fibers (Fig. 28E+G). The axons of HS and VS cells left the lobula plate in horizontal bundles like in wild-type animals; Therefore, repulsion between two neighboring HS or VS cell axons within one bundle was unlikely the reason for this phenotype. A more convincing hypothesis is that repelling *Dscam1* interactions between LPTCs and cells in the central brain caused single neurites to separate from the axon bundle prior to their destination areas. Misexpression of *Dscam1*^{+7.6.19.2} had however, no visible influence on the axonal pathway finding of LPTCs (Fig. 27J). It has been reported that TM1- and TM2-containing isoforms were sorted to different neuronal compartments (Zhan et al., 2004) which could be here the case. A restricted expression to the dendrites would explain why the misexpression of *Dscam1*^{+7.6.19.2} did not affect the axonal region of LPTCs.

The strength of the generated repulsive signal and resulting phenotypes depend on the expression level of particular *Dscam1* isoforms, the degree of overlap of the entire *Dscam1* repertoire and the developmental state of individual neurons (Zipursky and Gruber, 2013; Miura et al., 2013; Hutchinson et al., 2014). This might explain why in wild-type animals, dendritic neurites of the same LPTC and thus, expressing the exact same set of isoforms strictly avoided each other and never crossed. Partial overlap of the *Dscam1* repertoire in functionally related but different HS cells would then be sufficient to prevent an overall fasciculation but did not suppress crossing. *Dscam1* dependent growth but *Dscam1* independent dendrite spacing would explain the missing tiling in misexpression cells. Depending on the identity of single *Dscam1* isoforms, the elicited repelling signals resulted in a growth stop of the entire dendritic tree or only prohibited the outgrowth of higher order branches. The uniqueness of misexpression phenotypes has been observed before in olfactory and da neurons (Spletter et al., 2007; Zhu et al., 2006, Miura et al., 2013). Here, I did not further investigate whether other isoforms or misexpression of small sets of *Dscam1* isoforms could induce mosaic spacing of HS cell dendrites. Complete tiling of axonal processes in the fly visual system was suggested to depend on *Dscam2* (Millard et al., 2007, 2010) which might be interesting to examine in future studies.

Ectopic expression of *Dscam1*^{+7.6.19.2} caused a general reduction of higher order branches in the dendritic areas of HS cells that was confirmed by immunolabeling with α -Btx conjugated Alexa Fluor (Fig. 27N). Remaining branches were still expressing nAChRs but in lower density. In contrast, HS cells misexpressing *Dscam1*^{+11.31.25.1} displayed locally enriched receptor densities on their remaining branches (Fig. 28J). This might point to a local accumulation of synaptic input elements where presynaptic structures might follow their target structures despite their dislocation, similar to the observations made in the olfactory system (Zhu et al., 2006). There, positional shift of the dendrite of one projection neuron causes a corresponding shift of its partner, the axon of the olfactory receptor neuron. With that, connection specificity is maintained despite dendritic dislocation. In HS cells, such a pre- and postsynaptic matching mechanism independent from a precise dendritic positioning could be present. Evidences for an intact electrical coupling between neighboring HS cells were given by neurobiotin injection (Fig. 30). Here, functional

studies provided further insights into the network connectivities in *Dscam1* misexpression flies.

5.1.2 Correlations between anatomy and function

So far, I analyzed the anatomical changes of LPTCs caused by different genetic manipulations of the *Dscam1* code. Here, the functional implications of *Dscam1*^{+11.31.25.1} and *Dscam1*^{+7.6.19.2} misexpression were addressed by whole cell recording during visual stimulation of the fly. The entire electrophysiological study and analysis was performed by Bettina Schnell. Detailed descriptions of experimental setup and methods are provided in her PhD thesis. Complementary to the functional studies, I analyzed the anatomical structures of the recorded cells (s. 3.2.3) due to the variability in strength of the single *Dscam1* misexpression phenotypes. In this study, two major aspects were observed: contrast dependency and receptive field of single HS cells.

The recordings were done in control flies (DB331-Gal4; UAS-mCD8::GFP) and in flies with co-expression of *Dscam1*^{+11.31.25.1} or *Dscam1*^{+7.6.19.2}. To assign the recorded signal to a particular cell (HSN, HSE or HSS), cells were perfused with a red dye during the recording.

HS cells misexpressing *Dscam1*^{+11.31.25.1} did not show altered direction selectivity during the presentation of a stimulus that covered large areas of the field of view. This suggested that these cells still received input from local motion detectors. An explanation why there was no change observable might be provided by dendritic gain control. In the large dendrites of HS cells the contribution of individual synaptic currents to dendritic potential changes drop steeply with increasing stimulus size. This is because of an increase in conductance due to the opening of thousands of transmitter and voltage gated ion channels during the activation of not perfectly directionally selective input elements (Borst et al., 1995).

When the receptive fields of HS cells were mapped then differences between control and *Dscam1*^{+11.31.25.1} misexpression flies became evident. Control HS cells had much broader receptive fields than *Dscam1*^{+11.31.25.1} misexpression cells. Local stimuli presented in the frontal field of view caused reduced or no response in

Dscam1^{+11.31.25.1} cells. This motion blindness was in total accordance with the anatomical phenotype, in which additional repelling Dscam1^{+11.31.25.1} signals caused a lack of dendritic trees in the distal areas of HS cells. The deficit of dendritic branches resulted in disassembling of the input from local motion detectors in those areas (Schnell et al., 2012; Maisak et al., 2013; Mauss et al., 2014; Hiesinger et al., 2006; Fischbach and Hiesinger, 2008; Scott et al., 2003). Local motion stimuli presented in the lateral areas elicited stronger responses in Dscam1^{+11.31.25.1} cells compared to control HS cells. This functional aspect could explain the anatomical finding in which the remaining dendritic branches appeared to possess local accumulations of nAChRs. Further explanation can be provided by dendritic resistance and gain control properties of HS cell. Smaller dendrites in Dscam1^{+11.31.25.1} cells should have a high input resistance and lower leak conductance. Thus, local stimuli would cause higher voltage changes. Responses to contralateral presented stimuli were also slightly decreased. In the contrast dependency assay, the performances of Dscam1^{+11.31.25.1} cells were weaker compared to control cells, reaching a lower saturation plateau. This can be explained again by gain control mechanisms. It has been shown that the exact value of saturation in large-field motion detectors like HS cells is determined by the activation ratio of their excitatory and inhibitory input elements (Borst et al., 1995). Misexpression of Dscam1^{+11.31.25.1} in HS cells caused severe changes in their dendritic branching structure. Remaining branches did not resemble those of control cells. This might point to changes in the distribution of input elements and with that, an imbalance of excitatory and inhibitory input to the remaining branches. The new ratio of remaining input elements would therefore determine a new saturation value. The observed impact on the response to contralateral stimuli could be assigned to axonal misprojections of tangential cells that have their dendrites in the contralateral hemisphere of the brain (Schnell et al., 2010).

HS cells misexpressing Dscam1^{+7.6.19.2} with strong anatomical phenotypes were showing a total lack in response to ipsilateral provided stimuli whereas response to contralateral stimulation was unaltered. Those neurons displayed strong phenotypes with massive loss of dendritic branches. This result led to the assumption that those cells were missing input signals from columnar neurons, while information flow from contralateral projecting neurons was still maintained. The contrast dependence assay revealed a decreased but not abolished response to whole-field stimuli in those cells.

Like in *Dscam1*^{+11.31.25.1} misexpressing cells the ratio of input elements providing inhibitory and excitatory stimuli to the HS cells were most likely differing from those in wild-type cells. This can be attributed to the loss of higher order branches and thus, differing gain control mechanisms in those cells. In accordance with the variability in phenotypical strength, the saturation plateaus also varied. In general, we assumed a correlation between fluctuations in phenotypical strength and variations in individual cell performance, i.e. the more the dendritic branching pattern was differing from those of control cells, the more their function was impaired.

5.1.3 Correlations between anatomy and behavior

LPTCs play a important role in optomotor response (Heisenberg, 1971; Heisenberg and Götz, 1975; Heisenberg and Buchner, 1977; Heisenberg et al., 1978). To investigate whether HS cells with non wild-type morphologies cause behaviorally relevant changes in the neuronal circuitry, *Dscam1*^{+11.31.25.1} and *Dscam1*^{+7.6.19.2} were analyzed and compared to the performances of control flies (DB331-Gal4; UAS-mCD8::GFP/ BI). It has been suggested that compensatory yaw turning responses rely on visual processing in HS cells (Heisenberg et al., 1978; Heisenberg and Wolf, 1979). The behavioral study was carried out by Väinö Haikala. Detailed descriptions of experimental setup and methods can be found in his PhD thesis. Complementary to the behavioral experiments, I analyzed the anatomical structures of HS cells right after the fly's performance.

Here, visually guided, compensatory flight behavior was investigated. Periodic gratings that elicit compensatory yaw turning responses in wild-type flies were presented on a LED (Light Emmitting Diode) display to a tethered flying fly. The strength of a fly's response was analyzed by monitoring the stroke amplitude of the beating wings. By subtracting the amplitude of both wings, the strength of the executed turning behavior can be calculated (Götz, 1987; Dickinson et al., 1993).

Dscam1^{+11.31.25.1} and control flies showed identical yaw-turning responses when drifting gratings with a maximum contrast were displayed on the entire arena (360°). However, when a monocular motion stimulus (stimulus excluded the zone of binocular overlap (Schnell et al., 2010) was presented to the left or to the right eye then the strength of the elicited yaw-turning response was much decreased in

Dscam1^{+11.31.25.1} flies compared to control flies. Despite an unaltered correlation between yaw turning response and stimulus contrast, the saturation level reached only about 40% of the strength of that in control animals. Next, a small horizontal grating (10° in elevation, 100° in azimuth) moving at different elevations was presented to either eye of the fly. The biggest responses were elicited in control flies when stimuli were presented in the equatorial area that is covered by the dendrites of all 3 HS cells (Schnell et al., 2010; Scott et al., 2002). Again, *Dscam1*^{+11.31.25} flies exhibited much weaker behavioral responses at each elevation tested. In line with previous findings, the responses of *Dscam1*^{+11.31.25.1} flies to the contrast dependency assay were about 50% weaker to control flies. This result was in line with the obtained electrophysiological data.

In none of the tested assays *Dscam1*^{+11.31.25.1} flies were showing stronger responses to presented stimuli, which one would expect from the functional study. This discrepancy might be attributed to differences in the stimulus and the used read out. Electrophysiological recordings directly measure the activity of a certain cell whereas behavior is the result of the activity of an entire neuronal network. Neurons, other than HS cells might also contribute to the yaw turning response in *Drosophila*.

Taken together, we carried out a unique study on the function of *Dscam1* in HS cells. Anatomical results were complemented by electrophysiological and behavioral studies. The results let strongly suggest that *Dscam1* is necessary for correct pattern formation and target finding. Moreover, the anatomy of HS cells is pivotal for their function as motion detectors and strongly affects the execution of complex behavior in flies.

5.2 Efficacy of RicinA cell ablation

In this project, I demonstrated that the UAS>Stop>RicinA construct worked highly efficient for the purpose to isolate single LPTCs out of the dense expression pattern of DB331-Gal4 (Fig. 35). Cell vitality testing with PI convincingly demonstrated that the cell membranes of the remaining GFP labeled LPTCs in the DB331-Gal4 expression pattern were still intact (Fig. 35L). This result was in line with previous experiences with temperature sensitive RicinA constructs (Moffat et al., 1996), in which temperature sensitive RicinA expression has been shown to be restrictive to

those cells in which it was induced with no off-target effects. Nevertheless, for successful and targeted cell ablation, a clearly defined time-point of RicinA induction was essential. Beside the developmental time-point, the duration of heatshock was a crucial factor for the resulting ablation pattern (Gomez-Diaz and Alcorta, 2008). Therefore, time-point analysis was crucial for experimental success. In case of the DB331-Gal4 line, the time-frame turned out to be the late L3 which was a well-defined and recognizable stage when all larvae were attached to the walls of the vials. The heatshock protocol enabled a highly precise ablation of LPTCs. To decrease the number of ablated neurons other than LPTCs either heatshock induction at later stages or a more restricted heatshock window might provide solutions. However, experiments in later pupa stages turned out to induce RicinA very inefficiently in LPTCs. One explanation could be differing heat-protective mechanisms like the pupa shell or the adult cuticula, which are more protective than larval skin and therefore, might prohibit heatshock-induced flippase activity in later stages. Another explanation could be molecular mechanisms like DNA condensations that build a barrier against flippase activity (Oudman, 1991; Vermeulen and Loeschcke, 2007; Overgaard and Sørensen, 2008). Another theory for the lack of cell ablation in later stages could be a decrease in the number of mitotic dividing cells (Wu and Luo, 2006). This study demonstrated that flippase does not work in adult flies in which neurons are already differentiated.

To our surprise, there was not only a difference in the RicinA-induced ablation pattern between different flies but also within the optical lobes of one single fly. Both optical lobes possess different numbers and types of remaining LPTCs (Fig. 35E+F). Due to the method inhomogeneous heatshock treatment can be mostly excluded. This result rather points to a time difference in the development of LPTC precursor cells between both lobes. Different patterns of remaining LPTCs in the two optic lobes offer the advantage of testing two scenarios but also decrease the probability of having the same set of remaining LPTCs in both hemispheres. This might complicate the interpretation of behavioral experiments beside the variety of factors like motivation, flight experience, etc., of tested flies. Furthermore, assuming that LPTCs would play a key role in optomotor behavior of the fly, ablation of different sets of cells in both optic lobes would elicit a total misbalance in optic flow perception in both hemispheres. Previous studies have revealed network connectivities between both optical lobes (Schnell et al., 2010) and thus, disequilibrium between the numbers of

cells in both hemispheres might cause unpredictable changes in the fly optomotor response. Experiments with laser ablation of single HS and VS precursor cells at an early larval stage in *Musca* have demonstrated that these animals show reduced response to large-field regressive ND (Null Direction) stimuli whereas the response to progressive PD (Preferred Direction) stimuli is only slightly affected. In addition, object response to a single stripe hardly differs from wild-type (Geiger and Nässel, 1981; Nässel and Geiger, 1983). Due to the ablation differences in both optical lobes, in future studies the fly optomotor responses must be measured monocularly in order to prove whether specific alterations in optomotor behavior can be correlated with the lack of single LPTCs. In any case, it is necessary to analyze anatomically which LPTCs are missing, after each behavioral experiment.

5.2.1 Insights into developmental mechanisms

The *RicinA* project also allowed insights into cell-cell interactions during the development of LPTCs. Single LPTCs remained from *RicinA* ablation preserved normal dendritic branching patterns (Fig. 35) even in the total absence of other LPTCs (Fig. 35C), which were included in the expression pattern of *DB331-Gal4*. The results were in line with previous ablation studies in R7 photoreceptors that have shown that the loss of cells does not interfere with outgrowth and target finding of neighbored cells. However, photoreceptors differentiate in a defined sequence in which R7 is last emerging (Tomlinson, 1988). Regarding the development of LPTCs, it is still unclear whether LPTCs develop cell-autonomously or are guided through other *RicinA* unaffected neurons or molecular guidance cues. Columnar neurons presynaptic to LPTCs could still be intact in *RicinA* flies and thus guide outgrowing axonal and dendritic processes of remaining LPTCs to their target areas. On the other hand, mechanisms such as gradient cues could make single LPTCs independent of neighboring cells. It is well known that, during early development, gradients form guidance cues for embryonic development (Nüsslein-Volhard and Wieschaus, 1980) and for axonal targeting like in the case of the *robo/ slit* interaction (Kidd et al., 1999). The independent development of LPTCs is not surprising as motion detection is of vital importance for the fly and thus has to build upon mechanisms making this system less susceptible to perturbations.

5.2.2 Correlation between anatomy and behavior

Preliminary optomotor studies with *RicinA* flies were done in collaboration with Steven Fry and Vainö Heikala. In a wing-beat analyzer, the yaw torque of tethered flies was monitored and subsequently the anatomy of remaining LPTCs analyzed. However, more than 50% of all tested flies did not fly at all or flew only briefly. Others seemed to be blind and did not show any escape behavior (tested with an approaching hand). This observation presumably results from loss of all LPTCs but can also have another reason such as loss of motor neurons in the ventral ganglion. As the entire expression pattern of DB331-Gal4 has never been completely studied, both scenarios are possible. Furthermore, we could not distinguish between a lack of motivation and the inability to fly. Here, a walking paradigm (Strauss and Heisenberg, 1993) instead of tethered flight could be the solution in order to exclude the possibility of ablated flight motoneurons. However, from previous studies, it has been reported that many factors including flight experience, habituation to the torque and general environmental factors influence the optomotor response of flies (Hesselberg and Lehmann, 2009). By excluding flies with general gait impairment, all variations in the optomotor response can then be attributed to an altered motion detection system.

5.3 Recording cellular response properties with TN-XXL

Genetically encoded calcium indicators have great potential for the recording of neuronal activity (Hires et al., 2008). We used a FRT flanked 'Stop' cassette for controlling translation activation of TN-XXL with FLP activity and induced labeling only in small cell populations. In initial experiments, the generated UAS>Stop>TN-XXL transgenics allowed expression of the indicator to be restricted to only a few cells within the pattern of DB331-Gal4 (Fig. 36). This allows unambiguous identification of the neurons from which activity is measured (Hou et al., 2009). However, we still need to test whether the expression level and affinity of the indicator is sufficient in live imaging experiments.

5.4 Virus based neural tracer in *Drosophila*

The unique advantages of viral tracers have been demonstrated in numerous studies done in mammalian model organisms like *mus musculus* (Card, 1998; Wickersham et

al., 2007a, b). However, transferring this method to another organism that does not even belong to the same phylum was a challenge. Viruses are usually specific to certain replication machineries in the cells of their host animals. Our goal was to use EGFP encoding viruses for labeling and identifying columnar neurons that are presynaptically connected to LPTCs and, in long term, revealing all neurons involved in the motion detection network. In this thesis, we made the first preliminary steps towards this aim. Initial studies (data not shown) provided the evidence that VSVs were able to use the cellular machinery in *Drosophila* for replication. Viral spread was observable throughout several days of incubation in brain cultures.

For a specific targeting of VSVs, we used the EnvA/ TVA system (Balliet et al., 1999; Wickersham et al., 2007b). We successfully generated fly strains that express the TVA receptor (Fig. 37) and thereby, directed EnvA pseudotyped VSVs to LPTCs in brain cultures. The anatomical structures of labeled LPTCs (Fig. 38) were clearly identifiable which speaks for both, an even distribution of virus particles within the cells and a high viral replication rate. These findings are fundamental for future experiments as infectiousness, fertility, and vitality of the virus are necessary for targeting and spreading behavior (De Clercq et al., 1973; Aderka et al., 1985; Granstedt et al., 2010; Lancaster and Pfeiffer, 2010). The resulting detailed resolution anatomical given by EGFP expression was comparable to that reported from other studies (Granstedt et al., 2009). This is a very important criterion as presynaptically connected cells can only be identified based on their unique morphologies. In previous studies, the time-frame starting from infection of the host cell by rabies virus until spreading to the presynaptic neurons was reported to be around 3-4 days at 37°C in mammalian slice culture (Ugolini, 2010). However, for insects the optimum environmental temperature is 25°C that would result in an incubation time of 10-14 days. This period is much too long for recording any spreading behavior in brain cultures. Therefore, the next step would be to establish an *in vivo* assay. A preliminary injection protocol was tested successfully but needs to be refined. Furthermore, all generated transgenic G-protein expressing flies need to be tested. In this project, we paved the way towards a revolutionary technique that might enable retrograde tracing of neuronal networks in the fly.

6 Conclusion

In this thesis, it has been shown for the first time that it is possible to change the anatomy of LPTCs by manipulating the endogenous code of *Dscam1*. The resulting phenotypes were highly different from wild-type morphology and displayed characteristic aberrant features, which provided an ideal basis to study the correlation between anatomy and function of LPTCs. Further possibilities to study the role of LPTCs in behavior are provided by the elaborated RicinA protocol. The anatomy of the remaining LPTCs was not affected by the lack of neighboring cells and thus, the cells should be fully functional. Collaborative functional studies were in line with the anatomical observations thereby, showing for the first time that the function of motion detection strongly depends on the morphology of LPTCs in the retinotopic organized visual system.

Genetic tools are the key to study the function of a neuron and its role in the neuronal circuitry. The generated fly lines provide the opportunity to shed light on the input circuitry of LPTCs. The TN-XXL construct enables local functional observations of single LPTCs that might provide further insights into the information processing on the dendritic tree of LPTCs. By establishing the TVA/ EnvA system, the first steps towards a virus-based tool have been done. Preliminary tests showed successful targeting of the virus particles towards LPTCs. Further studies are needed to establish this system to the repertoire of genetic tools in *Drosophila*.

7 References

Adams MD, Sekelsky JJ.

From sequence to phenotype: reverse genetics in *Drosophila melanogaster*.

Nat Rev Genet. 2002 Mar; 3(3):189-98.

Aderka D, Novick D, Hahn T, Fischer DG, Wallach D.

Increase of vulnerability to lymphotoxin in cells infected by vesicular stomatitis virus and its further augmentation by interferon.

Cell Immunol. 1985 May; 92(2):218-25.

Andrews GL, Tanglao S, Farmer WT, Morin S, Brotman S, Berberoglu MA, Price H, Fernandez GC, Mastick GS, Charron F, Kidd T.

Dscam guides embryonic axons by Netrin-dependent and -independent functions.

Development. 2008 Dec; 135(23):3839-48.

Balliet JW, Berson J, D'Cruz CM, Huang J, Crane J, Gilbert JM, Bates P.

Production and characterization of a soluble, active form of Tva, the subgroup A avian sarcoma and leukosis virus receptor.

J Virol. 1999 Apr; 73(4):3054-61.

Basler K, Hafen E.

Dynamics of *Drosophila* eye development and temporal requirements of sevenless expression.

Development. 1989 Dec; 107(4):723-31.

Bausenwein B, Dittrich AP, Fischbach KF.

The optic lobe of *Drosophila melanogaster*. II. Sorting of retinotopic pathways in the medulla.

Cell Tissue Res. 1992 Jan; 267(1):17-28.

Bausenwein B, Fischbach KF.

Activity labeling patterns in the medulla of *Drosophila melanogaster* caused by motion stimuli.

Cell Tissue Res. 1992 Oct; 270(1):25-35.

Bharadwaj R, Kolodkin AL.

Descrambling Dscam diversity.

Cell. 2006 May 5; 125(3):421-4.

Borst A.

Neural Circuits for Elementary Motion Detection.

J Neurogenet. 2014 Mar 10.

References

Borst A, Egelhaaf M.

Principles of visual motion detection.

Trends Neurosci. 1989; 12:297-306.

Borst A, Egelhaaf M.

In vivo imaging of calcium accumulation in fly interneurons as elicited by visual motion stimulation.

Proc Natl Acad Sci U S A. 1992 May 1; 89(9):4139-43.

Borst A, Egelhaaf M, Haag J.

Mechanisms of dendritic integration underlying gain control in fly motion-sensitive interneurons.

J Comput Neurosci. 1995 Mar; 2(1):5-18.

Borst A, Haag J.

Neural networks in the cockpit of the fly.

J Comp Physiol A Neuroethol Sens Neural Behav Physiol. 2002 Jul; 188(6):419-37.

Borst A, Reisenman C, Haag J.

Adaptation of response transients in fly motion vision. II: Model studies.

Vision Res. 2003 May; 43(11):1309-22.

Boschek CB.

On the fine structure of the peripheral retina and lamina ganglionaris of the fly, *Musca domestica*.

Z. Zellforsch. 1971; 118:369-409.

Brand AH, Perrimon N.

Targeted gene expression as a means of altering cell fates and generating dominant phenotypes.

Development. 1993 Jun; 118(2):401-15.

Braitenberg V.

Patterns of projection in the visual system of the fly.

Exp. Brain Res. 1967; 3:271-298.

Brotz TM, Borst A.

Cholinergic and GABAergic receptors on fly tangential cells and their role in visual motion detection.

J Neurophysiol. 1996 Sep; 76(3):1786-99.

References

Brown V, Jin P, Ceman S, Darnell JC, O'Donnell WT, Tenenbaum SA, Jin X, Feng Y, Wilkinson KD, Keene JD, Darnell RB, Warren ST.

Microarray identification of FMRP-associated brain mRNAs and altered mRNA translational profiles in fragile X syndrome.

Cell. 2001 Nov 16; 107(4):477-87.

Buchner E, Buchner S.

Mapping stimulus-induced nervous activity in small brains by [³H] 2-deoxy-D-glucose.

Cell Tissue Res. 1980; 211(1):51-64.

Buchner E, Buchner S, Bülthoff H.

Identification of [³H]deoxyglucose-labeled interneurons in the fly from serial autoradiographs.

Brain Res. 1984 Jul 9; 305(2):384-8.

Card JP.

Exploring brain circuitry with neurotropic viruses: new horizons in neuroanatomy.

Anat Rec. 1998 Dec; 253(6):176-85.

Chen BE, Kondo M, Garnier A, Watson FL, Püettmann-Holgado R, Lamar DR, Schmucker D.

The molecular diversity of Dscam is functionally required for neuronal wiring specificity in *Drosophila*.

Cell. 2006 May 5; 125(3):607-20.

Conzelmann KK.

NONSEGMENTED NEGATIVE-STRAND RNA VIRUSES: Genetics and Manipulation of Viral Genomes.

Annu Rev Genet. 1998; 32:123-62.

Cook T, Desplan C.

Photoreceptor subtype specification: From flies to humans.

Semin.Cell Dev Biol. 2001; 12:509-518.

Corty MM, Matthews BJ, Grueber WB.

Molecules and mechanisms of dendrite development in *Drosophila*.

Development. 2009 Apr; 136(7):1049-61.

Cuntz H, Forstner F, Borst A, Häusser M.

One rule to grow them all: a general theory of neuronal branching and its practical application.

PLoS Comput Biol. 2010 Aug 5; 6(8): e1000877.

References

- Cuntz H, Forstner F, Haag J, Borst A.
The morphological identity of insect dendrites.
PLoS Comput Biol. 2008 Dec; 4(12): e1000251.
- Cvetkovska V, Hibbert AD, Emran F, Chen BE
Overexpression of Down syndrome cell adhesion molecule impairs precise synaptic targeting.
Nat Neurosci. 2013 Jun; 16(6):677-82.
- Darnell JC1, Van Driesche SJ, Zhang C, Hung KY, Mele A, Fraser CE, Stone EF, Chen C, Fak JJ, Chi SW, Licatalosi DD, Richter JD, Darnell RB.
FMRP stalls ribosomal translocation on mRNAs linked to synaptic function and autism.
Cell. 2011 Jul 22; 146(2):247-61.
- De Clercq E, Stewart WE 2nd, De Somer P.
Increased toxicity of double-stranded ribonucleic acid in virus-infected animals.
Infect Immun. 1973 Feb; 7(2):167-72.
- Dickinson MH, Lehmann FO, Götz KG.
The active control of wing rotation by *Drosophila*.
J Exp Biol. 1993 Sep; 182:173-89.
- Duffy JB.
GAL4 system in *Drosophila*: a fly geneticist's Swiss army knife.
Genesis. 2002 Sep-Oct; 34(1-2):1-15.
- Dvorak DR, Bishop LG, Eckert ME.
On the identification of movement detectors in the fly optic lobe.
J comp Physiol. 1975; 100:5-25.
- Elbashir SM, Martinez J, Patkaniowska A, Lendeckel W, Tuschl T.
Functional anatomy of siRNAs for mediating efficient RNAi in *Drosophila melanogaster* embryo lysate.
EMBO J. 2001 Dec 3; 20(23):6877-88.
- Enerly E, Larsson J, Lambertsson A.
Reverse genetics in *Drosophila*: from sequence to phenotype using UAS-RNAi transgenic flies.
Genesis. 2002 Sep-Oct; 34(1-2):152-5.
- Etessami R, Conzelmann KK, Marion R, Tsiang H, Ceccaldi PE.
Neuronal expression of foreign genes with recombinant rabies virus variants.
Rev Neurol (Paris). 2000 Mar; 156(3):236-41.

References

Farrow K, Borst A, Haag J.

Sharing receptive fields with your neighbors: tuning the vertical system cells to wide field motion. *J Neurosci.* 2005 Apr 13; 25(15):3985-93.

Fischbach KF, Dittrich APM.

The Optic Lobe of *Drosophila melanogaster*. Part I: A Golgi Analysis of Wild-Type Structure. *Cell Tissue Res.* 1989; 258:441-475.

Fischbach KF, Hiesinger PR.

Optic lobe development.

Adv Exp Med Biol. 2008; 628:115-36.

Franceschini N.

Sampling of the visual environment by the compound eye of the fly.

Photoreceptor optics. 1975; 98-125.

Fuerst PG, Koizumi A, Masland RH, Burgess RW.

Neurite arborization and mosaic spacing in the mouse retina require DSCAM.

Nature. 2008 Jan 24; 451(7177):470-4.

Garaschuk O, Griesbeck O.

Monitoring calcium levels with genetically encoded indicators.

Calcium Measurement Methods, 2009; vol. 43. Eds: A Verkhratsky, OH Petersen. Humana Press, Springer.

Geiger G, Nässel DR.

Visual orientation behavior of flies after selective laser beam ablation of interneurons.

Nature. 1981 Oct 1; 293(5831):398-9.

Glick DM.

Leucine scissors.

Glossary of Biochemistry and Molecular Biology (Revised ed.). London: Portland Press. 1997

Golic KG, Lindquist S.

The FLP recombinase of yeast catalyzes site-specific recombination in the *Drosophila* genome.

Cell. 1989 Nov 3; 59(3):499-509.

Gomez-Diaz C, Alcorta E.

Quantitative analysis of antennal mosaic generation in *Drosophila melanogaster* by the MARCM system.

References

Genesis. 2008 Jun; 46(6):283-8.

Götz KG.

Course-control, metabolism and wing interference during ultralong tethered flight in *Drosophila melanogaster*.

J Exp Biol. 1987 Oct; 128:35-48.

Granstedt AE, Szpara ML, Kuhn B, Wang SS, Enquist LW.

Fluorescence-based monitoring of in vivo neural activity using a circuit-tracing pseudorabies virus.

PLoS One. 2009 Sep 9; 4(9):e6923.

Granstedt AE, Kuhn B, Wang SS, Enquist LW.

Calcium-imaging of neuronal circuits in vivo using a circuit-tracing pseudorabies virus.

Cold Spring Harb Protoc. 2010 Apr; 2010(4):pdb.prot5410.

Grotewiel MS, Beck CD, Wu KH, Zhu XR, Davis RL.

Integrin-mediated short-term memory in *Drosophila*.

Nature. 1998 Jan 29; 391(6666):455-60.

Grueber WB1, Jan LY, Jan YN.

Tiling of the *Drosophila* epidermis by multidendritic sensory neurons.

Development. 2002 Jun; 129(12):2867-78.

Grueber WB, Sagasti A.

Self-avoidance and tiling: Mechanisms of dendrite and axon spacing.

Cold Spring Harb Perspect Biol. 2010 Sep; 2(9):a001750.

Haag J, Borst A.

Dye-coupling visualizes networks of large-field motion-sensitive neurons in the fly.

J Comp Physiol A Neuroethol Sens Neural Behav Physiol. 2005 May; 191(5):445-54.

Haag J, Borst A.

Neural mechanism underlying complex receptive field properties of motion-sensitive interneurons.

Nat Neurosci. 2004 Jun; 7(6):628-34.

Haag J, Denk W, Borst A.

Fly motion vision is based on Reichardt detectors regardless of the signal-to-noise ratio.

Proc Natl Acad Sci U S A. 2004 Nov 16; 101(46):16333-8.

References

- Hammond SM, Boettcher S, Caudy AA, Kobayashi R, Hannon GJ.
Argonaute2, a link between genetic and biochemical analyses of RNAi.
Science. 2001 Aug 10; 293(5532):1146-50.
- Hardie, RC.
In Functional Organization of the Fly Retina.
Berlin: Springer. 1985; 5 (ed. D. Ottoson):1-79.
- Hardie RC, Raghu P.
Visual transduction in Drosophila.
Nature. 2001 Sep 13; 413(6852):186-93.
- Hassenstein B, Reichardt W.
Systemtheoretische Analyse der Zeit-Reihenfolgen- und Vorzeichenauswertung bei der Bewegungsperezeption des Rüsselkäfers Chlorophanus.
Z. Naturforsch. 1956; 11b:513-524.
- Hattori D, Chen Y, Matthews BJ, Salwinski L, Sabatti C, Grueber WB, Zipursky SL.
Robust discrimination between self and non-self neurites requires thousands of Dscam1 isoforms.
Nature. 2009 Oct 1; 461(7264):644-8.
- Hattori D, Millard SS, Wojtowicz WM, Zipursky SL.
Dscam-mediated cell recognition regulates neural circuit formation.
Annu Rev Cell Dev Biol. 2008; 24:597-620.
- Hattori D, Demir E, Kim HW, Viragh E, Zipursky SL, Dickson BJ.
Dscam diversity is essential for neuronal wiring and self-recognition.
Nature. 2007 Sep 13; 449(7159):223-7.
- Hausen K.
Functional characterization and anatomical identification of motion-sensitive neurons in the lobula plate of the blowfly Calliphora erythrocephala.
Z. Naturforsch. 1976; C31:629-633.
- Hausen K, Wolburg-Buchholz W, Ribl WA.
The synaptic organization of visual interneurons in the lobula complex of flies. A light and electron microscopical study using silver-intensified cobalt-impregnations.
Cell Tissue Res. 1980; 208(3):371-87.

References

Hayashi S, Ito K, Sado Y, Taniguchi M, Akimoto A, Takeuchi H, Aigaki T, Matsuzaki F, Nakagoshi H, Tanimura T, Ueda R, Uemura T, Yoshihara M, Goto S.

GETDB, a database compiling expression patterns and molecular locations of a collection of Gal4 enhancer traps.

Genesis. 2002 Sep-Oct; 34(1-2):58-61.

Heisenberg M.

Separation of receptor and lamina potentials in the electroretinogram of normal and mutant *Drosophila*.

J Exp Biol. 1971 Aug; 55(1):85-100.

Heisenberg M, Götz KG.

The use of mutations for the partial degradation of vision in *Drosophila melanogaster*.

J Comp Physiol. 1975 Sep; 98(3):217-241.

Heisenberg M, Buchner E.

The role of retinula cell types in visual behavior of *Drosophila melanogaster*.

J comp Physiol. 1977; 117:127-162.

Heisenberg M, Wonneberger R, Wolf R.

Optomotor-blindH31-a *Drosophila* mutant of the lobula plate giant neurons.

J. comp. Physiol. 1978; 124:287-296.

Heisenberg M, Wolf R.

Vision in *Drosophila*.

Springer-Verlag, Berlin 1984; Vol. XII, of: Studies of Brain Function.

Heisenberg, M. and Wolf, R.

On the fine structure of yaw torque in visual flight orientation of *Drosophila melanogaster*.

J comp Physiol. 1979; 130:113–130.

Hengstenberg R, Hausen K, Hengstenberg B.

The number and structure of giant vertical cells (VS) in the lobula plate of the blowfly *Calliphora erythrocephala*.

Journal of Comparative Physiology A: Neuroethology, Sensory, Neural, and Behavioral Physiology 1982; 149(2):163-177.

Hesselberg T, Lehmann FO.

The role of experience in flight behaviour of *Drosophila*.

J Exp Biol. 2009 Oct; 212(Pt 20):3377-86.

References

Hiesinger PR, Zhai RG, Zhou Y, Koh TW, Mehta SQ, Schulze KL, Cao Y, Verstreken P, Clandinin TR, Fischbach KF, Meinertzhagen IA, Bellen HJ.

Activity-independent prespecification of synaptic partners in the visual map of *Drosophila*.

Curr Biol. 2006 Sep 19; 16(18):1835-43.

Hires SA, Tian L, Looger LL.

Reporting neural activity with genetically encoded calcium indicators.

Brain Cell Biol. 2008 Aug; 36(1-4):69-86.

Hou BH, Takanaga H, Griesbeck O, Frommer WB.

Osmotic induction of calcium accumulation in human embryonic kidney cells detected with a high sensitivity FRET calcium sensor.

Cell Calcium. 2009 Aug; 46(2):130-5.

Hughes ME, Bortnick R, Tsubouchi A, Bäumer P, Kondo M, Uemura T, Schmucker D.

Homophilic Dscam interactions control complex dendrite morphogenesis.

Neuron. 2007 May 3; 54(3):417-27.

Hummel T.

Neuronal development: neighbors have to be different.

Curr Biol. 2007 Dec 18; 17(24):R1050-2.

Hutchinson KM1, Vonhoff F, Duch C.

Dscam1 is required for normal dendrite growth and branching but not for dendritic spacing in *Drosophila* motoneurons.

J Neurosci. 2014 Jan 29; 34(5):1924-31.

Joesch M, Plett J, Borst A, Reiff DF.

Response properties of motion-sensitive visual interneurons in the lobula plate of *Drosophila melanogaster*.

Curr Biol. 2008 Mar 11; 18(5):368-74.

Joesch M, Schnell B, Raghu SV, Reiff DF, Borst A.

ON and OFF pathways in *Drosophila* motion vision.

Nature. 2010 Nov 11; 468(7321):300-4.

Kalb J, Egelhaaf M, Kurtz R.

Robust integration of motion information in the fly visual system revealed by single cell photoablation.

J Neurosci. 2006 Jul 26; 26(30):7898-906.

References

Kennerdell JR, Carthew RW.

Heritable gene silencing in *Drosophila* using double-stranded RNA.

Nat Biotechnol. 2000 Aug; 18(8):896-8.

Kidd T, Bland KS, Goodman CS.

Slit is the midline repellent for the robo receptor in *Drosophila*.

Cell. 1999 Mar 19; 96(6):785-94.

Kim JH1, Wang X, Coolon R, Ye B.

Dscam expression levels determine presynaptic arbor sizes in *Drosophila* sensory neurons.

Neuron. 2013 Jun 5; 78(5):827-38.

Kirschfeld K.

Die Projektion der optischen Umwelt auf das Raster der Rhabdomere im Komplexauge von *Musca*.

Exp. Brain Res. 1967; 3:248-270.

Kirschfeld K.

Das neurale Superpositionsauge.

Fortschr. Zool. 1973; 21:229-257.

Kirschfeld K., Franceschini N.

Optische Eigenschaften der Ommatidien im Komplexauge von *Musca*.

Kybernetik 1968; 5:47-52.

Kunes S, Steller H.

Ablation of *Drosophila* photoreceptor cells by conditional expression of a toxin gene.

Genes Dev. 1991 Jun; 5(6):970-83.

Lancaster KZ, Pfeiffer JK.

Limited trafficking of a neurotropic virus through inefficient retrograde axonal transport and the type I interferon response.

PLoS Pathog. 2010 Mar 5; 6(3):e1000791.

Land MF, Fernald RD.

The evolution of eyes.

Annu Rev Neurosci. 1992; 15:1-29.

Lee T, Luo L.

Mosaic analysis with a repressible cell marker (MARCM) for *Drosophila* neural development.

Trends Neurosci. 2001 May; 24(5):251-4.

References

Lee T, Luo L.

Mosaic analysis with a repressible cell marker (MARCM) for *Drosophila* neural development.

Trends Neurosci. 2001 May; 24(5):251-4.

Lefebvre JL, Kostadinov D, Chen WV, Maniatis T, Sanes JR.

Protocadherins mediate dendritic self-avoidance in the mammalian nervous system.

Nature. 2012 Aug 23; 488(7412):517-21.

Luan H, Peabody NC, Vinson CR, White BH.

Refined spatial manipulation of neuronal function by combinatorial restriction of transgene expression.

Neuron. 2006 Nov 9; 52(3):425-36.

Lue NF, Chasman DI, Buchman AR, Kornberg RD.

Interaction of GAL4 and GAL80 gene regulatory proteins in vitro.

Mol Cell Biol. 1987 Oct; 7(10):3446-51.

Luo L, Callaway EM, Svoboda K.

Genetic dissection of neural circuits.

Neuron. 2008 Mar 13; 57(5):634-60.

Ly A, Nikolaev A, Suresh G, Zheng Y, Tessier-Lavigne M, Stein E.

DSCAM is a netrin receptor that collaborates with DCC in mediating turning responses to netrin-1.

Cell. 2008 Jun 27; 133(7):1241-54.

Maisak MS1, Haag J, Ammer G, Serbe E, Meier M, Leonhardt A, Schilling T, Bahl A, Rubin GM, Nern A, Dickson BJ, Reiff DF, Hopp E, Borst A.

A directional tuning map of *Drosophila* elementary motion detectors.

Nature. 2013 Aug 8; 500(7461):212-6..

Mank M, Griesbeck O.

Genetically encoded calcium indicators.

Chem Rev. 2008 May; 108(5):1550-64.

Mank M, Santos AF, Drenth S, Mrcic-Flogel TD, Hofer SB, Stein V, Hendel T, Reiff DF, Levelt C, Borst A, Bonhoeffer T, Hübener M, Griesbeck O.

A genetically encoded calcium indicator for chronic in vivo two-photon imaging.

Nat Methods. 2008 Sep; 5(9):805-11.

References

- Matthews BJ, Grueber WB.
Dscam1-mediated self-avoidance counters netrin-dependent targeting of dendrites in *Drosophila*.
Curr Biol. 2011 Sep 13; 21(17):1480-7
- Matthews BJ, Kim ME, Flanagan JJ, Hattori D, Clemens JC, Zipursky SL, Grueber WB.
Dendrite self-avoidance is controlled by Dscam.
Cell. 2007 May 4; 129(3):593-604.
- Mauss AS1, Meier M, Serbe E, Borst A.
Optogenetic and pharmacologic dissection of feedforward inhibition in *Drosophila* motion vision.
J Neurosci. 2014 Feb 5; 34(6):2254-63.
- McGuire SE, Le PT, Osborn AJ, Matsumoto K, Davis RL.
Spatiotemporal rescue of memory dysfunction in *Drosophila*.
Science. 2003 Dec 5; 302(5651):1765-8.
- Mebatsion T, Konig M, Conzelmann KK.
Budding of rabies virus particles in the absence of the spike glycoprotein.
Cell. 1996 Mar 22; 84(6):941-51.
- Meier M, Serbe E, Maisak MS, Haag J, Dickson BJ, Borst A.
Neural circuit components of the *Drosophila* OFF motion vision pathway.
Curr Biol. 2014 Feb 17; 24(4):385-92.
- Meijers R, Puettmann-Holgado R, Skiniotis G, Liu JH, Walz T, Wang JH, Schmucker D.
Structural basis of Dscam isoform specificity.
Nature. 2007 Sep 27; 449(7161):487-91.
- Merriam JC, Lyon HS, Char DH.
Toxicity of a monoclonal F(ab')₂:ricin A conjugate for retinoblastoma in vitro.
Cancer Res. 1984 Aug; 44(8):3178-83.
- Millard SS, Flanagan JJ, Pappu KS, Wu W, Zipursky SL.
Dscam2 mediates axonal tiling in the *Drosophila* visual system.
Nature. 2007 Jun 7; 447(7145):720-4.
- Millard SS, Zipursky SL.
Dscam-mediated repulsion controls tiling and self-avoidance.
Curr Opin Neurobiol. 2008 Feb; 18(1):84-9.

References

- Millard SS, Lu Z, Zipursky SL, Meinertzhagen IA.
Drosophila dscam-proteins regulate postsynaptic specificity at multiple-contact synapses.
Neuron. 2010 Sep 9; 67(5):761-8.
- Miura SK, Martins A, Zhang KX, Graveley BR, Zipursky SL.
Probabilistic splicing of Dscam1 establishes identity at the level of single neurons.
Cell. 2013 Nov 21; 155(5):1166-77.
- Moffat KG, Gould JH, Smith HK, O'Kane CJ.
Inducible cell ablation in Drosophila by cold-sensitive ricin A chain.
Development. 1992 Mar; 114(3):681-7.
- Moses K.
Evolutionary biology: fly eyes get the whole picture.
Nature. 2006 Oct 12; 443(7112):638-9.
- Nässel DR, Geiger G.
Neuronal organization in fly optic lobes altered by laser ablations early in development or by mutations of the eye.
J Comp Neurol. 1983 Jun 10; 217(1):86-102.
- Neves G, Zucker J, Daly M, Chess A.
Stochastic yet biased expression of multiple Dscam splice variants by individual cells.
Nat Genet. 2004 Mar; 36(3):240-6.
- Nüsslein-Volhard C, Wieschaus E.
Mutations affecting segment number and polarity in Drosophila.
Nature. 1980 Oct 30; 287(5785):795-801
- Oudman L.
A locus in Drosophila melanogaster affecting heat resistance.
Hereditas. 1991; 114(3):285-7.
- Overgaard J, Sørensen JG.
Rapid thermal adaptation during field temperature variations in Drosophila melanogaster.
Cryobiology. 2008 Apr; 56(2):159-62.
- Pierantoni R.
A look into the cock-pit of the fly. The architecture of the lobular plate.
Cell Tissue Res. 1976 Aug 16; 171(1):101-22.

References

Qiu S, Adema CM, Lane T.

A computational study of off-target effects of RNA interference.

Nucleic Acids Res. 2005 Mar 30; 33(6):1834-47.

Raghu SV, Joesch M, Sigrist SJ, Borst A, Reiff DF.

Synaptic organization of lobula plate tangential cells in *Drosophila*: D α 7 cholinergic receptors.

J Neurogenet. 2009; 23(1-2):200-9.

Raghu SV, Joesch M, Borst A, Reiff DF.

Synaptic organization of lobula plate tangential cells in *Drosophila*: gamma-aminobutyric acid receptors and chemical release sites.

J Comp Neurol. 2007 Jun 1; 502(4):598-610.

Reichardt W.

Processing of optical information by the visual system of the fly.

Vision Res. 1986; 26(1):113-26.

Reichardt W.

Autocorrelation, a principle for the evaluation of sensory information by the central nervous system.

In: Rosenblith W.A, editor. Sensory communication.

MIT Press; Wiley; New York, NY; London, UK: 1961:303-317.

Reiff DF1, Plett J, Mank M, Griesbeck O, Borst A.

Visualizing retinotopic half-wave rectified input to the motion detection circuitry of *Drosophila*.

Nat Neurosci. 2010 Aug; 13(8):973-8.

Reiff DF, Ihring A, Guerrero G, Isacoff EY, Joesch M, Nakai J, Borst A.

In vivo performance of genetically encoded indicators of neural activity in flies.

J Neurosci. 2005 May 11; 25(19):4766-78.

Ro S, Rannala B.

A stop-EGFP transgenic mouse to detect clonal cell lineages generated by mutation.

EMBO Rep. 2004 Sep; 5(9):914-20.

Schmucker D, Chen B.

Dscam and DSCAM: complex genes in simple animals, complex animals yet simple genes.

Genes Dev. 2009 Jan 15; 23(2):147-56.

References

Schmucker D.

Molecular diversity of Dscam: recognition of molecular identity in neuronal wiring.

Nat Rev Neurosci. 2007 Dec; 8(12):915-20.

Schmucker D, Clemens JC, Shu H, Worby CA, Xiao J, Muda M, Dixon JE, Zipursky SL.

Drosophila Dscam is an axon guidance receptor exhibiting extraordinary molecular diversity.

Cell. 2000 Jun 9; 101(6):671-84.

Schnell B, Raghu SV, Nern A, Borst A.

Columnar cells necessary for motion responses of wide-field visual interneurons in Drosophila.

J Comp Physiol A Neuroethol Sens Neural Behav Physiol. 2012 May; 198(5):389-95.

Schnell B, Joesch M, Forstner F, Raghu SV, Otsuna H, Ito K, Borst A, Reiff DF.

Processing of horizontal optic flow in three visual interneurons of the Drosophila brain.

J Neurophysiol. 2010 Mar; 103(3):1646-57.

Scott EK, Raabe T, Luo L.

Structure of the vertical and horizontal system neurons of the lobula plate in Drosophila.

J Comp Neurol. 2002 Dec 23; 454(4):470-81.

Scott EK, Reuter JE, Luo L.

Dendritic development of Drosophila high order visual system neurons is independent of sensory experience.

BMC Neurosci. 2003 Jun 30; 4:14.

Seelig JD, Chiappe ME, Lott GK, Dutta A, Osborne JE, Reiser MB, Jayaraman V.

Two-photon calcium imaging from head-fixed Drosophila during optomotor walking behavior.

Nat Methods. 2010 Jul; 7(7):535-40.

Shi L1, Lee T.

Molecular diversity of Dscam and self-recognition.

Adv Exp Med Biol. 2012;739:262-75.

Shinomiya K, Karuppudurai T, Lin TY, Lu Z, Lee CH, Meinertzhagen IA.

Candidate Neural Substrates for Off-Edge Motion Detection in Drosophila.

Curr Biol. 2014 Apr 22; pii: S0960-9822(14)00343-1.

Silies M1, Gohl DM, Fisher YE, Freifeld L, Clark DA, Clandinin TR.

Modular use of peripheral input channels tunes motion-detecting circuitry.

Neuron. 2013 Jul 10; 79(1):111-27.

References

Single S, Borst A.

Dendritic integration and its role in computing image velocity.

Science. 1998 Sep 18; 281(5384):1848-50.

Soba P, Zhu S, Emoto K, Younger S, Yang SJ, Yu HH, Lee T, Jan LY, Jan YN.

Drosophila sensory neurons require Dscam for dendritic self-avoidance and proper dendritic field organization.

Neuron. 2007 May 3; 54(3):403-16.

Sokoloff L, Reivich M, Kennedy C, Des Rosiers MH, Patlak CS, Pettigrew KD, Sakurada O, Shinohara M.

The [14C] deoxyglucose method for the measurement of local cerebral glucose utilization: theory, procedure, and normal values in the conscious and anesthetized albino rat.

J Neurochem. 1977 May; 28(5):897-916.

Spalthoff C, Egelhaaf M, Tinnefeld P, Kurtz R.

Localized direction selective responses in the dendrites of visual interneurons of the fly.

BMC Biol. 2010 Apr 12; 8:36.

Spletter ML, Liu J, Liu J, Su H, Giniger E, Komiyama T, Quake S, Luo L.

Lola regulates Drosophila olfactory projection neuron identity and targeting specificity.

Neural Dev. 2007 Jul 16; 2:14.

Spradling AC, Rubin GM.

Transposition of cloned P-elements into Drosophila germ line chromosomes.

Science. 1982 Oct 22; 218(4570):341-7.

Strausfeld NJ.

Atlas of an insect brain.

Springer. 1976; 214 pp.

Strauss R, Heisenberg M.

A higher control center of locomotor behavior in the Drosophila brain.

J Neurosci. 1993 May; 13(5):1852-61.

Strother JA, Nern A, Reiser M.

Direct Observation of ON and OFF Pathways in the Drosophila Visual System.

Curr Biol. 2014 Apr 2.

References

Struhl G, Basler K.

Organizing activity of wingless protein in *Drosophila*.

Cell. 1993 Feb 26; 72(4):527-40.

Sweeney NT, Li W, Gao FB.

Genetic manipulation of single neurons in vivo reveals specific roles of Flamingo in neuronal morphogenesis.

Dev. Biol. 2002; 247:76-88.

Szymczak AL, Workman CJ, Wang Y, Vignali KM, Dilioglou S, Vanin EF, Vignali DA.

Correction of multi-gene deficiency in vivo using a single 'self-cleaving' 2A peptide-based retroviral vector.

Nat Biotechnol. 2004 May; 22(5):589-94.

Tamamaki N, Nakamura K, Furuta T, Asamoto K, Kaneko T.

Neurons in Golgi-stain-like images revealed by GFP-adenovirus infection in vivo.

Neurosci Res. 2000 Nov; 38(3):231-6.

Tang W, Ehrlich I, Wolff SB, Michalski AM, Wöfl S, Hasan MT, Lüthi A, Sprengel R.

Faithful expression of multiple proteins via 2A-peptide self-processing: a versatile and reliable method for manipulating brain circuits.

J Neurosci. 2009 Jul 8; 29(27):8621-9.

Takemura SY1, Bharioke A, Lu Z, Nern A, Vitaladevuni S, Rivlin PK, Katz WT, Olbris DJ, Plaza SM, Winston P, Zhao T, Horne JA, Fetter RD, Takemura S, Blazek K, Chang LA, Ogundeyi O, Saunders MA, Shapiro V, Sigmund C, Rubin GM, Scheffer LK, Meinertzhagen IA, Chklovskii DB.

A visual motion detection circuit suggested by *Drosophila* connectomics.

Nature. 2013 Aug 8; 500(7461):175-81.

Tian L, Hires SA, Mao T, Huber D, Chiappe ME, Chalasani SH, Petreanu L, Akerboom J, McKinney SA, Schreier ER, Bargmann CI, Jayaraman V, Svoboda K, Looger LL.

Imaging neural activity in worms, flies and mice with improved GCaMP calcium indicators.

J Neurosci. 2009 Jul 8; 29(27):8621-9.

Tomioka R, Rockland KS.

Improved Golgi-like visualization in retrogradely projecting neurons after EGFP-adenovirus infection in adult rat and monkey.

J Histochem Cytochem. 2006 May; 54(5):539-48.

References

Tomlinson A.

Cellular interactions in the developing *Drosophila* eye.

Development. 1988 Oct; 104(2):183-93.

Ugolini G.

Specificity of rabies virus as a transneuronal tracer of motor networks: transfer from hypoglossal motoneurons to connected second-order and higher order central nervous system cell groups.

J Comp Neurol. 1995 Jun 5; 356(3):457-80.

Ugolini G.

Advances in viral transneuronal tracing.

J Neurosci Methods. 2010 Dec 15; 194(1):2-20.

Van Haefen T, Wouterlood FG.

Neuroanatomical tracing at high resolution.

J Neurosci Methods. 2000 Nov 15; 103(1):107-16.

Vermeulen CJ, Loeschcke V.

Longevity and the stress response in *Drosophila*.

Exp Gerontol. 2007 Mar; 42(3):153-9.

Wässle H, Peichl L, Boycott BB.

Dendritic territories of cat retinal ganglion cells.

Nature. 1981 Jul 23; 292(5821):344-5.

Wang J, Zugates CT, Liang IH, Lee CH, Lee T.

Drosophila Dscam is required for divergent segregation of sister branches and suppresses ectopic bifurcation of axons.

Neuron. 2002 Feb 14; 33(4):559-71.

Wang J, Ma X, Yang JS, Zheng X, Zugates CT, Lee CH, Lee T.

Transmembrane/juxtamembrane domain-dependent Dscam distribution and function during mushroom body neuronal morphogenesis.

Neuron. 2004 Sep 2; 43(5):663-72.

Warzecha AK, Egelhaaf M, Borst A.

Neural circuit tuning fly visual interneurons to motion of small objects. I. Dissection of the circuit by pharmacological and photoinactivation techniques.

J Neurophysiol. 1993 Feb; 69(2):329-39.

References

- Wickersham IR, Finke S, Conzelmann KK, Callaway EM.
Retrograde neuronal tracing with a deletion-mutant rabies virus.
Nat Methods. 2007a Jan; 4(1):47-9.
- Wickersham IR, Lyon DC, Barnard RJ, Mori T, Finke S, Conzelmann KK, Young JA, Callaway EM.
Monosynaptic restriction of transsynaptic tracing from single, genetically targeted neurons.
Neuron. 2007b Mar 1; 53(5):639-47.
- Wojtowicz WM, Andre I, Qian B, Baker D, Zipursky SL.
A vast repertoire of Dscam binding specificities arises from modular interactions of variable Ig domains.
Cell. 2007 Sep 21; 130(6):1134-45.
- Wojtowicz WM, Flanagan JJ, Millard SS, Zipursky SL, Clemens JC.
Dscam generates axon guidance receptors that exhibit isoform-specific homophilic binding.
Cell. 2004 Sep 3; 118(5):619-33.
- Wu JS, Luo L.
A protocol for mosaic analysis with a repressible cell marker (MARCM) in Drosophila.
Nat Protoc. 2006; 1(6):2583-9.
- Yamagata M, Sanes JR.
Dscam and Sidekick proteins direct lamina-specific synaptic connections in vertebrate retina.
Nature. 2008 Jan 24; 451(7177):465-9.
- Yamagata M1, Sanes JR.
Synaptic localization and function of Sidekick recognition molecules require MAGI scaffolding proteins.
J Neurosci. 2010 Mar 10; 30(10):3579-88.
- Yamagata M, Sanes JR.
Expanding the Ig superfamily code for laminar specificity in retina: expression and role of contactins.
J Neurosci. 2012 Oct 10; 32(41):14402-14.
- Yamaguchi S, Wolf R, Desplan C, Heisenberg M.
Motion vision is independent of color in Drosophila.
Proc Natl Acad Sci USA. 2008; 105:4910-4915.
- Yamakawa K, Huot YK, Haendelt MA, Hubert R, Chen XN, Lyons GE, Korenberg JR.
DSCAM: a novel member of the immunoglobulin superfamily maps in a Down syndrome region and is involved in the development of the nervous system.
Hum Mol Genet. 1998 Feb; 7(2):227-37.

References

Yang D, Lu H, Erickson JW.

Evidence that processed small dsRNAs may mediate sequence-specific mRNA degradation during RNAi in *Drosophila* embryos.

Curr Biol. 2000 Oct 5; 10(19):1191-200.

Zamore PD, Tuschl T, Sharp PA, Bartel DP.

RNAi: double-stranded RNA directs the ATP-dependent cleavage of mRNA at 21 to 23 nucleotide intervals.

Cell. 2000 Mar 31; 101(1):25-33.

Zeidler MP, Tan C, Bellaïche Y, Cherry S, Häder S, Gayko U, Perrimon N.

Temperature-sensitive control of protein activity by conditionally splicing inteins.

Nat Biotechnol. 2004 Jul; 22(7):871-6.

Zhan XL, Clemens JC, Neves G, Hattori D, Flanagan JJ, Hummel T, Vasconcelos ML, Chess A, Zipursky SL.

Analysis of Dscam diversity in regulating axon guidance in *Drosophila* mushroom bodies.

Neuron. 2004 Sep 2; 43(5):673-86.

Zhu H, Hummel T, Clemens JC, Berdnik D, Zipursky SL, Luo L.

Dendritic patterning by Dscam and synaptic partner matching in the *Drosophila* antennal lobe.

Nat Neurosci. 2006 Mar; 9(3):349-55.

Zipursky SL, Grueber WB.

The molecular basis of self-avoidance.

Annu Rev Neurosci. 2013 Jul 8;36:547-68.

IV. Acknowledgement

I would like to express my gratitude to all those who enabled me to finish this thesis. I owe my deepest gratitude to Alexander Borst who enabled and allowed me to work in a unique laboratory environment where scientific questions can be approached in an amazing broad spectrum. I appreciated him very much as my doctor thesis adviser with whom I always could discuss about scientific and personal topics. He has always been guidance for me both, in research, and in social aspects. Furthermore, I thank Dierk Reiff who instructed me in all the projects I presented in this thesis. He was a great supervisor with many inspiring ideas for new experiments making his support available in a number of ways. I also would like to thank Karl Friedrich Förstner, a friend and member of my thesis committee for giving outstanding support in all aspects. I am indebted to my many of my colleagues and collaboration partner: Väinö Haikala, Bettina Schnell, Friedrich Förstner and Alexander Ghanem for great support. They opened up new dimensions in the projects and allowed me to look beyond my own backyard. I would like to show my gratitude to Klaus Conzelmann for collaboration in the virus project and for all insights about this alien system. Furthermore, I would like to thank Shamprasad Raghu for our intense discussions about project design and experiments. He helped me a lot in interpreting results and answering questions. I also enjoyed him very much as supervisor of the vGat project. Special thanks to our technicians Christian Theile and Wolfgang Eßbauer for taking care of the fly stocks, which was fundamental work for the success of all experiments. Thanks go also to the people in P1 for providing a nice atmosphere at my working place. I am indebted to my many of my colleagues to support me and therefore, would like to thank the entire Borst group for the wonderful time that I was able to spend in this lab. Finally yet importantly, I want to thank my parents and my family. They were very patient and supportive during the entire PhD time.